

1 Real-time UV-Index retrieval in Europe using Earth Observation 2 based techniques: system description and quality assessment 3 validation against ground-based measurements

4 Panagiotis G. Kosmopoulos¹, Stelios Kazadzis², Alois W. Schmalwieser³, Panagiotis I. Raptis¹,
5 Kyriakoula Papachristopoulou¹, Ilias Fountoulakis^{1,4}, Akriti Masoom⁵, Alkiviadis F. Bais⁶, Julia Bilbao⁷,
6 Mario Blumthaler⁸, Axel Kreuter^{8,9}, Anna Maria Siani¹⁰, Kostas Eleftheratos¹¹, Chrysanthi Topaloglou⁶,
7 Julian Gröbner², Bjørn Johnsen¹², Tove M. Svendby¹³, Jose Manuel Vilaplana¹⁴, Lionel Doppler¹⁵, Ann
8 R. Webb¹⁶, Marina Khazova¹⁷, Hugo De Backer¹⁸, Anu Heikkilä¹⁹, Kaisa Lakkala²⁰, Janusz Jaroslowski²¹,
9 Charikleia Meleti⁵, Henri Diémoz⁴, Gregor Hülsen², Barbara Klotz⁸, John Rimmer¹⁶, Charalampos
10 Kontoes¹

11
12 ¹National Observatory of Athens, Athens, Greece

13 ²Physikalisch-Meteorologisches Observatorium Davos, World Radiation Center, Davos Dorf, Switzerland

14 ³University of Veterinary Medicine, Vienna, Austria

15 ⁴Environmental Protection Agency of Aosta Valley, Aosta, Italy

16 ⁵Indian Institute of Technology Roorkee, India

17 ⁶Aristotle University of Thessaloniki, Greece

18 ⁷Valladolid University, Valladolid, Spain

19 ⁸Innsbruck Medical University, Innsbruck, Austria

20 ⁹-Luftblick OG, Innsbruck, Austria

21 ¹⁰Sapienza University of Rome, Rome, Italy

22 ¹¹National and Kapodistrian University of Athens, Athens, Greece

23 ¹²Norwegian Radiation and Nuclear Safety Authority, Bærum, Norway

24 ¹³NILU - Norwegian Institute for Air Research, KjellerBærum, Norway

25 ¹⁴National Institute for Aerospace Technology, Torrejón de Ardoz, Spain

26 ¹⁵German Weather Service, Offenbach, Germany

27 ¹⁶University of Manchester, Manchester, UK

28 ¹⁷Public Health England, London, UK

29 ¹⁸Royal Meteorological Institute of Belgium, Bruxelles, Belgium

30 ¹⁹Finnish Meteorological Institute, Helsinki, Finland

31 ²⁰Finnish Meteorological Institute, Sodankylä, Finland

32 ²¹Institute of Geophysics, Polish Academy of Sciences, Warsaw, Poland

33
34 *Correspondence to:* P.G. Kosmopoulos (pkosmo@noa.gr)

35 **Abstract.** This study introduces an Earth observation (EO)-based system which is capable of operationally estimating and
36 continuously monitoring the ultraviolet index (UVI) in Europe. The UVIOS (i.e. UV-Index Operating System) exploits a

37 synergy of radiative transfer models with high performance computing and EO data from satellites (Meteosat Second
38 Generation and Meteorological Operational Satellite-B), and retrieval processes (Tropospheric Emission Monitoring Internet
39 Service, Copernicus Atmosphere Monitoring Service and the Global Land Service). It provides a near-real-time now-casting
40 and short-term forecasting service for UV radiation over Europe. The main atmospheric inputs for the UVI simulations include
41 ozone, clouds and aerosols while the impacts of ground elevation and surface albedo are also taken into account. The UVIOS
42 output is the UVI at high spatial and temporal resolution (5 km and 15 minutes, respectively) for Europe (i.e. 1.5 million pixels)
43 in real-time. The UVI is empirically related to biologically important UV dose rates and the reliability of this EO-based solution
44 was verified against ground-based measurements from 17 stations across Europe. Stations are equipped with spectral,
45 broadband or multi-filter instruments and cover a range of topographic and atmospheric conditions. A period of over one year
46 of forecasted 15-min retrievals under all sky conditions were compared with the ground-based measurements. UVIOS
47 forecasts were within ± 0.5 of measured UVI for at least 70% of the data compared at all stations. For clear sky conditions the
48 agreement was better than 0.5 UVI for 80% of the data. A sensitivity analysis of EO inputs and UVIOS outputs was performed
49 in order to quantify the level of uncertainty in the derived products, and to identify the covariance between the accuracy of the
50 output and the spatial and temporal resolution, and the quality of the inputs. Overall, UVIOS slightly overestimated UVI due
51 to observational uncertainties in inputs of cloud and aerosol. This service will hopefully contribute to EO capabilities and will
52 assist the provision of operational early warning systems that will help raise awareness among European Union citizens of the
53 health implications of high UVI doses.

54 **Keywords.** Ultraviolet Index; Earth Observation; Radiative Transfer; High Performance Computing; Clouds; Aerosols;
55 Ozone; Solar Zenith Angle; Ground Elevation; Surface Albedo

56 **1 Introduction**

57 Human exposure to ultraviolet (UV) radiation (<400 nm) has both beneficial and harmful effects (Andrady et al., 2015;
58 Juzeniene et al., 2011; Lucas et al., 2006). Overexposure to UV radiation (UVR) has a number of implications, such as the
59 acute response of erythema, the risk of skin cancer and a number of eye diseases (snow blindness, cataract). Nevertheless,
60 exposure to solar UVB radiation (290-315 nm) is the main mechanism for the synthesis of Vitamin D in the human skin
61 (Holick, 2002; Webb and Engelsen, 2008; Webb et al., 2011). Low levels of the Vitamin D are associated with depression of
62 the immune system and there is evidence that is linked to a number of medical implications (Lucas et al., 2015).

63 The UV index was introduced by WHO/WMO in 1994 (WMO, 1995), as a simple method of informing the general public
64 about the erythema effective (sun-burning) UV. It is a unitless, scaled version of erythemally-weighted UV determined by
65 multiplying the erythema weighted irradiance (in W/m^2) by $40 m^2/W$ (Fioletov et al., 2010 ; Vanicek et al., 2000; WHO, 2002).
66 The response of UV radiation to climatic changes is of great concern (Bais et al., 2019; Bais et al., 2018; McKenzie et al.,

67 2011). According to the latest work of Bais et al. (2019) greater values of UV are expected by the end of 21st century, relative
68 to the present decade, at low latitudes, while at higher latitudes UV will decrease but these projections are associated with
69 high uncertainty (up to 30%).

70 There are many factors affecting UV irradiance reaching Earth's surface (Kerr and Fioletov, 2008). The dependence of UV
71 irradiance on astronomical and geometrical parameters is generally well understood, and in many cases the changes are
72 periodical (e.g., (Blumthaler et al., 1997; Gröbner et al., 2017; Larkin et al., 2000; Seckmeyer et al., 2008)). Atmospheric gases
73 play a crucial role in attenuating UV irradiance, specifically NO₂ is a major absorber in the UV is spectral region (e.g., Cede et
74 al. (2006)), while O₃ is the main absorber at lower (UVB) wavelengths. Other gases that have significant absorption in the UV
75 include SO₂ (Fioletov et al., 1998) and HCHO (Gratien et al., 2007), but their –usually- smaller atmospheric abundances,
76 result in minor effects to incoming UV (with major exceptions such as volcanic incidents). Aerosols are another important
77 parameter controlling UV irradiance levels at the surface (e.g., Kazadzis et al. (2009b)). Aerosol optical depth (AOD) that
78 quantifies the attenuation of the direct solar beam by aerosols is a parameter varying with wavelength, as well as sSingle
79 scattering albedo (SSA), which determines the scattering ratio to total extinction, is also a spectrally variant parameter. Several
80 recent studies based on incoming surface UV irradiance measurements or calculations reveal the enhanced absorption by
81 aerosols in the UV relative to the visible spectral range. ~~They show the~~ Finally, a number of studies have highlighted the
82 importance of using representative SSA in the UV spectral region, instead of interpolating SSA at visible wavelengths to the
83 UV, or directly using SSA at visible wavelengths, options that systematically overestimate UV irradiance (Corr et al., 2009;
84 Fountoulakis et al., 2019; Kazadzis et al., 2016; Mok et al., 2018; Raptis et al., 2018).

85 All the aforementioned parameters are particularly important under cloud free conditions. The cloudy sky complicates the
86 propagation of solar radiation, predominantly in the troposphere, through multiple cloud - radiation interactions. Nonetheless,
87 UVR is less affected than the total solar radiation by clouds (e.g., Badosa et al. (2014)). Bais et al. (1993) quantified that for
88 the city of Thessaloniki the change from 0 to 8 oktas for cloud coverage corresponds to 80% reduction in the UVR and pointed
89 out that there is very low wavelength dependence of UVR attenuation by cloud cover. Although, the transmittance of clouds
90 does not vary significantly with wavelength, some studies (Mayer et al., 1998; Seckmeyer et al., 1996) have found that the
91 diffuse component of the surface UVR is affected by clouds in a spectrally dependent way, due to more efficient scattering
92 and absorption of shorter UV wavelengths, in case of large air masses. In cases of partially cloudy sky but unobscured sun,
93 UVR tends to be higher than in clear sky conditions (e.g., Badosa et al. (2014)), as is the case for total solar radiation. For short
94 timescale analysis the variability of UVR introduced by clouds should be considered.

95 Solar UV irradiance at the surface increases with increasing surface albedo. This increment affects the UV radiant exposure,
96 which becomes crucial for outdoor human activities (Schmalwieser and Siani, 2018; Schmalwieser, 2020; Siani et al., 2008).
97 Measurements and computations of effective surface albedo for heterogeneous surfaces reveal its strong spectral dependence,
98 with snow-covered surfaces having significantly higher values of albedo for short wavelengths compared to total solar radiation
99 (Blumthaler and Ambach, 1988; Kreuter et al., 2014). Stronger enhancement of the UV relative to visible radiation over highly
100 reflective surfaces is also due to the more effective multiple scattering of shorter wavelengths in the atmosphere.

101 Any systematic changes in any of the parameters described in previous paragraphs have the potential to lead to changes for
102 UVR. These changes vary significantly throughout the globe and are attributed to different possible drivers (Bernhard and
103 Stierle, 2020; Fountoulakis et al., 2018; McKenzie et al., 2019). Fountoulakis et al. (2020a) gives a review of recent
104 publications concerning UV trends since 1990s, and associated factors, summarizing these as positive trends for South and
105 Central Europe and negative trends at higher latitudes, and recognizing the important role of aerosols and cloud coverage for
106 these trends. ~~Findings from the same study demonstrated that the long-term changes of UV irradiance recorded at four stations
107 around Europe during the last two decades are mainly attributed to aerosols, cloud coverage and surface albedo variations,
108 with total ozone changes being of minor importance.~~ Chubarova et al. (2020) found a long term increase of 3% per decade in
109 UV at Northern Eurasia for the 1979-2015 period. For the northern mid-latitudes Zerefos et al. (2012) showed that the long-
110 term (1995-2006) positive trend in total ozone wasn't enough to compensate for, let alone reverse, the UVB increase attributed
111 to tropospheric aerosol decline (brightening effect). Since 2007, a slowdown or even a possible turning point in the positive
112 UVB trend was detected, which was attributed to the continued upward trend in total ozone overwhelming the aerosol effect
113 (Zerefos et al., 2012). By contrast, the long-term variability of UVB irradiance over northern high latitudes was determined by
114 ozone and not by aerosol trends, as shown by Eleftheratos et al. (2015) who found a statistically significant negative trend of
115 -3.9% per decade for the UVB irradiance during the time period 1999-2011, ~~from ground-based measurements at 7 stations.~~
116 ~~This was~~ in agreement with statistically significant increase of spaceborne measured total ozone by about 1.5% per decade
117 (ozone recovery) for the same area. ~~For Arctic regions changes in snow cover have a great impact on UV trends according to
118 Bernhard (2011), who concluded that the future Arctic UV climate may be affected more by a warming climate changing the
119 snow cover than changes in stratospheric ozone concentrations.~~

120 The continuous monitoring of the UV index is currently performed by about 160 stations from 25 countries around Europe
121 (Schmalwieser et al., 2017), with all monitoring instruments having the potential to provide other effective doses such as the
122 effective dose for the production of vitamin D in human skin (e.g., Fioletov et al. (2009)).

123 There are three types of instruments for UV irradiance measurements; those measuring the integral of UV irradiance
124 (broadband sensors) tailored to a specific response, narrow band instruments such as filter radiometers with coarse spectral
125 resolution, and instruments performing high resolution spectral measurements – the most versatile but most challenging and
126 least robust instruments. Concerning the current UV monitoring measurement accuracy; The European reference UV
127 spectroradiometer (QASUME) is a traveling instrument which provides a common standard through inter-comparison on-site
128 (Gröbner et al., 2005; Hülsen et al., 2016). During the period 2000-2005 the QASUME visited 27 spectroradiometers sites.
129 Out of the 27 instruments, 13 showed deviations of less than 4% relative to the QASUME reference spectroradiometer in the
130 UVB (for 15 instruments in the UVA) for solar zenith angles below 75°. The expanded relative uncertainty (coverage factor
131 $k=2$) of solar UV irradiance measurements by QASUME, for SZA smaller than 75° and wavelengths longer than 310 nm, was
132 4.6% in 2002 – 2014 (Gröbner and Sperfeld, 2005), and has been 2 % since 2014 (Hülsen et al., 2016). For broadband
133 instruments, the current instrument uncertainties are summarized in (Hülsen et al., 2020; Hülsen et al., 2008). In 2017, 75
134 broad-band instruments measuring the UV index, the UVB or/and the UVA irradiance participated in the solar UV broadband

135 radiometer comparison in Davos Switzerland. Using the instrument/user calibration factors, the differences between the
136 datasets by the broad-band instruments and the reference (QASUME) dataset were within $\pm 5\%$ for 32 (43 %) of the instrument
137 datasets, $\pm 10\%$ for 48 (64 %), and exceeded $\pm 10\%$ for 27 (35 %).

138 Although ground-based monitoring of solar UVR is more accurate than satellite retrievals, ground based stations are sparse,
139 and the only way for continuous monitoring of the UVR on a global scale is through satellites. In recent decades instruments
140 on-board satellites have provided the necessary data for estimates of UV irradiance reaching the Earth surface on a global scale
141 (Herman, 2010) and hence satellite-derived UVR climatological studies have been conducted (Vitt et al., 2020; Verdebout,
142 2004). The satellite UV irradiance record started with the Total Ozone Mapping Spectrometer (TOMS) on-board Nimbus-7 in
143 1978 and continued with Ozone Monitoring Instrument (OMI) on-board NASA's satellite EOS-Aura. The OMI retrieval
144 algorithm for surface UVR estimates was based on the experience gained from TOMS (Levelt et al., 2018; Levelt et al., 2006).
145 The early surface UVR retrieval algorithms from satellite data didn't account for the enhanced aerosol absorption in the UV
146 spectral range, resulting in overestimated values (Krotkov et al., 1998). A lot of scientific effort has been put into correcting
147 the products (Arola et al., 2009). TROPospheric Monitoring Instrument (TROPOMI) onboard Sentinel – 5 Precursor (Lindfors
148 et al., 2018) is the current satellite instrument that provides the surface UVR product on a daily basis with global coverage,
149 including 36 UVR parameters. As the aforementioned instruments were installed onboard polar orbiting satellites, providing
150 global spatial coverage, the temporal resolution of the data is daily since there are only one or two overpasses per day for every
151 point. Geostationary satellites provide continuous (in time) measurements over wide areas. The geostationary meteorological
152 satellites Meteosat monitor the full Earth Disk including Europe and their frequent data acquisition of rapidly changing
153 parameters e.g., cloud is essential for estimating daily UV doses (Verdebout, 2000).

154 -Comparison of OMI surface UV irradiance estimates with ground-based measurements for Thessaloniki, Greece showed that
155 OMI irradiances overestimate surface observations for UVB wavelengths by between $\sim 1.5\%$ to 13.5% in contrast to
156 underestimated satellite values for UVA wavelengths (Zempila et al., 2016). Results from the validation of TROPOMI surface
157 UV radiation product showed that most of the satellite data agreed within $\pm 10\%$ with ground-based measurements for snow-
158 free surfaces (Lakkala et al., 2020). Larger differences between satellite data and ground-based measurements were observed
159 for sites with non-homogeneous topography and non-homogeneous surface albedo conditions. The differences between
160 ground-based and satellite UVR data are mostly due to uncertainties in the input parameters to the satellite algorithm used to
161 retrieve the UV irradiance at the surface. Based on a recent study of Garane et al. (2019) a mean bias of 0-1.5% and a mean
162 standard deviation of 2.5 – 4.5 % was found for the relative difference between TROPOMI total ozone column (TOC) product
163 and ground based quality assured Brewer and Dobson TOC measurements.

164 In this study we introduce a novel UV-Index Operating System, called UVIOS, which is able to efficiently combine
165 information on geophysical input parameters from different modelled and satellite-based data sources in order to provide for
166 the European region the best possible UV-Index (UVI) estimates operationally and in real-time. ~~UVIOS is based on pre-~~
167 ~~calculated radiative transfer model simulations in the form of analytical look up tables (LUT) in conjunction with geophysical~~
168 ~~input parameters and high performance computing for instantaneous outputs.~~ The reliability of the UVIOS input and output

169 parameters was tested for the year 2017 against ground-based measurements and an analytical sensitivity analysis was
170 performed in order to quantify the uncertainties and to provide information about the limitations and about the optimum
171 operating conditions of the proposed system. ~~Since UVIOS can produce massive UVI outputs of the order of 1.5 million
172 simulations in less than 5 minutes following the proposed simulation and computing architecture (see section 2.1.2), this means
173 that it can be used for both operational applications and real-time estimations. The exact use of UVIOS depends only on the
174 available input data sources. For this study both nowcasts (clouds) and forecasts (ozone, aerosol) were used as inputs to the
175 system. The nowcasts represent the continuous monitoring dimension (i.e. what is happening now) in terms of cloud
176 microphysics data every 15 minutes retrieved in real-time by the geostationary satellite Meteosat Second Generation (MSG).
177 The forecasts represent the future estimations (day-ahead in our study) of aerosol optical properties and total ozone column
178 based on deterministic approaches (ECMWF) and assimilated satellite data for better accuracy. As a result, UVIOS under
179 cloudless conditions operates as a forecast system since it uses forecasted inputs and provides the clear sky UVI forecasts
180 operationally. By adding the nowcast cloud information as input to UVIOS (i.e. all-sky conditions), the whole procedure will
181 follow the time steps of MSG cloud microphysics data collocated and synchronized with the forecast data. So, following the
182 proposed operation method of this study, the UVIOS can be used as a UVI forecast system for cloudless conditions or as a
183 UVI nowcast system for all-sky conditions.~~

184 In Section 2 we describe the UVIOS ~~and~~, the input data sources, ~~while and~~ Section 3 presents the ground-based measurements
185 used as well as for the evaluation/validation methodology. Section ~~4~~ 3 analyses/presents the results in terms of model
186 performance and factors that affect the UVIOS retrievals and the overall accuracy. Finally, Section ~~5~~ 4 summarizes the findings
187 and the main conclusions of this study and provides a brief description of the future plans with this system.

188 2 The UV Index operating system (UVIOS) Data and Methodology

189 2.1 System description The UV Index operating system (UVIOS)

190 2.1.1 UVIOS modelling

191 The UVIOS system is a novel model that uses real-time and forecasted atmospheric inputs based on satellite retrievals and
192 modelling techniques and databases in order to nowcast and forecast the UVI with a spatial resolution of 5 km and a temporal
193 resolution of 15 minutes. The UVIOS calculation scheme is based on the libRadtran library of radiative transfer models (RTM)
194 (Mayer and Kylling, 2005) within which all the available inputs (i.e. solar elevation, cloud and aerosol optical properties,
195 ozone) can be integrated in real-time into the radiative transfer code and calculate the UVI for each pixel. Afterwards, post
196 processing correction for the elevation of each location and the surface albedo is also performed. In order to be able to simulate
197 the UVI for 1.5 million pixels in real-time we use pre-determined spectral solar irradiance LUTs based on the Libradtran RTM,
198 in combination with high performance computing (HPC) architectures that speed up the process of choosing and

199 interpolating/extrapolating the right combinations from the LUTs (Kosmopoulos et al., 2018; Taylor et al., 2016). The result
200 is the retrieval of UVI for 1.5 million pixels covering the European domain in less than 5 minutes after receiving all necessary
201 input parameters.

202 As mentioned the UVIOS architecture does not include a clear sky model and the subsequent calculation of individual sources
203 of UV attenuation, but instead it directly uses the following parameters: solar zenith angle (SZA), the aerosol optical depth
204 (AOD) and other aerosol optical properties (e.g., single scattering albedo (SSA), asymmetry parameter, and Ångström
205 exponent (AE)), the total ozone column (TOC), the cloud optical thickness (COT), as well as the surface elevation (ELE) and
206 the surface albedo (ALB) as RTM inputs. Table 1 presents the EO data used as inputs for the UVI real time simulations, their
207 description and sources. The Meteosat Second Generation (MSG4) cloud microphysics includes the nowcasted cloud optical
208 thickness (COT) at 550 nm, and cloud phase (CPH) obtained at a spatial and temporal resolutions of 5 km (average, depending
209 on latitude) and 15 minutes, respectively. Typical values of other cloud properties (e.g., cloud height, cloud thickness) have
210 been assumed based on the cloud type (information which is also available from MSG) (for more detailed information see
211 Taylor et al. (2016)). The 1-day forecast CAMS aerosol optical depth (AOD) at 550 nm is obtained at a spatial and temporal
212 resolutions of 40 km and 3 h, respectively and the monthly aerosol optical properties obtained from AeroCom (Kinne, 2019)
213 includes asymmetry parameter, single scattering albedo (SSA) and Ångström exponent (AE) at $1^\circ \times 1^\circ$ (latitude x longitude)
214 spatial resolution. Solar elevation is taken from the Astronomical model (NREL) (5 km – 15 minutes) (Reda and Andreas,
215 2008) and climatological surface albedo (ALB) is retrieved from Copernicus Global Land Service (CGLS) (1 km – 12 days)
216 (Carrer et al., 2010). Surface elevation (ELE) is obtained from the Digital Elevation Model (DEM) of NOAA (NOAA, 1988).
217 The Tropospheric Emission Monitoring Internet Service (TEMIS) 1-day forecast of total ozone column (TOC) is at a spatial
218 resolution of $1^\circ \times 1^\circ$ – 1 day with assimilated ozone fields from GOME-2 (METOP-B) (Eskes et al., 2003). We have to mention
219 also here that the selection of the RTM inputs has been decided based on their real-time availability.

220 **2.1.2 ~~UVIOS~~ real-time processing concept**

221 The LUT approach, despite its large size (almost 2.5 million spectral RTM simulations for clear and all sky conditions)
222 (Kosmopoulos et al., 2018), still provides estimates at discrete input parameters values. To overcome this mathematical issue,
223 we performed a multi-parametric interpolation technique to correct the input-output parameter intervals. This solution is
224 computationally more costly than a continuous function-approximation model, i.e. a Neural Network (NN) model
225 (Kosmopoulos et al., 2018), but the accuracy improvement is significant. Indicatively, using a test set of 1 million RTM
226 simulations for UVI from the developed LUT, we applied the NN developed in Kosmopoulos et al. (2018) and found a mean
227 execution time of around 144 seconds followed by a mean absolute error (MAE) of 0.0321, while by using the proposed
228 UVIOS multi-parametric interpolation exploiting the HPC and distributed computing benefits we found for the same test set
229 an execution time of 295 seconds with a MAE of 0.0001. The inclusion of many parameters (in this study we incorporated

230 eight, i.e. AOD, SZA, TOC, COT, ELE, ALB, AE, SSA) with small step sizes dramatically increase the LUT size, followed
231 by high computing requirements for the multi-parametric interpolation/extrapolation procedures.
232 For the UVIOS simulations performed in this study, a 32-core UNIX server was used equipped with 256 Gb of RAM and 12
233 Tb of storage system working in a RAID10 architecture. The combination of the HPC with the analytical LUTs, which were
234 developed by using the libRadtran RTM, allow a high speed multi-parametric interpolation and polynomial reconstruction
235 (Gal, 1986) to increase accuracy between the LUT records following a mathematical equation relating the UVIOS outputs to
236 the EO inputs.

237 An example of the UVIOS input output data is presented in Figure 1 through a flowchart illustration of the modelling technique
238 scheme. The inputs, including the solar and surface elevation, albedo, aerosol, ozone forecasts and the cloud observations as
239 described in Table 1, are fed to the real-time solver that results in spectrally weighted output of UVI for the European region.
240 Figure 2 shows the memory usage and error statistics for a range of different LUT sizes. The LUT error decreases as the LUT
241 size increases, regardless of the function being approximated. The LUT sizes in Figure 2 fit into cache on our HPC
242 environment, thus performance in terms of processing speed and overall output accuracy vary only slightly between the table
243 sizes shown. In our case, UVIOS shows that LUT transformation can provide a significant performance increase without
244 incurring an unreasonable amount of error, provided there is sufficient memory available. We note that the cache size is a
245 critical factor for LUT performance, while under a HPC environment practically there is no limit. Such techniques can be
246 implemented in hardware with distributed computing that operates in parallel to provide optimum performance.

247 Since UVIOS can produce massive UVI outputs of the order of 1.5 million simulations in less than 5 minutes following the
248 proposed simulation and computing architecture (see section 2.1.2), this means that it can be used for both operational
249 applications and real-time estimations. The exact use of UVIOS depends only on the available input data sources. For this
250 study both nowcasts (clouds) and forecasts (ozone, aerosol) were used as inputs to the system. The nowcasts represent the
251 continuous monitoring dimension (i.e. what is happening now) in terms of cloud microphysics data every 15 minutes retrieved
252 in real-time by the geostationary satellite ~~Meteosat Second Generation (MSG)~~. The forecasts represent the future estimations
253 (day ahead in our study) of aerosol optical properties and total ozone column based on deterministic approaches (ECMWF)
254 and assimilated satellite data for better accuracy. As a result, UVIOS under cloudless conditions operates as a forecast system
255 since it uses forecasted inputs and provides the clear-sky UVI forecasts operationally. By adding the nowcast cloud information
256 as input to UVIOS (i.e. all sky conditions), the whole procedure will follow the time steps of MSG cloud microphysics data
257 collocated and synchronized with the forecast data. So, following the proposed operation method of this study, the UVIOS can
258 be used as a UVI forecast system for cloudless conditions or as a UVI nowcast system for all sky conditions.

259
260 **2.32 Input dataThe description of the geophysical parameters**

261 The Cloud Optical Thickness (COT) data from Meteosat was used, whose retrieval algorithm is based on 0.6 and 1.6 micron
262 channel radiances of Meteosat's Spinning Enhanced Visible and InfraRed Imager (SEVIRI). MSG products have been
263 described in Derrien and Le Gléau (2005) and the MétéoFrance (2013) technical report. The COT impact uncertainty on UVI
264 deals with the MSG COT reliability and accuracy and hence introduces errors into the UVIOS simulations (Derrien and Le
265 Gléau, 2005; Pfeifroth et al., 2016). In addition, comparison principles of (point) station UVI measurements with a 5 km MSG
266 COT matrix are possibly responsible for at least part of the observed deviations (e.g., Kazadzis et al. (2009a)). For instance,
267 when a MSG pixel is partly cloudy, the ground measurements of UVI could fluctuate more than 100%, depending on whether
268 the sun is visible or whether clouds attenuate the direct component of the solar irradiance. The result is that in cases of partly
269 covered MSG pixels and in the absence of clouds between the ground measurement and the sun, the ground truth UVI would
270 be much higher than the UVIOS one. Of course, the presence of small clouds which have not been identified by MSG and
271 cover (part of) the sun disk, is plausible as well, consequently causing an overestimation of the modelled UVI (Koren et al.,
272 2007). Furthermore, sensors onboard geostationary satellites suffer from the parallax error, which contributes to the spatial
273 errors of the images and the overall uncertainty of the products (Bieliński, 2020; Henken et al., 2011). The error depends on
274 the altitude of the cloud and the viewing angle (parallax errors are more significant for high viewing angles).

275 UVIOS calculations at high solar zenith angles (>70 deg) are retrieved assuming cloudless skies since the MSG COT product
276 is not available in these conditions, facing reliability issues (Kato and Marshak, 2009). This has an effect on the quality of the
277 UVIOS overall performance at high solar zenith angles, where there is no cloud information as input to the model in order to
278 quantify the consequent impact on UVI. However, such measurements under high solar zenith angles are accompanied with
279 very low UVI levels (<1) both in the performed RTM simulations and in the ground-based measurements. This inconsistency,
280 even if does not affect UVIOS UVI results associated with dangerous effects on human health, nevertheless it is still affected
281 by the rest of input parameters (i.e. ozone, aerosol etc) mitigating the UVIOS uncertainty in the absence of cloud information
282 under such high solar zenith angles. There is more discussion in the next section on how we use these data for the UVIOS
283 validation.

284 For the total aerosol optical depth, we used 1-day forecast data from the Copernicus Atmospheric Monitoring Service (CAMS)
285 as the basic input parameter. These forecasts are based on the Monitoring Atmospheric Composition and Climate (MACC)
286 analysis and provide accurate data of aerosol optical depth (AOD) at 550 nm with a time step of 1 h and spatial resolution of
287 0.4°. For aerosol single scattering albedo properties climatological values from MACv2 aerosol climatology (Kinne, 2019)
288 was utilized. Monthly means of single scattering albedo at 310nm were acquired from global gridded data at a 1° x 1° spatial
289 resolution. Also, in order to derive the Angstrom exponent, monthly means of AOD at 340nm and 550nm were used. The
290 calculated Ångström exponent was then applied to the 550 nm AOD (from CAMS) in order to get AOD in the UV.

291 The surface albedo data were obtained from the Copernicus global land service (CGLS: Geiger et al., 2008; Carrer et al., 2010).
292 As a global surface ALB product is not available in the UV region, for this study we have used the climatological product of
293 CGLS (in the visible range) (Lacaze et al., 2013) as follows: based on the findings of Feister and Grewe (1995), we used a UV
294 albedo of 0.05 for non-snow cases and a UV ALB equal with CGLS when CGLS exceeded 0.5 (snow cover). The total ozone

295 column forecasts were obtained from Tropospheric Emission Monitoring Internet Service (TEMIS) which is a near- real time
296 service which uses the satellite observations of total ozone column by the Global Ozone Monitoring Experiment (GOME) and
297 SCIAMACHY assimilated in a transport model, driven by the European Centre for Medium-Range Weather Forecasts
298 (ECMWF) forecast meteorological fields (Eskes et al., 2003). The elevation data was obtained from the 5-minute Gridded
299 Global Relief Data (ETOPO5) database, which provides land and seafloor elevation information at a 5-minute
300 latitude/longitude grid, with a 1-meter precision in the region of Europe and is freely available from NOAA (NOAA, 1988).
301 An analytical description of the above geophysical parameters including their specifications and resolution can be found in
302 Table 1, followed by the corresponding references for more technical details. Figure 3 shows an example of the input-output
303 UVIOS parameters. An extensive validation of the MACC analysis and forecasting system products were performed by Eskes
304 et al. (2015). The aerosol optical properties were validated against 3-year (Apr. 2011 – Aug. 2014) near real time level 1.5
305 AERONET measurements and for AOD at 550 nm an overall overestimation was exhibited. Due to dedicated validation
306 activity of the MACC service a validation report that covers the time period of this study (Eskes et al., 2018) is also available,
307 presenting an overall positive modified normalized mean bias during 2017, ranging from 0 to 0.4, with the same range of
308 values over the study region (Europe). This overestimation of AOD at 550 nm may explain some of the UVI underestimation
309 under clear sky conditions (see section [4.3.2.2](#)).

310 **3 Ground measurements and evaluation methodology**

311 **2.3.1 Ground-based measurements**

312 In order to validate the UVIOS results 17 ground based stations were selected, for which measurements of the UVI were
313 available during 2017. The stations are shown in Fig. 4. Comparisons were performed with a 15-minute step. The ground based
314 measurements were obtained from spectrophotometers (Brewer), spectroradiometers (Bentham), filter radiometers (GUV) and
315 broadband instruments (SL501 and YES) as Table 2 shows. Note that UV data in table 2 has been calibrated, processed and
316 provided directly by the responsible scientists for each station. References wherein more information for the data quality of
317 particular instruments can be found are also provided. Brewer spectrophotometers measure the global spectral UV irradiance
318 with a step of 0.5 nm, and a resolution which is approximately 0.5 nm (usually between 0.4 and 0.6 nm). Depending on their
319 type the spectral range is usually 290-325 nm (MKII, MKIV) or 290-363 nm (MKIII). Since Brewer spectrophotometers
320 measure the spectrum up to a wavelength which is shorter than 400 nm, extension of the spectrum up to 400 nm in order to
321 calculate the UV index is usually achieved using empirical methods (e.g., (Fioletov et al., 2003; Slaper et al., 1995)). The
322 additional uncertainty in the UVI due to the latter approximation is well below the overall uncertainty in the measurements.
323 Bentham spectroradiometers measure the whole UV spectrum (290 – 400 nm) with step and resolution which can be
324 determined by the operator. The spectra from AOS and LIN (measured by Bentham spectroradiometers) used in this study
325 have been recorded with a step of either 0.25 or 0.5 nm and a resolution of ~ 0.5 nm. The Brewer Spectrophotometer measures

326 the total column of ozone using the differential absorption method, i.e. measuring the direct solar irradiance at four wavelengths
327 and then comparing the intensity at wavelengths that are weakly and strongly absorbed by ozone (Kerr et al., 1985). Brewer
328 TOC measurements are used in the present document to validate the TEMIS forecasts. The Ground-based Ultraviolet (GUV)
329 instrument is a multichannel radiometer that measures UV radiation in five spectral bands having central wavelengths as 305,
330 313, 320, 340 and 380 nm. However, in addition to UV irradiances, other data that can be obtained from GUV instruments are
331 total ozone and the cloud optical depth (Dahlback, 1996; Lakkala et al., 2018). GUV measurements are used for LAN station
332 of Norway. At stations AKR, INN and VIE, the surface UV was measured using Solar Light (SL) 501 radiometers. It provides
333 direct observation of UV index with a frequency of one minute. The Yankee Environmental System (YES) has been used for
334 VAL station.

335 The low latitude stations include AKR, ARE, ATH, ROM, THE, and VAL. AKR has minimum altitude of 23 m and VAL has
336 maximum altitude of 705 m above sea level. The middle latitude locations are AOS, DAV, INN, BEL, LIN, MAN, UCC, and
337 VIE among which the minimum altitude is 10 m in LAN and maximum altitude is in DAV at 1610 m above mean sea level.
338 HEL, LAN, and SOD represent the high latitude zone, with HEL having an altitude of 48 m and SOD an altitude of 185 m
339 above mean sea level (Table 2). A summary of basic climatic information for the validation locations was obtained from the
340 Köppen climate classification (Chen and Chen, 2013) and it is summarized here. THE, AKR, ARE, ROM, ATH and VAL
341 have a Mediterranean climate comprising of mild, wet winters and dry summers. MAN experiences maritime climate (cool
342 summer and cool, but not very cold, winter). AOS, UCC, LAN, BEL, HEL, LIN and VIE experience humid continental climate
343 with warm to hot summers, cold winters and precipitation distributed throughout the year. DAV and INN experience boreal
344 climate characterised by long, usually very cold winters, and short, cool to mild summers. SOD has subarctic climate having
345 very cold winters and mild summers.

346 **3.2.4 Evaluation methodology**

347 The time series period covers the whole year 2017 at 15-min intervals, following the MSG available time steps. A
348 synchronization between the UVIOS simulations and the ground-based measurements was performed in order to match the
349 15-min intervals of UVIOS to the measured data. The UVIOS data availability is 93%, while for the ground stations it reaches
350 almost 79% enabling a direct UVI data comparison of 77% of the 2017 time steps. For the comparison we used the closest
351 instrument measurements to the 15-min intervals with a maximum deviation of 3 minutes in order to avoid solar elevation and
352 cloud presence mismatches. Additionally, the UVIOS comparisons included measurements up to 70 degrees SZA. The
353 rationale for this cutoff was that UVIOS retrievals at high SZA are retrieved as cloudless as COT is unavailable from MSG.
354 In addition, the comparison is also impacted by limitation of the horizon of ground-based sites (e.g., Davos, Innsbruck, Aosta)
355 where the diffuse component and in some cases the direct component of solar UV irradiance are affected by obstacles
356 (mountains) on the horizon. The contribution of this mainly diffuse irradiance to the total budget is a function of solar elevation
357 and azimuth (day of the year) and also cloudiness. Although UVIOS simulations were corrected for changing UVI with respect

358 to altitude (see Section 3.2.3), the correction cannot be perfect for higher altitude stations. The reason is that it is not possible
359 to take into account all different factors (aerosol load and properties, atmospheric pressure, surface albedo) (e.g., Blumthaler
360 et al., 1997; Chubarova et al., 2016) which affect the change of UVI with altitude. This explains some of the deviations in the
361 results as the UVIOS retrieves UVI assuming a flat horizon. Clear sky conditions were defined as the UVIOS retrieval where
362 MSG COT equals to zero. Further discussion on the uncertainties introduced by this choice is mentioned in the cloud effect
363 section.

364 Most of the comparisons have been performed using the absolute (mean bias or median) UVI differences (model –
365 measurements). In addition, median values of the percentage differences (100* (model – measurements)/measurements) have
366 been used. UVIOS estimations were also evaluated in terms of mean bias and root mean square error (MBE and RMSE,
367 respectively), defined as follows:

$$368 \quad \text{MBE} = \bar{\varepsilon} = \frac{1}{N} \sum_{i=1}^N \varepsilon_i \quad (1) \quad \text{RMSE} = \sqrt{\frac{1}{N} \sum_{i=1}^N \varepsilon_i^2} \quad (2)$$

369 Where $\varepsilon_i = x_f - x_o$ are the residuals (UVIOS errors), calculated as the difference between the simulated values (x_f) and the
370 ground-based values (x_o), and where N is the total number of values. MBE quantifies the overall bias and detects whether the
371 UVIOS overestimates (MBE>0) or underestimates (MBE<0). RMSE quantifies the spread of the error distribution. Finally,
372 the correlation coefficient (r), as well as the coefficient of determination (R^2) were used to represent the proportion of the
373 variability between modeled and measured values.

374 **4.3 Results**

375 **4.3.1 Overall performance of the UVIOS system**

376 Fig. 5 presents a density scatterplot of the UVIOS simulations for all stations as compared to the ground-based measurements,
377 in which a pattern of shaded squares represents the counts of the points falling in each square and which shows is followed by
378 a correlation coefficient (r) of 0.944. For a more detailed view of the UVIOS performance, Fig. 6 depicts a Taylor diagram
379 with the overall model accuracy for all ground stations under all sky and clear sky conditions as a function of the correlation
380 coefficient, normalized standard deviation and RMSE. For both, clear sky and all sky conditions, the results are similar. The
381 absolute differences between the UVIOS and the measured UVI are within ± 0.5 , and the correlation coefficients are between
382 0.85 and 0.99 for all stations. The RMSE is for most stations less than 0.5. Under all sky conditions the RMSE is higher
383 relative to the RMSE for clear skies for MAN, DAV and SOD, which is probably due to misclassification of cloudy pixels
384 (see also the Appendix A section). Relative differences can be misleading as they may correspond to very small absolute
385 differences without physical meaning, especially for low levels of the UVI. Thus, we focused on absolute differences in order
386 to have a more representative assessment of the actual effect (UV Index) and its results. The differences were categorized to
387 low (less than 0.5), moderate (0.5 - 1) and high (more than 1). In the Appendix A, relative differences are also discussed.

388 In Table 3, U1.0 and U0.5 represent the percentage of cases with absolute differences between modelled and ground based
389 UVI measurements within 1 and 0.5, respectively, for all comparisons between the 15-minute model retrievals and the
390 corresponding ground-based measurements. As shown in Table 3, for all stations and for both, clear- and all sky conditions,
391 differences were within 0.5 UVI for at least 70% of the cases. Under clear sky conditions, AOS, BEL, HEL, LAN, LIN, SOD
392 and THE had above 90% of U0.5 cases, while others have 75-90% of U0.5 cases. All stations but DAV had above 90% of
393 U1.0 cases for clear skies, while the correlation coefficients for most of the stations were above 0.9 (exceptions are ATH and
394 MAN). For all-skies differences were within 1 UVI for 90% of the cases for all stations with the correlation coefficients
395 exceeding 0.9 for most of them (exceptions are DAV, MAN and SOD). Median differences for all skies for every station were
396 well within ± 0.2 UVI, with the 25-75 percentiles being within ± 0.5 UVI and the 5-95 percentiles within ± 1 UVI. For clear
397 skies the corresponding values are ± 0.1 , ± 0.4 and ± 0.8 respectively. In the following sections we try to investigate the factors
398 that contribute to the differences between UVIOS and ground-based measurements.

399 **4.3.2 Factors affecting UVIOS retrievals**

400 **4.3.2.1 Ozone effect**

401 All the available collocated Total Ozone Column (TOC) measurements for the stations used in UVIOS evaluation have been
402 obtained from the WOUDC (<https://woudc.org/>) database. In this database 8 out of 17 UVIOS evaluation stations (AOS, ATH,
403 DAV, MAN, ROM, SOD, THE and UCC) were found, providing TOC ground-based measurements. TOC comparison has
404 been performed by calculating daily means of ground-based measurements and the TOC from TEMIS. In order to quantify the
405 effect of the uncertainty of the forecasted TOC used as input at UVIOS we have calculated the mean differences of the
406 forecasted and measured TOCs and used a radiative transfer model to investigate their effect on UVIOS retrieved UVI. Table
407 4 shows the mean differences in D.U. from TEMIS TOC (used as inputs in UVIOS) as compared to the WOUDC ground-
408 based measurements for one year of comparison data. It is seen that for the stations AOS, DAV, MAN and UCC the values of
409 the TEMIS observations are higher as compared to the ground-based measurements (by 7.6, 1.9, 5, and 2.9 DU respectively)
410 while for the other stations TEMIS observations are lower (by 0.9, 5.4, 9.9, and 2.2 DU for ATH, ROM, SOD, and THE
411 respectively). The negative bias is seen to be highest for ROM station (-9.9) and the positive bias is highest for AOS station
412 (7.6). Part of the large differences over the complex terrain sites can be explained by the difference between the actual altitude
413 of the station and the average altitude of the corresponding grid points of TEMIS. For example, for AOS the average altitude
414 of the pixel is 2000 m while the real altitude of the station is 570 m, resulting in an underestimation of the tropospheric column
415 of ozone by TEMIS. In general, differences can be explained by the combined effects of uncertainties in TOC retrieval from
416 satellite and ground-based platforms (Rimmer et al., 2018; Boynard et al., 2018; Garane et al., 2018). Figure 7 shows the effect
417 of this TOC bias on the calculated UVIOS. As seen in Table 4, there is a mix of small underestimation and overestimation
418 cases in the TOCs used within UVIOS, with average absolute differences of 4-5 DU. Worst TOC UVIOS inputs were found
419 in AOS and ROM (7.6 and -9.9 DU) leading to maximum (at 30 degrees SZA) differences in UVI of -0.22 and 0.3 for AOS

420 and ROM, respectively. In general, in most of the cases UVI mean differences are less than 0.1. It has to be noted that the TOC
421 differences have a larger impact when expressed in percent at higher SZAs, while in Figure 7 higher absolute differences for
422 low SZA's are associated with higher UVIs at these SZAs. Detailed comparisons for each station are shown in the Appendix
423 A figures.

424 **4.3.2.2 Aerosol effect**

425 Aerosol optical depth measurements used for the UVIOS aerosol input evaluation have been collected from the AERONET-
426 NASA web site (Giles et al., 2019) for 12 out of our total 17 stations (AKR, ARE, ATH, DAV, HEL, LIN, ROM, SOD, THE,
427 UCC, VAL and VIE. AERONET (level 2, version 3) values of AOD at 500 nm were interpolated at 550nm using the
428 AERONET derived 440-870nm Angstrom exponent for each individual measurement. In order to compare those
429 measurements with CAMS forecasted AOD used for the UVIOS their daily means were derived. The comparison of forecasted
430 and measured daily means was based on all available data due to gaps in the AERONET time series. The AOD MBE and
431 RMSE statistical scores are shown in Table 5 in absolute units and correlation coefficient as well. All the stations have a mean
432 positive bias up to 0.071 except UCC which is showing a mean negative bias of 0.007. The comparison of all individual
433 stations with CAMS data used as inputs on UVIOS showed that under all cases CAMS AOD is higher than that from
434 AERONET with a mean difference of 0.07 at 550nm. The correlation between the modeled and the measured values varies
435 from 0.10 for VIE to 0.91 for ARE with most of the stations showing the correlation coefficient above 0.7. As in the case of
436 the TOC, AOD CAMS data are forecasts from the previous day and real time WOUDC or AERONET level 2.0 data do not
437 exist. Although real time TOC (and in due course AOD in the UV) is available from Eubrewnet (López-Solano et al., 2018;
438 Rimmer et al., 2018), it is only for particular locations and not for the whole European domain. Thus, the only choice in
439 providing for a real time UV Index for Europe is using the CAMS (for AOD) and the TEMIS (for TOC) data.

440 In order to evaluate the effect of AOD on UVI, UVI differences between the UVIOS using both AOD datasets (CAMS and
441 AERONET) as UVIOS inputs were analyzed. Figure 8 shows the mean bias error of the CAMS – AERONET AOD impact on
442 UVI for all stations with available ground based AOD data as a function of SZA together with the uncertainty range ($\pm 1 \sigma$).
443 It can be seen that UVIOS with CAMS AOD input underestimates UVI compared to the UVIOS with AERONET data, except
444 for the UCC station. This is consistent with CAMS overestimations of AOD compared to the AERONET measurements,
445 except for the station UCC as shown in Table 5. Higher aerosol levels in the atmosphere tend to lower the UVI. Highest
446 difference in UVI is observed for the stations HEL, SOD, VIE. Since, the aerosol level at the stations HEL and SOD is very
447 low, the percent difference between the AOD from CAMS and AERONET is larger for these stations (although the absolute
448 difference is similar) relative to stations with higher AOD, leading to higher differences in the UVI. Aerosol content for VIE
449 is higher than HEL and SOD but still within 0.2 which might be the reason for the higher UVI difference. In terms of SZA, it
450 is observed that the mean bias decreases with an increase in the SZA as the values of UVI also decrease with SZA and the

451 most deviation is for station VIE which is consistent with the poor correlation between the CAMS forecasted input and the
452 measurements for this station as seen from Table 5.

453 The use of single scattering albedo in the UV region is a difficult task and many studies have shown that such measurements
454 need extra effort and it is not possible to perform them worldwide (Arola et al., 2009; Kazadzis et al., 2016; Raptis et al.,
455 2018). The monthly values of the single scattering albedo used in UVIOS for the UV region were derived from the MACv2
456 database at the 310 nm wavelength (Kinne, 2019). Fig 9 shows the intra annual variability of SSA for the 17 stations. For all
457 stations, SSA values range from 0.76 to 0.93, with most of them having SSA values between 0.83 to 0.93, and relatively small
458 variability. In contrast, there are stations like ARE, BEL, INN, LIN, VIE and THE which have relatively smaller SSA values
459 (0.76-0.9) and greater variability than the other stations.

460 **4.3.2.3 Albedo effect & surface elevation correction**

461 Surface albedo at UV wavelengths is small (2 – 5%) for most types of surfaces (Feister and Grewe, 1995; Madronich, 1993)
462 except for features like sand (with a typical albedo of ~0.3) and snow (up to 1 for fresh snow) (Meinander et al., 2013; Myhre
463 and Myhre, 2003; Vanicek et al., 2000; Henderson-Sellers and Wilson, 1983). Renaud et al. (2000), found an enhancement of
464 about 15 to 25% in UVI for clear-skies and snow conditions due to the multiple ground-atmosphere reflections and this relative
465 increment was about 80% larger for overcast conditions. The combined effect of aerosols and snow lead to an enhancement of
466 about 50% in UVI in cloud-free condition for moderately polluted atmospheres (Badosa and Van Weele, 2002). Fig. 10 (a)
467 presents the effect of surface albedo on the UVI percentage difference (i.e. for various albedo values under clear sky conditions)
468 as a function of SZA, while Fig. 10 (b) shows the effect of surface elevation on UVI as a function of the percentage difference
469 for various total ozone columns. It is observed that the UVI percentage difference increases almost linearly with albedo for a
470 particular SZA and the variation is found to be almost identical for all SZA. This indicates that the UVI percentage difference
471 is independent of the SZA and increases with surface albedo. The UVI percentage difference is found also to increase almost
472 linearly with the increase in elevation for a particular total ozone column. The percentage difference is similar for all ozone
473 columns up to 1km, after which the differences with ozone column become more apparent. That is, at a particular elevation,
474 the percentage difference is higher for less total ozone column. A 1% fluctuation (decline or increase) in column ozone can
475 lead to about a 1.2% fluctuation (increase or decline) in the UV Index (Fioletov et al., 2003; Probst et al., 2012). Indicatively,
476 the average maximum surface elevation correction in terms of UVI for the DAV station (due to UVIOS input deviation from
477 to actual elevation) was of the order of 1.6 (15%), while for INN and AOS it was 0.5 and 0.6 respectively (6%) and for the
478 VAL station close to 0.8 (8%).

479 Uncertainties introduced in UVIOS from the use of a constant surface albedo value of 0.05 for non-snow conditions are quite
480 low. For the case of albedo values used for snow conditions based on the CGLS monthly mean product uncertainties can be
481 related to: the small difference of UV and visible albedo values; the fact that the CGLS provides an albedo of a certain area
482 around the station that does not necessarily coincide with the “effective” albedo area affecting UV measurements; and finally

483 that the monthly albedo product represents a monthly average while a real time CGLS product represents the last 12 days
484 (dynamically changing albedo). In order to investigate this last point, we have compared the UV effects from the use of the
485 two albedo datasets for DAV station, where the average difference between an example ground-based dataset and UVIOS was
486 found to be 0.14 UVI (Gröbner, 2021). In Fig. 11, the effect of surface albedo correction is shown for the Davos station, for a
487 period with snow cover and low percentage cloudiness. The climatological and the dynamically changing albedo are presented
488 in terms of percentage differences between modelled and ground measurements as a function of SZA. In the case of
489 climatological albedo, most of the percentage difference between forecasted and the measured UVI value is found to vary from
490 -30% to 10% for SZA between 20° to 70°, showing more underestimation than overestimation from the UVIOS simulations.
491 Similarly, in the case of dynamically changing albedo, most of the percentage difference between forecasted and the measured
492 UVI value is found to vary from -20% to 10% for SZA between 20° to 70°. The mean percentage difference between the results
493 using the two different albedo inputs is -2.76% in terms of accuracy improvement. However, beyond 70 degree SZA, there is
494 a huge variation in the percentage difference with mostly underestimations from the UVIOS simulations (not shown in Fig.
495 11).

496 **43.2.4 Cloud effect**

497 For the evaluation we used measurements at SZA lower than 70 degrees, based on the lack of cloud input from MSG for higher
498 SZAs. The lack of MSG data results in an overestimation of UVIOS in high SZAs and the UVI is systematically overestimated
499 for long periods during winter at high latitude regions when SZA does not get below 70 degrees during the day. However,
500 based on the simulations performed by UVIOS, this overestimation is low in terms of absolute UVI and does not usually
501 exceed 0.2 UVI because maximum UVIs at such SZAs rarely exceed UVI=1.

502 COT retrieved from the MSG satellite has been used as input for the UVIOS together with typical optical properties of the
503 clouds as discussed in Sect. 2.1. The evaluation of all stations for cloudless and cloudy conditions can be seen in Figure 12
504 that shows the relative frequency distribution of all stations (colours) and the mean (black line) for cloudless (upper plot) and
505 cloudy conditions (lower plot). Mean bias error of the modeled by UVIOS and measured UVI for all- and clear sky conditions
506 and the percentage of clear sky time steps data is presented in Figure 13. The mean bias for clear sky conditions is found to be
507 less than that for the all sky conditions for the stations AKR, ATH and THE (having most days of the year being cloudless as
508 the clear sky percentage is above 70%). The MBE for DAV, LIN and MAN is less for clear sky relative to all sky conditions
509 even though most days of the year are cloudy (clear sky annual percentage less than 45%) at the particular stations. While,
510 stations BEL, HEL, INN, LAN, SOD, UCC and VIE, that have mostly cloudy skies throughout the year (clear sky annual
511 percentage less than 50%), are having more MBE for clear sky conditions than the all sky condition. This can be due to the
512 erroneous classification of a cloudy sky as clear sky, which is also discussed in the following section. MBE is also larger for
513 AOS and ARE which have mostly clear skies throughout the year. Stations ROM and VAL have comparatively much smaller
514 MBE for clear sky conditions.

515 As shown in Table 6 there are 45.4% of cases with underestimations and 54.6% cases with overestimations for cloudless
516 conditions (COT=0). For all the other cases, overestimations (62.5%) are more predominant than underestimations (37.5%).
517 The difference in the modelled and the measured values goes beyond ± 1 UVI for only 5.1% cases for cloudless conditions
518 and 14.7% for all other cases. In general, under cloudy conditions, UVIOS shows an overestimation for UVI in contrast to the
519 ground measurements. One explanation for the overestimations could be the erroneous determination of COT from MSG above
520 the ground-based stations, giving cloud input that can be overestimated or underestimated. The results show that there is a
521 general tendency for a small underestimation of MSG COT that leads to a systematic but small UVIOS UVI overestimation
522 under cloudy conditions. Another possible explanation is the spatial representativeness of MSG COT. The MSG COT
523 determination is available at 5 by 5 km pixels that may differ from the actual situation of the cloud prevailing above the station,
524 especially in broken cloud conditions and in case when it blocks the direct radiation from the sun. Moreover, for lower solar
525 elevations, the direct sun irradiance can be blocked by cloud in neighbouring pixels. The first effect has been explored in the
526 relative frequency distribution of Figure 12 that shows a higher number ($\sim 63\%$) of data on the right of the zero UVI difference
527 vertical line for cloudy skies. When comparing data outside the 0.5 and 1 difference limits we also see that 1 – 4 times more
528 data show a UVIOS overestimation as compared to the clear sky case. This shows that in general there is a small (in UVI
529 terms) but significant UVIOS overestimation for non-zero COT conditions. Moreover, for clear skies, as determined from the
530 MSG, we observe a less pronounced UVIOS overestimation that corresponds to the fact that even if MSG defines the situation
531 as completely cloudless, in reality there may be some cases where clouds near the ground-based station affect the measured
532 UVI. This effect is easier to understand when showing these differences as a function of solar zenith angle which is explored
533 through Figure 14. It is observed that the absolute difference between the modelled and the measured values decreases with
534 increasing solar zenith angle and most of the difference lies within ± 4 UVI. The seasonal variation of the percentage UVI
535 difference as a function of SZA shows that while absolute UVI is small in winter the percentage difference is higher compared
536 to other seasons.

537 Figure 15 (a) shows the shadow volume at the surface level of a cloud, relative to the SEVIRI angle view, as a function of
538 cloud height and SZA, highlighting the ray tracing in the presence of clouds and the accompanied angular dependence due to
539 the 3D geometry. 15 (b) shows the scatter of the UVI difference under clear sky conditions for all stations as a function of
540 SZA. It is observed that there is an obvious pattern of scattered data for UVI differences higher than 1.5 compared with the
541 ones for differences less than -1.5. These data represent UVIOS overestimation for UVI retrievals due to the underestimation
542 of the cloudiness just above the stations. These data illustrate the well-known spatial representativeness issues whereby a COT
543 value for a satellite grid is not fully representative of a point measurement station. In addition, absolute and percentage relative
544 differences are shown in Fig. 15 (c) and (d) respectively for SZA up to 65 degrees. The differences between the UVIOS and
545 the ground-based UVI decreases in absolute level but increases in percent with an increase in SZA. This is due to the decrease
546 of UVI with increasing SZA. Modelled and the measured UVI difference is close to zero both for mean and median values.
547 For SZA below 30 degrees, differences are 0 to -0.2, while 20 to 80 percentiles range from -0.6 to -0.2. Percentage difference
548 increases with SZA as absolute UVI decreases with the 20 to 80 percentiles showing differences between -10% and 10%.

549 54. Summary and conclusions and future plans

550 In this study, a fast RTM model of UVI, the so-called UVIOS, using inputs of the SZA, aerosol optical depth, total ozone
551 column, cloud optical depth, elevation and surface albedo that implicitly includes temporal effects and the effect of cloud and
552 aerosol physics, allows for the generation of high-resolution maps of UVI. Ground based measurements of UV are the most
553 accurate way to determine this important health related parameter. However, such stations are sparse and hence, satellite
554 observations can be used in order to have a nowcasted UV service. To date, polar orbiting satellites like TOMS, OMI and
555 recently TROPOMI provided a global UV dataset with a major disadvantage being the temporal resolution (one measurement
556 per day). This, combined with the large temporal variability of clouds can lead to huge deviations from reality when a single
557 daily measurement is included. Geostationary satellite, MSG, have been used in order to try to improve on such limitations
558 using cloud information every 15 minutes.

559 Comparison of the forecasted and the ground-based measurements indicated that at least 70% and 80% of comparisons were
560 within 0.5 UVI difference for all sky condition and clear sky, respectively. The mean differences between TEMIS TOC and
561 the ground measured TOC from the WOUDC for one year of comparison data showed that TEMIS tends to slightly
562 overestimate the TOC for some stations along with underestimating it for other stations. While, in general, in most of the cases
563 UVI mean differences are less than 0.1, the TOC differences have a larger impact in percent UVI differences at higher SZAs.
564 Such small differences can also be the result of daily TOC variation not captured in TEMIS.

565 CAMS AOD seems to be slightly overestimated as compared with AERONET data that leads to a UVIOS underestimation.
566 CAMS data are found to overestimate the AOD from AERONET measurements with a mean difference of 0.07 at 500 nm.
567 All the stations have a mean positive bias up to 0.071 except one station that had a mean negative bias of 0.007. The analysis
568 of the impact of the mean bias error of the CAMS – AERONET AOD impact on UVI for all stations showed that the mean
569 bias decreases with an increase in the SZA as the values of UVI also decreases with SZA. The greatest deviation is for station
570 VIE which is consistent with the poor correlation between the CAMS forecasted input and the measurements for this station.
571 The real time data provision approach of UVIOS requires using a maximum of one-day ozone and aerosol forecast using the
572 TEMIS and CAMS service respectively. Uncertainties in the used SSA increase the overall uncertainty of the simulated UVI,
573 especially for high levels of atmospheric aerosols. However, as systematic SSA measurements in the UV region are not
574 available, quantification of these uncertainties were not possible.

575 Cloudy conditions show high percentage differences but low UVI differences, and have a general tendency to lead to a UVIOS
576 overestimation. It was found that 45.4% of cases have underestimations while 54.6% cases have overestimations for the
577 cloudless conditions, while overestimations (62.5%) were more predominant than underestimations (37.5%) for all the other
578 cases. In general, UVIOS showed an overestimation for UVI in contrast to the ground measurements under cloudy conditions
579 with the difference in the modeled and the measured values going beyond ± 1 for 5.1% cases for cloudless conditions and
580 14.7% for all other cases. At individual stations the results for cloudless sky conditions, which are the most important for
581 health related issues, showed good agreement. In general, ~85% of all and 95% of cloudless cases are within 1 UVI difference.

582 The relative percentage biases can be large for low UVI cases due to clouds or at high SZAs, above 75°, due to the absence of
583 accurate information for clouds. The results show that there is a general tendency of small underestimation of MSG COT that
584 leads to a systematic but small UVIOS overestimation under cloudy conditions. Another possible explanation is the spatial
585 representativeness issues between a satellite and a single point on the ground.

586 Using climatological surface albedo has little impact at low albedo sites but mainly leads to underestimations in UVIOS
587 simulations for high albedo situations (snow cover). Most of the percentage difference between forecasted and the measured
588 UVI values varied from -30% to 10% for SZA between 20° to 70° (climate albedo), while it was found to vary from -20% to
589 10% for dynamically changing albedo. Since high surface albedo conditions correspond to winter months (i.e. high SZAs and
590 relatively low UVI) for the stations used in the study, the corresponding absolute differences in the UVI are generally smaller
591 than 2 UVI. However, there was a huge variation in the percentage difference beyond 70 degree SZA with mostly
592 underestimations from the UVIOS simulations. Finally, for uncertainties in elevation inputs, the UVI percentage difference is
593 found to increase almost linearly with the increase in elevation for a particular total ozone column and beyond that, it is seen
594 that the rate of increase in the percentage difference decreases with increase in the total ozone column.

595 UVIOS system forms a novel tool for widespread estimations of UVI using real-time and forecasted EO inputs. UVIOS utilizes
596 the MSG domain with high spatiotemporal resolution, producing outputs within acceptable limits of accuracy for UV health
597 related applications. It captures basic cloud features and all major atmospheric and geospatial parameters that affect UVI.
598 Under cloudless conditions it performs to within the uncertainty of the ground based measurements to which it has been
599 compared. Further development and improvement of the model can be achieved in the future. Meteosat Third Generation
600 (MTG) satellites are expected to be launched in the following years and give aerosol and cloud products which would improve
601 the performance of nowcast and forecast UV models when used as inputs. A future goal is to compare the UVIOS accuracy
602 under cloudy conditions by using, (i) the current MSG cloud information (5 km, 15 min), (ii) the ECMWF forecast cloud
603 information (4 km, 1 hour) and (iii) the forthcoming MTG cloud information (500m, 5 min), in order to quantify the
604 uncertainties of the forecasted cloud data as compared to the satellite observations, as well as the overall improvement of the
605 MTG data compared to the MSG due to the MTG's higher resolution.

606 The future plans with the UVIOS system include open access to the operational UVI product through European online map-
607 based user interfaces, data hubs and cloud platforms for Earth Observation data (e.g. GEOSS Portal and NextGEOSS). A real-
608 time correction and quality assurance of the outputs is also scheduled by assimilating ground measurements in collaboration
609 with the stations used in this study. In addition, the short-term and long-term forecasting horizons will be exploited for further
610 added value as an early warning system that raises awareness among citizens of the health implications of high UVI doses. To
611 this direction, numerical weather prediction models and computer vision techniques (Kosmopoulos et al., 2020) will be utilized
612 as complements to the UVIOS system in order to capture the cloud movement forecast and effect on the UVI levels. Finally,
613 a historical database of UVI will be developed by using climatological input data sources for past years aiming to study climatic
614 trends and to make the system a holistic platform for scientific and social value deployment.

615

616 **Author contribution**

617 PGK was responsible for the design of the study and the whole analysis, with support from SK, AWS, PIR, KP, IF, AM and
618 J-G. PGK and SK are the developers of UVIOS. All authors contributed to editing the paper.

619 **Code/Data availability**

620 All data used as inputs to the UVIOS system are open access, while all data sets produced by the UVIOS for the purposes of
621 this paper can be requested from the corresponding author. The ground-based measurements can be requested from the PIs of
622 the stations. The UVIOS suite of algorithms and LUTs can be used for various applications after consultation with the
623 corresponding author.

624 **Competing interests**

625 The authors declare that they have no conflict of interest.

626 **Acknowledgements**

627 We acknowledge the Eumetsat SAFNWC, the Copernicus and TEMIS services as well as the Aerocom and GOME teams for
628 providing all the necessary data used in this study. We would like to thank the 17 site instrument operators and technical staff
629 that made the ground based measurements feasible.

630 **Financial support**

631 The UVIOS development received no specific grant from any funding agency in the public, commercial, or not-for-profit
632 sectors. The evaluation part of this study has been partly funded by the European Commission project EuroGEO e-shape (grant
633 agreement No 820852).

634 **References**

635 Andrady, A.L., Aucamp, P.J., Austin, A.T., Bais, A.F., Ballare, C.L., Barnes, P.W., Bernhard, G.H., Bornman, J.F., Caldwell,
636 M.M., de Grijl, F.R., and Erickson, D.J.: Environmental effects of ozone depletion and its interactions with climate change:
637 2014 assessment executive summary. Photochemical and Photobiological Sciences 14(1), 14-18, 10.1039/c4pp90042a, 2015.

- 638 Arola, A., Kazadzis, S., Lindfors, A., Krotkov, N., Kujanpää, J., Tamminen, J., Bais, A., di Sarra, A., Villaplana, J. M.,
639 Brogniez, C., Siani, A. M., Janouch, M., Weihs, P., Webb, A., Koskela, T., Kouremeti, N., Meloni, D., Buchard, V., Auriol,
640 F., Ialongo, I., Staneck, M., Simic, S., Smedley, A., and Kinne, S.: A new approach to correct for absorbing aerosols in OMI
641 UV, *Geophysical Research Letters*, 36, 10.1029/2009gl041137, 2009.
- 642 Badosa, J., and Van Weele, M.: Effects of aerosols on UV-index, KNMI Scientific Report WR-2002-07, 2002.
- 643 Badosa, J., Calbó, J., McKenzie, R., Liley, B., González, J.-A., Forgan, B., and Long, C. N.: Two Methods for Retrieving UV
644 Index for All Cloud Conditions from Sky Imager Products or Total SW Radiation Measurements, *Photochemistry and*
645 *Photobiology*, 90, 941-951, <https://doi.org/10.1111/php.12272>, 2014.
- 646 Bais, A. F., Zerefos, C. S., Meleti, C., Ziomas, I. C., and Tourpali, K.: Spectral measurements of solar UVB radiation and its
647 relations to total ozone, SO₂, and clouds, *Journal of Geophysical Research: Atmospheres*, 98, 5199-5204, 10.1029/92jd02904,
648 1993.
- 649 Bais, A. F., Lucas, R. M., Bornman, J. F., Williamson, C. E., Sulzberger, B., Austin, A. T., Wilson, S. R., Andrady, A. L.,
650 Bernhard, G., McKenzie, R. L., Aucamp, P. J., Madronich, S., Neale, R. E., Yazar, S., Young, A. R., de Gruijl, F. R., Norval,
651 M., Takizawa, Y., Barnes, P. W., Robson, T. M., Robinson, S. A., Ballaré, C. L., Flint, S. D., Neale, P. J., Hylander, S., Rose,
652 K. C., Wängberg, S. Å., Häder, D. P., Worrest, R. C., Zepp, R. G., Paul, N. D., Cory, R. M., Solomon, K. R., Longstreth, J.,
653 Pandey, K. K., Redhwi, H. H., Torikai, A., and Heikkilä, A. M.: Environmental effects of ozone depletion, UV radiation and
654 interactions with climate change: UNEP Environmental Effects Assessment Panel, update 2017, *Photochemical &*
655 *Photobiological Sciences*, 17, 127-179, 10.1039/c7pp90043k, 2018.
- 656 Bais, A. F., Bernhard, G., McKenzie, R. L., Aucamp, P. J., Young, P. J., Ilyas, M., Jöckel, P., and Deushi, M.: Ozone–climate
657 interactions and effects on solar ultraviolet radiation, *Photochemical & Photobiological Sciences*, 18, 602-640,
658 10.1039/c8pp90059k, 2019.
- 659 ~~Bernhard, G.: Trends of solar ultraviolet irradiance at Barrow, Alaska, and the effect of measurement uncertainties on trend~~
660 ~~detection, *Atmos. Chem. Phys.*, 11, 13029–13045, 10.5194/acp-11-13029-2011, 2011.~~
- 661 Bernhard, G., and Stierle, S.: Trends of UV Radiation in Antarctica, *Atmosphere*, 11, 10.3390/atmos11080795, 2020.
- 662 Bieliński, T.: A Parallax Shift Effect Correction Based on Cloud Height for Geostationary Satellites and Radar Observations,
663 *Remote Sensing*, 12, 10.3390/rs12030365, 2020.
- 664 Blumthaler, M., and Ambach, W.: SOLAR UVB-ALBEDO OF VARIOUS SURFACES, *Photochemistry and Photobiology*,
665 48, 85-88, <https://doi.org/10.1111/j.1751-1097.1988.tb02790.x>, 1988.
- 666 Blumthaler, M., Ambach, W., and Ellinger, R.: Increase in solar UV radiation with altitude, *Journal of Photochemistry and*
667 *Photobiology B: Biology*, 39, 130-134, [https://doi.org/10.1016/S1011-1344\(96\)00018-8](https://doi.org/10.1016/S1011-1344(96)00018-8), 1997.
- 668 Boynard, A., Hurtmans, D., Garane, K., Goutail, F., Hadji-Lazaro, J., Koukouli, M. E., Wespes, C., Vigouroux, C., Keppens,
669 A., Pommereau, J. P., Pazmino, A., Balis, D., Loyola, D., Valks, P., Sussmann, R., Smale, D., Coheur, P. F., and Clerbaux,
670 C.: Validation of the IASI FORLI/EUMETSAT ozone products using satellite (GOME-2), ground-based (Brewer–Dobson,
671 SAOZ, FTIR) and ozonesonde measurements, *Atmos. Meas. Tech.*, 11, 5125-5152, 10.5194/amt-11-5125-2018, 2018.
- 672 Carrer, D., Roujean, J.-L., and Meurey, C.: Comparing Operational MSG/SEVIRI Land Surface Albedo Products From Land
673 SAF With Ground Measurements and MODIS, *IEEE Transactions on Geoscience and Remote Sensing*, 48, 1714-1728,
674 10.1109/TGRS.2009.2034530, 2010.

675 Cede, A., Herman, J., Richter, A., Krotkov, N., and Burrows, J.: Measurements of nitrogen dioxide total column amounts using
676 a Brewer double spectrophotometer in direct Sun mode, *Journal of Geophysical Research: Atmospheres*, 111,
677 <https://doi.org/10.1029/2005JD006585>, 2006.

678 Chubarova, N., Zhdanova, Y., and Nezval, Y.: A new parameterization of the UV irradiance altitude dependence for clear-sky
679 conditions and its application in the on-line UV tool over Northern Eurasia. *Atmos. Chem. Phys.*, 16, 11867-11881,
680 [10.5194/acp-16-11867-2016](https://doi.org/10.5194/acp-16-11867-2016), 2016.

681 Chubarova, N.E., Pastukhova, A.S., Zhdanova, E.Y., Volpert, E.V., Smyshlyaev, S.P., and Galin, V.Y.: Effects of ozone and
682 clouds on temporal variability of surface UV radiation and UV resources over Northern Eurasia derived from measurements
683 and modeling. *Atmosphere*, 11(1), 59, [10.3390/atmos11010059](https://doi.org/10.3390/atmos11010059), 2020.

684 Corr, C. A., Krotkov, N., Madronich, S., Slusser, J. R., Holben, B., Gao, W., Flynn, J., Lefer, B., and Kreidenweis, S. M.:
685 Retrieval of aerosol single scattering albedo at ultraviolet wavelengths at the T1 site during MILAGRO, *Atmos. Chem. Phys.*,
686 9, 5813-5827, [10.5194/acp-9-5813-2009](https://doi.org/10.5194/acp-9-5813-2009), 2009.

687 Czerwińska, A. E., Krzyścin, J. W., Jarosławski, J., and Posyniak, M.: Effects of urban agglomeration on surface-UV doses: a
688 comparison of Brewer measurements in Warsaw and Belsk, Poland, for the period 2013–2015, *Atmos. Chem. Phys.*, 16,
689 [13641-13651](https://doi.org/10.5194/acp-16-13641-2016), [10.5194/acp-16-13641-2016](https://doi.org/10.5194/acp-16-13641-2016), 2016.

690 Dahlback, A.: Dahlback, Measurements of biologically effective UV doses, total ozone abundances, and cloud effects with
691 multichannel, moderate bandwidth filter instruments, *Appl. Opt. Vol. 35, No. 33*, 1996. Further references, see. Eg. Bernhard
692 et al, Johnsen et al. *JGR*, 2008, *Applied Optics*, 35, 6514 - 6521, [10.1364/AO.35.006514](https://doi.org/10.1364/AO.35.006514), 1996.

693 De Bock, V., De Backer, H., Van Malderen, R., Mangold, A., and Delcloo, A.: Relations between erythemal UV dose, global
694 solar radiation, total ozone column and aerosol optical depth at Uccle, Belgium, *Atmos. Chem. Phys.*, 14, 12251-12270,
695 [10.5194/acp-14-12251-2014](https://doi.org/10.5194/acp-14-12251-2014), 2014.

696 Derrien, M., and Le Gléau, H.: MSG/SEVIRI cloud mask and type from SAFNWC, *International Journal of Remote Sensing*,
697 26, 4707-4732, [10.1080/01431160500166128](https://doi.org/10.1080/01431160500166128), 2005.

698 Eleftheratos, K., Kazadzis, S., Zerefos, C. S., Tourpali, K., Meleti, C., Balis, D., Zyrichidou, I., Lakkala, K., Feister, U.,
699 Koskela, T., Heikkilä, A., and Karhu, J. M.: Ozone and Spectroradiometric UV Changes in the Past 20 Years over High
700 Latitudes, *Atmosphere-Ocean*, 53, 117-125, [10.1080/07055900.2014.919897](https://doi.org/10.1080/07055900.2014.919897), 2015.

701 Eskes, H., Huijnen, V., Arola, A., Benedictow, A., Blechschmidt, A. M., Botek, E., Boucher, O., Bouarar, I., Chabrillat, S.,
702 Cuevas, E., Engelen, R., Flentje, H., Gaudel, A., Griesfeller, J., Jones, L., Kapsomenakis, J., Katragkou, E., Kinne, S.,
703 Langerock, B., Razingar, M., Richter, A., Schultz, M., Schulz, M., Sudarchikova, N., Thouret, V., Vrekoussis, M., Wagner,
704 A., and Zerefos, C.: Validation of reactive gases and aerosols in the MACC global analysis and forecast system, *Geosci. Model*
705 *Dev.*, 8, 3523-3543, [10.5194/gmd-8-3523-2015](https://doi.org/10.5194/gmd-8-3523-2015), 2015.

706 Eskes, H. J., Velthoven, P. F. J. V., Valks, P. J. M., and Kelder, H. M.: Assimilation of GOME total-ozone satellite observations
707 in a three-dimensional tracer-transport model, *Quarterly Journal of the Royal Meteorological Society*, 129, 1663-1681,
708 <https://doi.org/10.1256/qj.02.14>, 2003.

709 Eskes, H. J., Wagner, A., Schulz, M., Christophe, Y., Ramonet, M., Basart, S., Benedictow, A., Bennouna, Y., Blechschmidt,
710 A.-M., Chabrillat, S., Clark, H., Cuevas, E., Flentje, H., Hansen, K. M., IM, U., Kapsomenakis, J., Langerock, B., Petersen,
711 K., Richter, A., Sudarchikova, N., Thouret, V., Warneke, T., and Zerefos, C.: Validation report of the cams near-real-time
712 global atmospheric composition service: period September-November 2017., *Copernicus Atmosphere Monitoring Service*
713 (CAMS) Report, [CAMS84_2015SC3_D84.1.1.10_2017SON_V1.pdf](https://doi.org/10.5194/cams84_2015SC3_D84.1.1.10_2017SON_V1.pdf), February 2018., 2018.

- 714 Feister, U., and Grewe, R.: SPECTRAL ALBEDO MEASUREMENTS IN THE UV and VISIBLE REGION OVER
715 DIFFERENT TYPES OF SURFACES, *Photochemistry and Photobiology*, 62, 736-744, <https://doi.org/10.1111/j.1751-1097.1995.tb08723.x>, 1995.
- 717 Fioletov, V., Kerr, J. B., and Fergusson, A.: The UV Index: Definition, Distribution and Factors Affecting It, *Canadian Journal of Public Health*, 101, I5-I9, 10.1007/bf03405303, 2010.
- 719 Fioletov, V. E., Kerr, J. B., McArthur, L. J. B., Wardle, D. I., and Mathews, T. W.: Estimating UV Index Climatology over
720 Canada, *Journal of Applied Meteorology and Climatology*, 42, 417-433, 10.1175/1520-0450(2003)042<0417:EUIOC>2.0.CO;2, 2003.
- 722 Fioletov, V. E., McArthur, L. J. B., Mathews, T. W., and Marrett, L.: On the relationship between erythemal and vitamin D
723 action spectrum weighted ultraviolet radiation, *Journal of Photochemistry and Photobiology B: Biology*, 95, 9-16,
724 <https://doi.org/10.1016/j.jphotobiol.2008.11.014>, 2009.
- 725 Fioletov, V.E., Griffioen, E., Kerr, J.B., Wardle, D.I., and Uchino, O.: Influence of volcanic sulfur dioxide on spectral UV
726 irradiance as measured by Brewer spectrophotometers. *Geophysical Research Letters*, 25(10), 1665-1668, 1998.
- 727 Fountoulakis, I., Bais, A. F., Fragkos, K., Meleti, C., Tourpali, K., and Zempila, M. M.: Short- and long-term variability of
728 spectral solar UV irradiance at Thessaloniki, Greece: effects of changes in aerosols, total ozone and clouds, *Atmos. Chem. Phys.*, 16, 2493-2505, 10.5194/acp-16-2493-2016, 2016.
- 730 Fountoulakis, I., Zerefos, C. S., Bais, A. F., Kapsomenakis, J., Koukouli, M.-E., Ohkawara, N., Fioletov, V., De Backer, H.,
731 Lakkala, K., Karppinen, T., and Webb, A. R.: Twenty-five years of spectral UV-B measurements over Canada, Europe and
732 Japan: Trends and effects from changes in ozone, aerosols, clouds, and surface reflectivity, *Comptes Rendus Geoscience*, 350,
733 393-402, <https://doi.org/10.1016/j.crte.2018.07.011>, 2018.
- 734 Fountoulakis, I., Natsis, A., Siomos, N., Drosoglou, T., and Bais, F. A.: Deriving Aerosol Absorption Properties from Solar
735 Ultraviolet Radiation Spectral Measurements at Thessaloniki, Greece, *Remote Sensing*, 11, 10.3390/rs11182179, 2019.
- 736 Fountoulakis, I., Diémoz, H., Siani, A.-M., Laschewski, G., Filippa, G., Arola, A., Bais, A. F., De Backer, H., Lakkala, K.,
737 Webb, A. R., De Bock, V., Karppinen, T., Garane, K., Kapsomenakis, J., Koukouli, M.-E., and Zerefos, C. S.: Solar UV
738 Irradiance in a Changing Climate: Trends in Europe and the Significance of Spectral Monitoring in Italy, *Environments*, 7,
739 10.3390/environments7010001, 2020a.
- 740 Fountoulakis, I., Diémoz, H., Siani, A. M., Hülsen, G., and Gröbner, J.: Monitoring of solar spectral ultraviolet irradiance in
741 Aosta, Italy, *Earth Syst. Sci. Data*, 12, 2787-2810, 10.5194/essd-12-2787-2020, 2020b.
- 742 Gal, S.: Computing elementary functions: A new approach for achieving high accuracy and good performance, *Accurate Scientific Computations*, Berlin, Heidelberg, 1986, 1-16,
- 744 Garane, K., Bais, A. F., Kazadzis, S., Kazantzidis, A., and Meleti, C.: Monitoring of UV spectral irradiance at Thessaloniki
745 (1990–2005): data re-evaluation and quality control, *Ann. Geophys.*, 24, 3215-3228, 10.5194/angeo-24-3215-2006,
746 2006.
- 747 Garane, K., Lerot, C., Coldewey-Egbers, M., Verhoelst, T., Koukouli, M. E., Zyrichidou, I., Balis, D. S., Danckaert, T.,
748 Goutail, F., Granville, J., Hubert, D., Keppens, A., Lambert, J. C., Loyola, D., Pommereau, J. P., Van Roozendael, M., and
749 Zehner, C.: Quality assessment of the Ozone_cci Climate Research Data Package (release 2017) – Part 1: Ground-based
750 validation of total ozone column data products, *Atmos. Meas. Tech.*, 11, 1385-1402, 10.5194/amt-11-1385-2018, 2018.

- 751 Garane, K., Koukouli, M. E., Verhoelst, T., Lerot, C., Heue, K. P., Fioletov, V., Balis, D., Bais, A., Bazureau, A., Dehn, A.,
752 Goutail, F., Granville, J., Griffin, D., Hubert, D., Keppens, A., Lambert, J. C., Loyola, D., McLinden, C., Pazmino, A.,
753 Pommereau, J. P., Redondas, A., Romahn, F., Valks, P., Van Roozendael, M., Xu, J., Zehner, C., Zerefos, C., and Zimmer,
754 W.: TROPOMI/S5P total ozone column data: global ground-based validation and consistency with other satellite missions,
755 *Atmos. Meas. Tech.*, 12, 5263-5287, 10.5194/amt-12-5263-2019, 2019.
- 756 Giles, D. M., Sinyuk, A., Sorokin, M. G., Schafer, J. S., Smirnov, A., Slutsker, I., Eck, T. F., Holben, B. N., Lewis, J. R.,
757 Campbell, J. R., Welton, E. J., Korkin, S. V., and Lyapustin, A. I.: Advancements in the Aerosol Robotic
758 Network (AERONET) Version 3 database – automated near-real-time quality control algorithm with improved cloud
759 screening for Sun photometer aerosol optical depth (AOD) measurements, *Atmos. Meas. Tech.*, 12, 169-209, 10.5194/amt-12-
760 169-2019, 2019.
- 761 Gratien, A., Nilsson, E., Doussin, J.F., Johnson, M.S., Nielsen, C.J., Stenstrøm, Y., and Picquet-Varrault, B.: UV and IR
762 absorption cross-sections of HCHO, HCDO, and DCDO. *The journal of Physical Chemistry, A*, 111(45), 11506-11513, 2007.
- 763 Gröbner, J., Schreder, J., Kazadzis, S., Bais, A. F., Blumthaler, M., Görts, P., Tax, R., Koskela, T., Seckmeyer, G., Webb, A.
764 R., and Rembges, D.: Traveling reference spectroradiometer for routine quality assurance of spectral solar ultraviolet irradiance
765 measurements, *Applied Optics*, 44, 5321-5331, 10.1364/ao.44.005321, 2005.
- 766 Gröbner, J., and Sperfeld, P.: Direct traceability of the portable QASUME irradiance scale to the primary irradiance standard
767 of the PTB, *Metrologia*, 42, 134-139, 10.1088/0026-1394/42/2/008, 2005.
- 768 Gröbner, J., Kröger, I., Egli, L., Hülsen, G., Riechelmann, S., and Sperfeld, P.: The high-resolution extraterrestrial solar
769 spectrum (QASUMEFTS) determined from ground-based solar irradiance measurements, *Atmos. Meas. Tech.*, 10, 3375-3383,
770 10.5194/amt-10-3375-2017, 2017.
- 771 Gröbner, J.: Example datasets from PMOD/WRC Davos, Switzerland with the double Brewer B163 and QASUME II
772 compared with the UVIOS model. *Atmos. Meas. Tech. (supplement comment)*, 10.5194/amt-2020506-CC1, 2021.
- 773 Heikkilä, A., Kaurola, J., Lakkala, K., Karhu, J. M., Kyrö, E., Koskela, T., Engelsen, O., Slaper, H., and Seckmeyer, G.:
774 European UV DataBase (EUVDB) as a repository and quality analyser for solar spectral UV irradiance monitored in
775 Sodankylä, *Geosci. Instrum. Method. Data Syst.*, 5, 333-345, 10.5194/gi-5-333-2016, 2016.
- 776 Henderson-Sellers, A., and Wilson, M. F.: Surface albedo data for climatic modeling, *Reviews of Geophysics*, 21, 1743-1778,
777 <https://doi.org/10.1029/RG021i008p01743>, 1983.
- 778 Henken, C. C., Schmeits, M. J., Deneke, H., and Roebeling, R. A.: Using MSG-SEVIRI Cloud Physical Properties and Weather
779 Radar Observations for the Detection of Cb/TCu Clouds, *Journal of Applied Meteorology and Climatology*, 50, 1587-1600,
780 2011.
- 781 Herman, J. R.: Global increase in UV irradiance during the past 30 years (1979–2008) estimated from satellite data, *Journal*
782 *of Geophysical Research: Atmospheres*, 115, 10.1029/2009jd012219, 2010.
- 783 Holick, M. F.: Vitamin D: the underappreciated D-lightful hormone that is important for skeletal and cellular health, *Current*
784 *Opinion in Endocrinology, Diabetes and Obesity*, 9, 2002.
- 785 Hülsen, G., Gröbner, J., Bais, A., Blumthaler, M., Disterhoft, P., Johnsen, B., Lantz, K. O., Meleti, C., Schreder, J., Vilaplana
786 Guerrero, J. M., and Ylianttila, L.: Intercomparison of erythral broadband radiometers calibrated by seven UV calibration
787 facilities in Europe and the USA, *Atmos. Chem. Phys.*, 8, 4865-4875, 10.5194/acp-8-4865-2008, 2008.

- 788 Hülsen, G., Gröbner, J., Nevas, S., Sperfeld, P., Egli, L., Porrovecchio, G., and Smid, M.: Traceability of solar UV
789 measurements using the Qasume reference spectroradiometer, *Applied Optics*, 55, 7265 - 7275, 10.1364/AO.55.007265, 2016.
- 790 Hülsen, G., Gröbner, J., Bais, A., Blumthaler, M., Diemoz, H., Bolsee, D., Rodríguez, A. D., Fountoulakis, I., Naranen, E.,
791 Schreder, J., Stefania, F., and Vilaplana Guerrero, J. M.: Second solar ultraviolet radiometer comparison campaign UVC-II,
792 *Metrologia*, 2020.
- 793 [Johnsen B., Kjeldstad B., Aalerud T.N., Nilsen L.T., Schreder J., Blumthaler M., Bernhard G., Topaloglou C., Meinander O.,](#)
794 [Bagheri A., Slusser J.R. and Davis J.: Intercomparison and harmonization of UV index measurements from multiband filter](#)
795 [radiometers, *J. Geophys. Res.* 113, D15206. doi:10.1029/2007JD009731, 2008.](#)
- 796 Juzeniene, A., Brekke, P., Dahlback, A., Andersson-Engels, S., Reichrath, J., Moan, K., Holick, M. F., Grant, W. B., and
797 Moan, J.: Solar radiation and human health, *Reports on Progress in Physics*, 74, 066701, 10.1088/0034-4885/74/6/066701,
798 2011.
- 799 Kato, S., and Marshak, A.: Solar zenith and viewing geometry-dependent errors in satellite retrieved cloud optical thickness:
800 Marine stratocumulus case. *Journal of Geophysical Research*, 114, D01202, 10.1029/2008JD010579, 2009.
- 801 Kazadzis, S., Bais, A., Balis, D., Kouremeti, N., Zempila, M., Arola, A., Giannakaki, E., Amiridis, V., and Kazantzidis, A.:
802 Spatial and temporal UV irradiance and aerosol variability within the area of an OMI satellite pixel, *Atmos. Chem. Phys.*, 9,
803 4593-4601, 10.5194/acp-9-4593-2009, 2009a.
- 804 Kazadzis, S., Kouremeti, N., Bais, A., Kazantzidis, A., and Meleti, C.: Aerosol forcing efficiency in the UVA region from
805 spectral solar irradiance measurements at an urban environment, *Ann. Geophys.*, 27, 2515-2522, 10.5194/angeo-27-2515-
806 2009, 2009b.
- 807 Kazadzis, S., Raptis, P., Kouremeti, N., Amiridis, V., Arola, A., Gerasopoulos, E., and Schuster, G. L.: Aerosol absorption
808 retrieval at ultraviolet wavelengths in a complex environment, *Atmos. Meas. Tech.*, 9, 5997-6011, 10.5194/amt-9-5997-2016,
809 2016.
- 810 Kerr, J. B., Evans, W. F. J., and Asbridge, I. A.: Recalibration of Dobson Field Spectrophotometers with a Travelling Brewer
811 Spectrophotometer Standard, *Atmospheric Ozone*, Dordrecht, 1985, 381-386,
- 812 Kerr, J. B., and Fioletov, V. E.: Surface ultraviolet radiation, *Atmosphere-Ocean*, 46, 159-184, 10.3137/ao.460108, 2008.
- 813 Kinne, S.: The MACv2 aerosol climatology, *Tellus B: Chemical and Physical Meteorology*, 71, 1-21,
814 10.1080/16000889.2019.1623639, 2019.
- 815 Koren, I., Remer, L. A., Kaufman, Y. J., Rudich, Y., and Martins, J. V.: On the twilight zone between clouds and aerosols,
816 *Geophysical Research Letters*, 34, <https://doi.org/10.1029/2007GL029253>, 2007.
- 817 Kosmopoulos, P. G., Kazadzis, S., Taylor, M., Raptis, P. I., Keramitsoglou, I., Kiranoudis, C., and Bais, A. F.: Assessment of
818 surface solar irradiance derived from real-time modelling techniques and verification with ground-based measurements,
819 *Atmos. Meas. Tech.*, 11, 907-924, 10.5194/amt-11-907-2018, 2018.
- 820 [Kosmopoulos, P.G., Kouroutsidis, D., Papachristopoulou, K., Raptis, P.I., Masoom, A., Saint-Drenan, Y-M., Blanc, P.,](#)
821 [Kontoes, C. and Kazadzis, S.: Short-Term Forecasting of Large-Scale Clouds Impact on Downwelling Surface Solar](#)
822 [Irradiation. *Energies*, 13\(24\), 6555. <https://doi.org/10.3390/en13246555>, 2020.](#)

- 823 Kreuter, A., Buras, R., Mayer, B., Webb, A., Kift, R., Bais, A., Kouremeti, N., and Blumthaler, M.: Solar irradiance in the
824 heterogeneous albedo environment of the Arctic coast: measurements and a 3-D model study, *Atmos. Chem. Phys.*, 14, 5989-
825 6002, 10.5194/acp-14-5989-2014, 2014.
- 826 Krotkov, N. A., Bhartia, P. K., Herman, J. R., Fioletov, V., and Kerr, J.: Satellite estimation of spectral surface UV irradiance
827 in the presence of tropospheric aerosols: 1. Cloud-free case, *Journal of Geophysical Research: Atmospheres*, 103, 8779-8793,
828 <https://doi.org/10.1029/98JD00233>, 1998.
- 829 Lacaze, R., Smets, B., Trigo, I., Calvet, J.C., Jann, A., Camacho, F., Baret, F., Kidd, R., Defourny, P., Tansey, K., et al.: The
830 Copernicus Global Land Service: Present and future. In *Proceedings of the EGU General Assembly*, Vienna, Austria, 7-12
831 April, 2013.
- 832 Lakkala, K., Arola, A., Heikkilä, A., Kaurola, J., Koskela, T., Kyrö, E., Lindfors, A., Meinander, O., Tanskanen, A., Gröbner,
833 J., and Hülsen, G.: Quality assurance of the Brewer spectral UV measurements in Finland, *Atmos. Chem. Phys.*, 8, 3369-3383,
834 10.5194/acp-8-3369-2008, 2008.
- 835 Lakkala, K., Redondas, A., Meinander, O., Thölix, L., Hamari, B., Almansa, A. F., Carreno, V., García, R. D., Torres, C.,
836 Deferrari, G., Ochoa, H., Bernhard, G., Sanchez, R., and de Leeuw, G.: UV measurements at Marambio and Ushuaia during
837 2000–2010, *Atmos. Chem. Phys.*, 18, 16019-16031, 10.5194/acp-18-16019-2018, 2018.
- 838 Lakkala, K., Kujanpää, J., Brogniez, C., Henriot, N., Arola, A., Aun, M., Auriol, F., Bais, A. F., Bernhard, G., De Bock, V.,
839 Catalfamo, M., Deroo, C., Diémoz, H., Egli, L., Forestier, J. B., Fountoulakis, I., Garcia, R. D., Gröbner, J., Hassinen, S.,
840 Heikkilä, A., Henderson, S., Hülsen, G., Johnsen, B., Kalakoski, N., Karanikolas, A., Karppinen, T., Lamy, K., León-Luis, S.
841 F., Lindfors, A. V., Metzger, J. M., Minvielle, F., Muskatel, H. B., Portafaix, T., Redondas, A., Sanchez, R., Siani, A. M.,
842 Svendby, T., and Tamminen, J.: Validation of TROPOMI Surface UV Radiation Product, *Atmos. Meas. Tech. Discuss.*, 2020,
843 1-37, 10.5194/amt-2020-121, 2020.
- 844 Larkin, A., Haigh, J. D., and Djavidnia, S.: The Effect of Solar UV Irradiance Variations on the Earth's Atmosphere, *Space*
845 *Science Reviews*, 94, 199-214, 10.1023/a:1026771307057, 2000.
- 846 Levelt, P. F., Oord, G. H. J. v. d., Dobber, M. R., Malkki, A., Huib, V., Johan de, V., Stammes, P., Lundell, J. O. V., and Saari,
847 H.: The ozone monitoring instrument, *IEEE Transactions on Geoscience and Remote Sensing*, 44, 1093-1101,
848 10.1109/tgrs.2006.872333, 2006.
- 849 Levelt, P. F., Joiner, J., Tamminen, J., Veefkind, J. P., Bhartia, P. K., Stein Zweers, D. C., Duncan, B. N., Streets, D. G., Eskes,
850 H., van der A, R., McLinden, C., Fioletov, V., Carn, S., de Laat, J., DeLand, M., Marchenko, S., McPeters, R., Ziemke, J., Fu,
851 D., Liu, X., Pickering, K., Apituley, A., González Abad, G., Arola, A., Boersma, F., Chan Miller, C., Chance, K., de Graaf,
852 M., Hakkarainen, J., Hassinen, S., Ialongo, I., Kleipool, Q., Krotkov, N., Li, C., Lamsal, L., Newman, P., Nowlan, C.,
853 Suleiman, R., Tilstra, L. G., Torres, O., Wang, H., and Wargan, K.: The Ozone Monitoring Instrument: overview of 14 years
854 in space, *Atmos. Chem. Phys.*, 18, 5699-5745, 10.5194/acp-18-5699-2018, 2018.
- 855 López-Solano, J., Redondas, A., Carlund, T., Rodríguez-Franco, J. J., Diémoz, H., León-Luis, S. F., Hernández-Cruz, B.,
856 Guirado-Fuentes, C., Kouremeti, N., Gröbner, J., Kazadzis, S., Carreño, V., Berjón, A., Santana-Díaz, D., Rodríguez-Valido,
857 M., De Bock, V., Moreta, J. R., Rimmer, J., Smedley, A. R. D., Boulkelia, L., Jepsen, N., Eriksen, P., Bais, A. F., Shirovov,
858 V., Vilaplana, J. M., Wilson, K. M., and Karppinen, T.: Aerosol optical depth in the European Brewer Network, *Atmos. Chem.*
859 *Phys.*, 18, 3885-3902, 10.5194/acp-18-3885-2018, 2018.
- 860 Lucas, R., McMichael, T., Smith, W., Armstrong, B. K., Prüss-Üstün, A., and World Health, O.: Solar ultraviolet radiation :
861 global burden of disease from solar ultraviolet radiation / Robyn Lucas ... [et al.] ; editors, Annette Prüss-Üstün ... [et al.].
862 *Environmental burden of disease series ; no. 13*, World Health Organization, Geneva, 2006.

- 863 Lucas, R. M., Byrne, S. N., Correale, J., Ilschner, S., and Hart, P. H.: Ultraviolet radiation, vitamin D and multiple sclerosis,
864 *Neurodegenerative Disease Management*, 5, 413-424, 10.2217/nmt.15.33, 2015.
- 865 Madronich, S.: *Environmental UV Photobiology*, *Environ. UV Photobiol.*, 10.1007/978-1-4899-2406-3, 1993.
- 866 Mayer, B., Kylling, A., Madronich, S., and Seckmeyer, G.: Enhanced absorption of UV radiation due to multiple scattering in
867 clouds: Experimental evidence and theoretical explanation, *Journal of Geophysical Research: Atmospheres*, 103, 31241-
868 31254, <https://doi.org/10.1029/98JD02676>, 1998.
- 869 Mayer, B., and Kylling, A.: Technical note: The libRadtran software package for radiative transfer calculations - description
870 and examples of use, *Atmos. Chem. Phys.*, 5, 1855-1877, 10.5194/acp-5-1855-2005, 2005.
- 871 McKenzie, R., Bernhard, G., Liley, B., Disterhoft, P., Rhodes, S., Bais, A., Morgenstern, O., Newman, P., Oman, L., Brogniez,
872 C., and Simic, S.: Success of Montreal Protocol Demonstrated by Comparing High-Quality UV Measurements with “World
873 Avoided” Calculations from Two Chemistry-Climate Models, *Scientific Reports*, 9, 12332, 10.1038/s41598-019-48625-z,
874 2019.
- 875 McKenzie, R. L., Aucamp, P. J., Bais, A. F., Björn, L. O., Ilyas, M., and Madronich, S.: Ozone depletion and climate change:
876 impacts on UV radiation, *Photochemical & Photobiological Sciences*, 10, 182-198, 10.1039/c0pp90034f, 2011.
- 877 Meinander, O., Kazadzis, S., Arola, A., Riihelä, A., Räisänen, P., Kivi, R., Kontu, A., Kouznetsov, R., Sofiev, M., Svensson,
878 J., Suokanerva, H., Aaltonen, V., Manninen, T., Roujean, J. L., and Hautecoeur, O.: Spectral albedo of seasonal snow during
879 intensive melt period at Sodankylä, beyond the Arctic Circle, *Atmos. Chem. Phys.*, 13, 3793-3810, 10.5194/acp-13-3793-
880 2013, 2013.
- 881 MétéoFrance: Algorithm theoretical basis document for cloud products (CMA-PGE01 v3.2, CT-PGE02 v2.2 & CTTH-PGE03
882 v2.2), Technical Report SAF/NWC/CDOP/MFL/SCI/ATBD/01, Paris: MétéoFrance, 2013.
- 883 Mok, J., Krotkov, N. A., Torres, O., Jethva, H., Li, Z., Kim, J., Koo, J. H., Go, S., Irie, H., Labow, G., Eck, T. F., Holben, B.
884 N., Herman, J., Loughman, R. P., Spinei, E., Lee, S. S., Khatri, P., and Campanelli, M.: Comparisons of spectral aerosol single
885 scattering albedo in Seoul, South Korea, *Atmos. Meas. Tech.*, 11, 2295-2311, 10.5194/amt-11-2295-2018, 2018.
- 886 Myhre, G., and Myhre, A.: Uncertainties in Radiative Forcing due to Surface Albedo Changes Caused by Land-Use Changes,
887 *Journal of Climate*, 16, 1511-1524, 10.1175/1520-0442(2003)016<1511:uirfdt>2.0.co;2, 2003.
- 888 NOAA: Data Announcement 88-MGG-02, Digital relief of the surface of the Earth. NOAA, National Geophysical Data Center,
889 Boulder, Colorado, 1988.
- 890 Noël, S., Mieruch, S., Bovensmann, H., and Burrows, J. P.: Preliminary results of GOME-2 water vapour retrievals and first
891 applications in polar regions, *Atmos. Chem. Phys.*, 8, 1519-1529, 10.5194/acp-8-1519-2008, 2008.
- 892 Peeters, P., Simon, P. C., Hansen, G., Meerkoetter, R., Verdebout, J., Seckmeyer, G., Taalas, P., and Slaper, H.: MAUVE: A
893 European Initiative for Developing and Improving Satellite Derived Ultraviolet Maps, *Radiation Protection Dosimetry*, 91,
894 201-202, 10.1093/oxfordjournals.rpd.a033200, 2000.
- 895 Pfeifroth, U., Kothe, S., and Trentmann, J.: Validation report: Meteosat solar surface radiation and effective cloud albedo
896 climate data record (Sarah 2), EUMETSAT SAF CM Validation report with reference number SAF/CM/DWD/VAL/
897 METEOSAT/HEL, 2.1, https://doi.org/10.5676/EUM_SAF_CM/SARAH/V002, 2016.

- 898 Probst, P., Rizzi, R., Tosi, E., Lucarini, V., and Maestri, T.: Total cloud cover from satellite observations and climate models,
899 Atmospheric Research, 107, 161-170, <https://doi.org/10.1016/j.atmosres.2012.01.005>, 2012.
- 900 Raptis, I.-P., Kazadzis, S., Eleftheratos, K., Amiridis, V., and Fountoulakis, I.: Single Scattering Albedo's Spectral Dependence
901 Effect on UV Irradiance., Atmosphere, 9, 10.3390/atmos9090364, 2018.
- 902 Reda, I., and Andreas, A.: Solar position algorithm for solar radiation applications. NREL Technical Report, NREL/TP-560-
903 34302, Prepared under Task No. WU1D5600, 2008.
- 904 Renaud, A., Staehelin, J., Fröhlich, C., Philipona, R., and Heimo, A.: Influence of snow and clouds on erythral UV radiation:
905 Analysis of Swiss measurements and comparison with models, Journal of Geophysical Research: Atmospheres, 105, 4961-
906 4969, <https://doi.org/10.1029/1999JD900160>, 2000.
- 907 Rimmer, J. S., Redondas, A., and Karppinen, T.: EuBrewNet – A European Brewer network (COST Action ES1207), an
908 overview, Atmos. Chem. Phys., 18, 10347-10353, 10.5194/acp-18-10347-2018, 2018.
- 909 Schmalwieser, A., and Siani, A.: Review on Non-Occupational Personal Solar UV Exposure Measurements, Photochemistry
910 and Photobiology, 94, 10.1111/php.12946, 2018.
- 911 Schmalwieser, A. W., Gröbner, J., Blumthaler, M., Klotz, B., De Backer, H., Bolsée, D., Werner, R., Tomsic, D., Metelka, L.,
912 Eriksen, P., Jepsen, N., Aun, M., Heikkilä, A., Duprat, T., Sandmann, H., Weiss, T., Bais, A., Toth, Z., Siani, A.-M., Vaccaro,
913 L., Diémoz, H., Grifoni, D., Zipoli, G., Lorenzetto, G., Petkov, B. H., di Sarra, A. G., Massen, F., Yousif, C., Aculinin, A. A.,
914 den Outer, P., Svendby, T., Dahlback, A., Johnsen, B., Biszczuk-Jakubowska, J., Krzyscin, J., Henriques, D., Chubarova, N.,
915 Kolarž, P., Mijatovic, Z., Groselj, D., Pribulova, A., Gonzales, J. R. M., Bilbao, J., Guerrero, J. M. V., Serrano, A., Andersson,
916 S., Vuilleumier, L., Webb, A., and O'Hagan, J.: UV Index monitoring in Europe, Photochemical & Photobiological Sciences,
917 16, 1349-1370, 10.1039/c7pp00178a, 2017.
- 918 Schmalwieser, A. W.: Possibilities to estimate the personal UV radiation exposure from ambient UV radiation measurements,
919 Photochemical & Photobiological Sciences, 19, 1249-1261, 10.1039/d0pp00182a, 2020.
- 920 Seckmeyer, G., Erb, R., and Albold, A.: Transmittance of a cloud is wavelength-dependent in the UV-range, Geophysical
921 Research Letters, 23, 2753-2755, <https://doi.org/10.1029/96GL02614>, 1996.
- 922 Seckmeyer, G., Pissulla, D., Glandorf, M., Henriques, D., Johnsen, B., Webb, A., Siani, A.-M., Bais, A., Kjeldstad, B.,
923 Brogniez, C., Lenoble, J., Gardiner, B., Kirsch, P., Koskela, T., Kaurola, J., Uhlmann, B., Slaper, H., Den Outer, P., Janouch,
924 M., Werle, P., Gröbner, J., Mayer, B., De La Casiniere, A., Simic, S., and Carvalho, F.: Variability of UV Irradiance in Europe,
925 Photochemistry and Photobiology, 84, 172-179, 10.1111/j.1751-1097.2007.00216.x, 2008.
- 926 Siani, A. M., Casale, G. R., Diémoz, H., Agnesod, G., Kimlin, M. G., Lang, C. A., and Colosimo, A.: Personal UV exposure
927 in high albedo alpine sites, Atmos. Chem. Phys., 8, 3749-3760, 10.5194/acp-8-3749-2008, 2008.
- 928 Slaper, H., Reinen, H. A. J. M., Blumthaler, M., Huber, M., and Kuik, F.: Comparing ground-level spectrally resolved solar
929 UV measurements using various instruments: A technique resolving effects of wavelength shift and slit width, Geophysical
930 Research Letters, 22, 2721-2724, 10.1029/95gl02824, 1995.
- 931 Smedley, A. R. D., Rimmer, J. S., Moore, D., Toumi, R., and Webb, A. R.: Total ozone and surface UV trends in the United
932 Kingdom: 1979–2008, International Journal of Climatology, 32, 338-346, 10.1002/joc.2275, 2012.

933 ~~Svendby, T., Hansen, G. H., Bäcklund, A., and Dahlback, A.: Monitoring of the atmospheric ozone layer and natural ultraviolet~~
934 ~~radiation: Annual report 2018, NILU M 1462 | 2019, 39, 2018.~~

- 935 Taylor, M., Kosmopoulos, P. G., Kazadzis, S., Keramitsoglou, I., and Kiranoudis, C. T.: Neural network radiative transfer
936 solvers for the generation of high resolution solar irradiance spectra parameterized by cloud and aerosol parameters, *Journal*
937 *of Quantitative Spectroscopy and Radiative Transfer*, 168, 176-192, <https://doi.org/10.1016/j.jqsrt.2015.08.018>, 2016.
- 938 Vanicek, K., Frei, T., Litynska, Z., and Schmalwieser, A.: *UV-Index for the Public*, European Union, 2000.
- 939 Verdebot, J.: A method to generate surface UV radiation maps over Europe using GOME, Meteosat and ancillary geophysical
940 data. *Journal of Geophysical Research: Atmospheres*, 105(D4), 5049-5058, 2000.
- 941 Vitt, R., Laschewski, G., Bais, A. F., Diémoz, H., Fountoulakis, I., Siani, A.-M., and Matzarakis, A.: UV-Index Climatology
942 for Europe Based on Satellite Data, *Atmosphere*, 11, 10.3390/atmos11070727, 2020.
- 943 Webb, A. R., and Engelsen, O.: Ultraviolet Exposure Scenarios: Risks of Erythema from Recommendations on Cutaneous
944 Vitamin D Synthesis, in: *Sunlight, Vitamin D and Skin Cancer*, edited by: Reichrath, J., Springer New York, New York, NY,
945 72-85, 2008.
- 946 Webb, A. R., Slaper, H., Koepke, P., and Schmalwieser, A. W.: Know Your Standard: Clarifying the CIE Erythema Action
947 Spectrum, *Photochemistry and Photobiology*, 87, 483-486, 10.1111/j.1751-1097.2010.00871.x, 2011.
- 948 WHO: *Global Solar UV Index: A Practical Guide*, No. WHO/SD., Geneva, Switzerland, 2002.
- 949 WMO: *Report of the WMO Meeting of Experts on UVB Measurements, Data Quality and Standardization of UV Indices*,
950 1994, 1995.
- 951 Zempila, M.-M., Koukouli, M.-E., Bais, A., Fountoulakis, I., Arola, A., Kouremeti, N., and Balis, D.: OMI/Aura UV product
952 validation using NILU-UV ground-based measurements in Thessaloniki, Greece, *Atmospheric Environment*, 140, 283-297,
953 <https://doi.org/10.1016/j.atmosenv.2016.06.009>, 2016.
- 954 Zerefos, C. S., Tourpali, K., Eleftheratos, K., Kazadzis, S., Meleti, C., Feister, U., Koskela, T., and Heikkilä, A.: Evidence of
955 a possible turning point in solar UV-B over Canada, Europe and Japan, *Atmos. Chem. Phys.*, 12, 2469-2477, 10.5194/acp-12-
956 2469-2012, 2012.
- 957
- 958
- 959
- 960
- 961
- 962
- 963
- 964
- 965
- 966

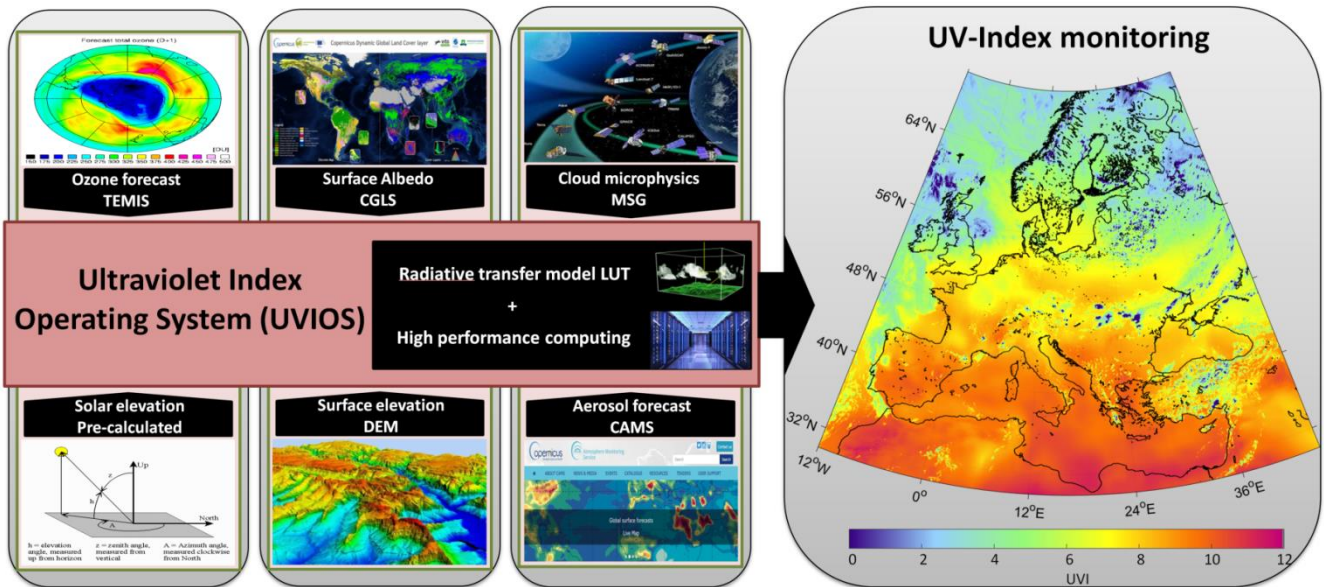
967
 968
 969
 970
 971
 972
 973
 974
 975
 976

Table 1: UVIOS model input parameters

Parameter	Description (spatial – temporal resolution)	Source	Reference
Cloud microphysics	Nowcast cloud optical thickness (COT), cloud phase (CPH) (5 km – 15 minutes)	Meteosat Second Generation (MSG4) NOA Antenna	(MétéoFrance, 2013)
Aerosol optical depth	1-day forecast aerosol optical depth (AOD) (40 km – 3 hours)	Copernicus Atmosphere Monitoring Service (CAMS) – FTP access	(Eskes et al., 2015)
Aerosol optical properties	Single scattering albedo (SSA), Angstrom exponent (AE) (1 x 1 degrees – 1 month)	Aerosol Comparisons between Observations and Models (Aerocom)	(Kinne, 2019)
Solar elevation	Solar zenith angle (SZA) (5 km – 15 minutes)	Astronomical model In-house software (NOA)	(Reda and Andreas, 2008)
Surface albedo	Surface albedo (ALB) (1 km – 12 days)	Copernicus Global Land Service (CGLS)	(Carrer et al., 2010)
Water vapor	H ₂ O observation (40 x 80 km – 1day)	Global Ozone Monitoring Experiment 2 Level 2 data (GOME-2 L2)	(Noël et al., 2008)
Surface elevation	Elevation observation (ELE) (1 m – fixed)	Digital Elevation Model (DEM) In-house database (NOAA)	(NOAA, 1988)
Ozone	1-day forecast total ozone column (TOC) (1 x 1 degrees – 1 day)	Tropospheric Emission Monitoring Internet Service (TEMIS) with Assimilated Ozone Fields from GOME-2 (METOP-B)	(Eskes et al., 2003)

977
 978
 979
 980
 981
 982
 983
 984
 985
 986

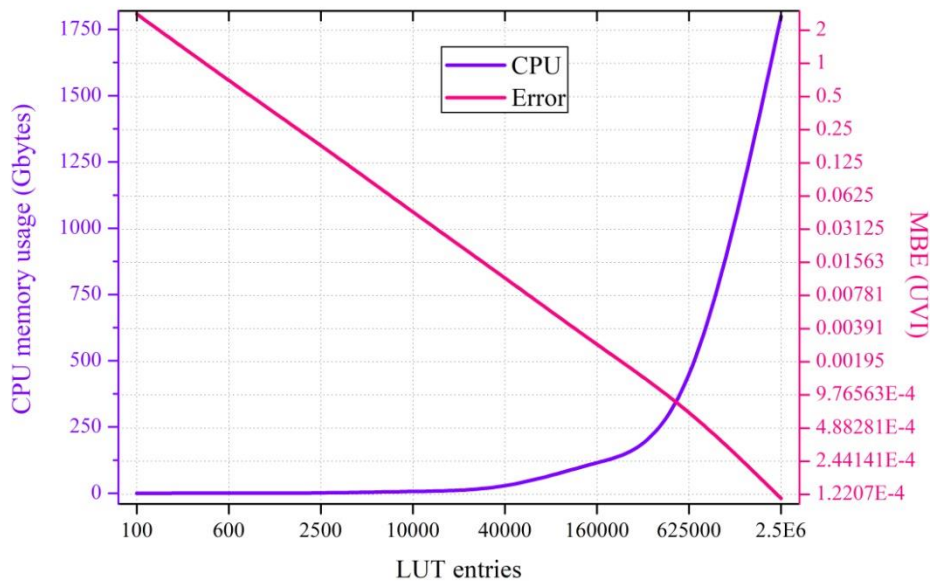
987
988
989
990
991
992
993
994
995
996



997
998
999
1000
1001
1002
1003
1004
1005
1006
1007

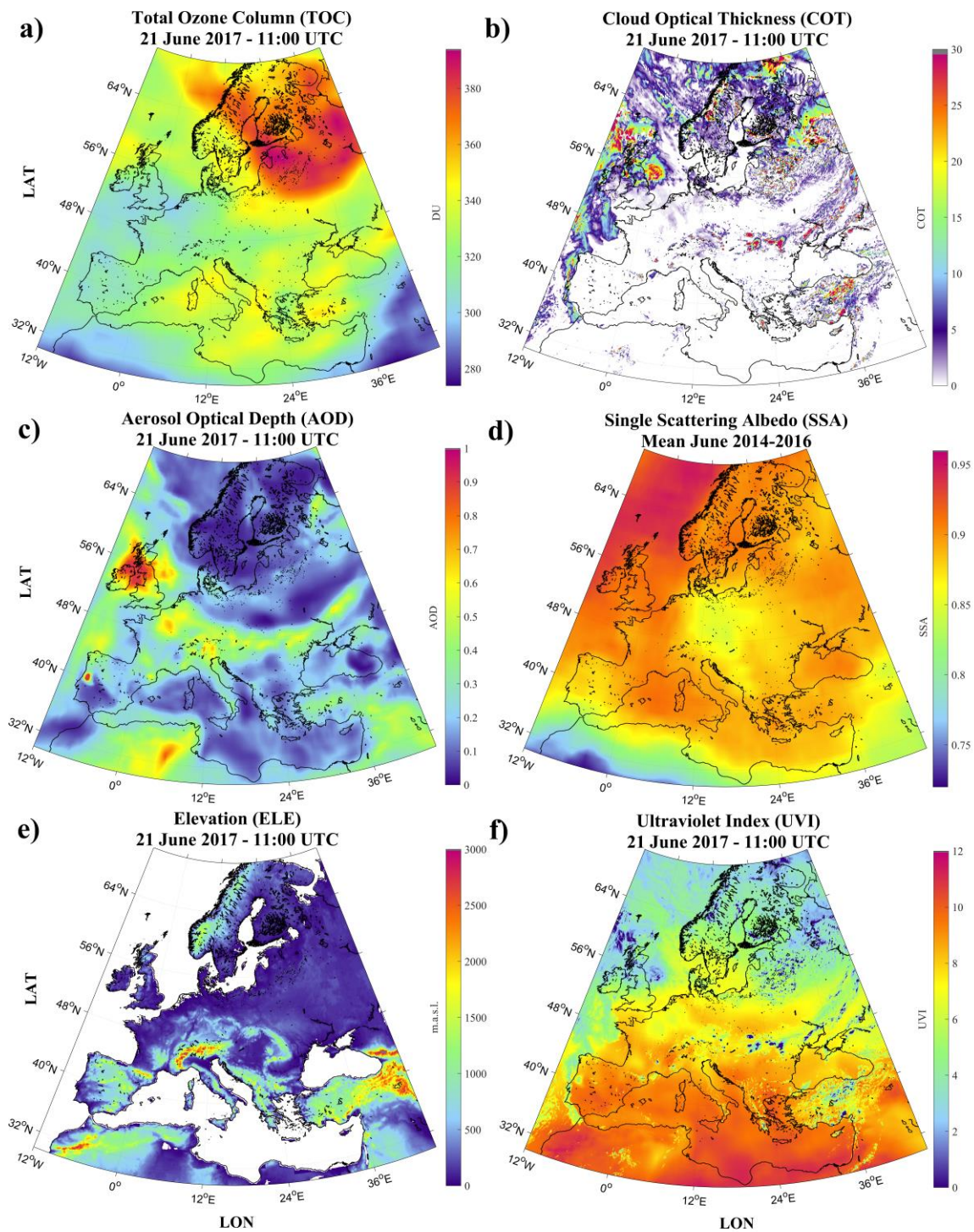
Figure 1: Flowchart illustration of the UVIOS modelling technique scheme. The pre-calculated effects of solar and surface elevation and albedo followed by the aerosol and ozone forecasts and the real-time cloud observations to the UVIOS solver result in the spectrally weighted output of UVI for the European region.

1008
1009
1010
1011
1012
1013
1014
1015
1016



1017
1018
1019
1020
1021
1022
1023
1024
1025
1026

Figure 2: UVIOS memory usage and error statistics in terms of mean bias error (MBE) for a range of different LUT sizes.

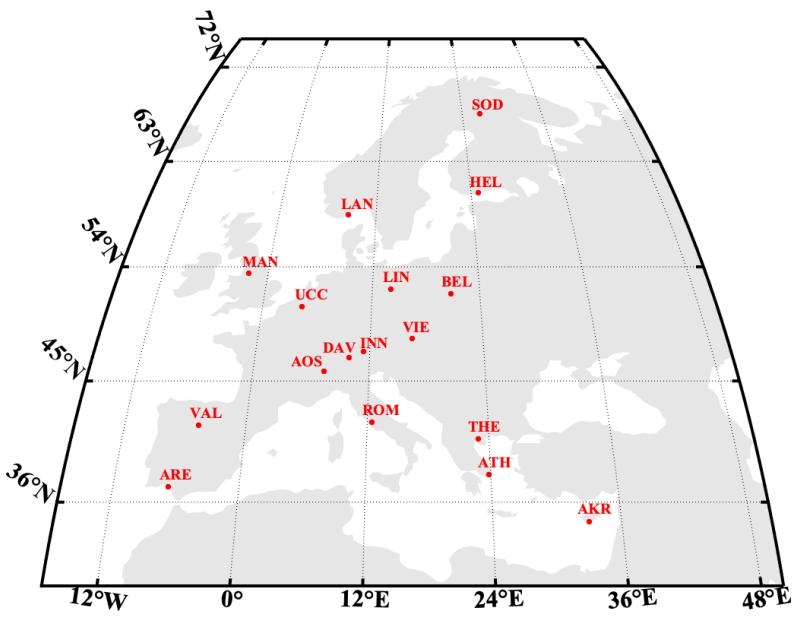


1027

1028
1029

Figure 3: An example of the input TOC (a), COT (b), AOD (c), SSA (d), ELE (e) and output UVI (f) maps based on the UVIOS modelling technique applied for the 21st of June 2017 at 11:00 UTC.

1030
1031
1032
1033
1034
1035
1036
1037
1038
1039



1040
1041
1042
1043
1044
1045
1046
1047
1048
1049
1050
1051

Figure 4: Study region and UVI ground measurement locations.

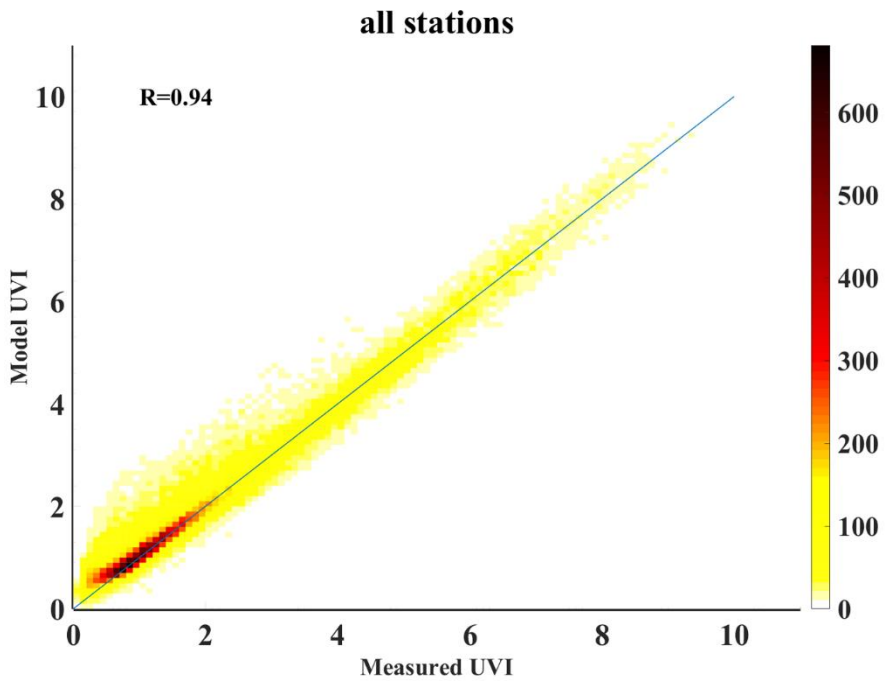
1052
 1053
 1054
 1055
 1056
 1057
 1058
 1059

Table 2: Coordinates (degrees), instrument type, height (metres above sea level) and maximum UVI measured levels of the European stations used for the comparison.

Station	Country	Code	Latitude (°N)	Longitude (°E)	Instrument	Height (m.a.s.l.)	UVI _{max}	Reference
Akrotiri	Cyprus	AKR	34.59	32.99	SL501	23	9.14	
Aosta	Italy	AOS	45.74	7.36	Bentham DTMc300	570	9.60	(Fountoulakis et al., 2020b)
El Arenosillo	Spain	ARE	37.10	-6.73	Brewer MKIII	52	9.78	
Athens	Greece	ATH	37.99	23.78	Brewer MKIV	180	10.20	
Belsk	Poland	BEL	51.84	20.79	Brewer MKIII	176	7.54	(Czerwińska et al., 2016)
Davos	Switzerland	DAV	46.81	9.84	Brewer MKIII	1590	10.57	
Helsinki	Finland	HEL	60.20	24.96	Brewer MKIII	48	5.68	(Lakkala et al., 2008)
Innsbruck	Austria	INN	47.26	11.38	SL501	577	8.35	(Hülßen et al., 2020)
Landvik	Norway	LAN	58.33	8.52	GUV-541	10	6.65	(Johnsen Svendby et al., 2018)
Lindenberg	Germany	LIN	52.21	14.11	Bentham DTMc300	127	8.86	
Manchester	United Kingdom	MAN	53.47	-2.23	Brewer MKII	76	7.30	(Smedley et al., 2012)
Rome	Italy	ROM	41.90	12.50	Brewer MKIV	75	8.38	
Sodankyla	Finland	SOD	67.37	26.63	Brewer MKIII	179	4.51	(Heikkilä et al., 2016; Lakkala et al., 2008)
Thessaloniki	Greece	THE	40.63	22.96	Brewer MKIII	60	10.40	(Fountoulakis et al., 2016; Garane et al., 2006)
Uccle	Belgium	UCC	50.80	4.35	Brewer MKIII	100	8.99	(De Bock et al., 2014)
Valladolid	Spain	VAL	41.66	-4.71	YES	705	10.32	(Hülßen et al., 2020)
Vienna	Austria	VIE	48.26	16.43	SL501	153	8.09	(Hülßen et al., 2020)

1060
 1061
 1062
 1063
 1064

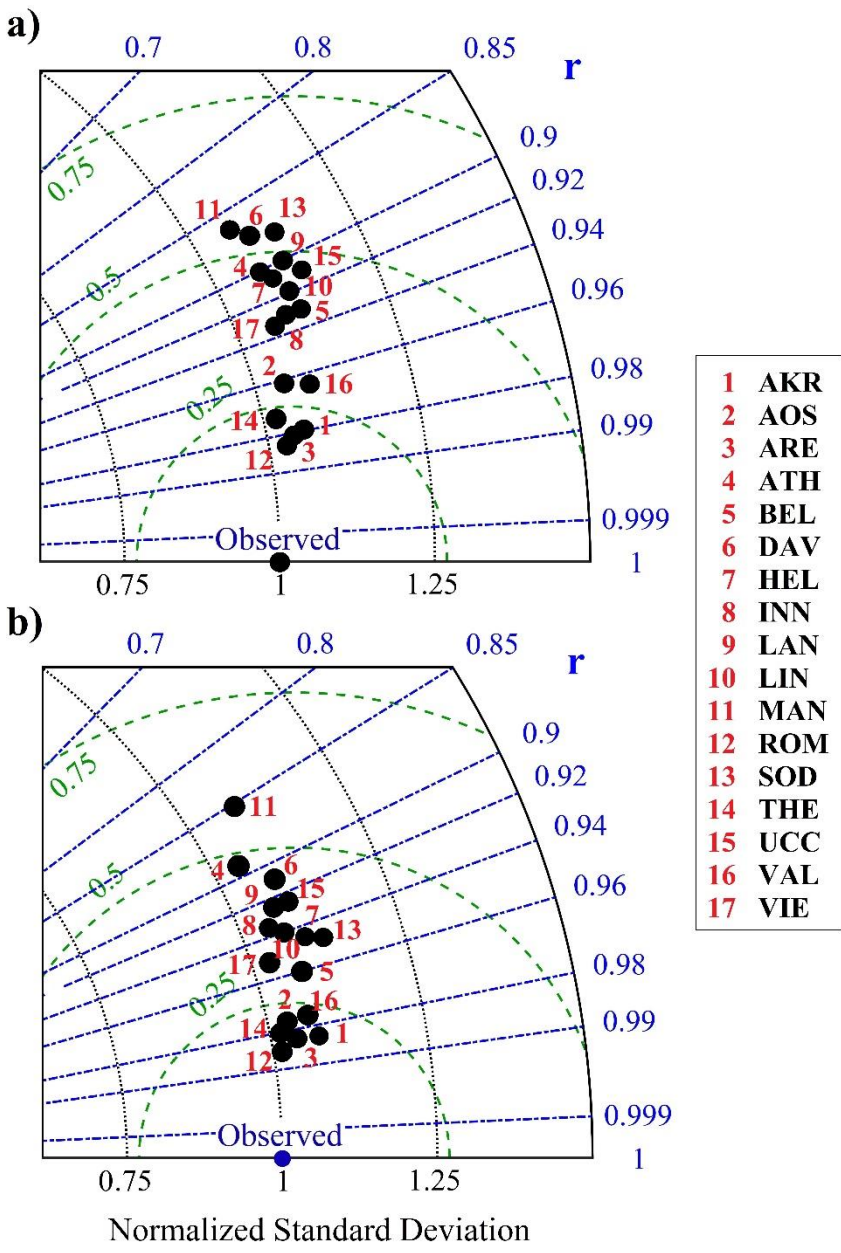
1065
1066
1067
1068
1069
1070
1071
1072
1073
1074



1075
1076
1077
1078
1079
1080
1081
1082
1083
1084

Figure 5: Density sScatter-plot of the overall UVIOS performance for all stations. The analytical statistics for each station can be found in the Appendix A.

1085
1086
1087



1088
1089
1090
1091

Figure 6: Taylor diagram for the overall UVIOS accuracy for all ground-stations under all sky (a) and clear sky (b) conditions.

1092
 1093
 1094
 1095
 1096
 1097
 1098
 1099
 1100
 1101
 1102
 1103
 1104
 1105
 1106
 1107
 1108
 1109
 1110
 1111
 1112
 1113

Table 3: Absolute difference between UVIOS and ground-based UVI measurements in terms of percentages (%) of data that are within 0.5 and 1 UVI of difference (U0.5 and U1.0, respectively) as well as the correlation coefficient (r) for all sky and clear sky conditions.

STATION	ALL SKY			CLEAR SKY		
	U0.5	U1.0	r	U0.5	U1.0	r
AKR	82.25	96.02	0.980	84.57	97.48	0.987
AOS	86.81	94.40	0.961	92.23	97.07	0.978
ARE	85.15	95.73	0.981	87.99	96.86	0.986
ATH	84.99	94.29	0.902	88.98	96.35	0.891
BEL	83.07	93.28	0.933	91.30	96.50	0.960
DAV	74.20	86.43	0.873	76.19	87.06	0.912
HEL	86.53	94.79	0.909	94.13	97.70	0.944
INN	79.96	92.17	0.932	87.09	95.23	0.937
LAN	84.94	93.46	0.900	92.34	96.52	0.925
LIN	81.58	91.86	0.919	90.95	96.31	0.941
MAN	77.72	90.44	0.862	87.85	94.27	0.852
ROM	87.69	96.19	0.985	89.55	97.00	0.991
SOD	90.86	97.26	0.883	95.69	98.94	0.947
THE	88.98	95.91	0.974	92.51	97.35	0.981
UCC	71.18	87.68	0.913	83.23	92.15	0.926
VAL	85.86	93.93	0.962	86.61	95.22	0.976
VIE	76.65	91.53	0.936	83.37	94.42	0.952

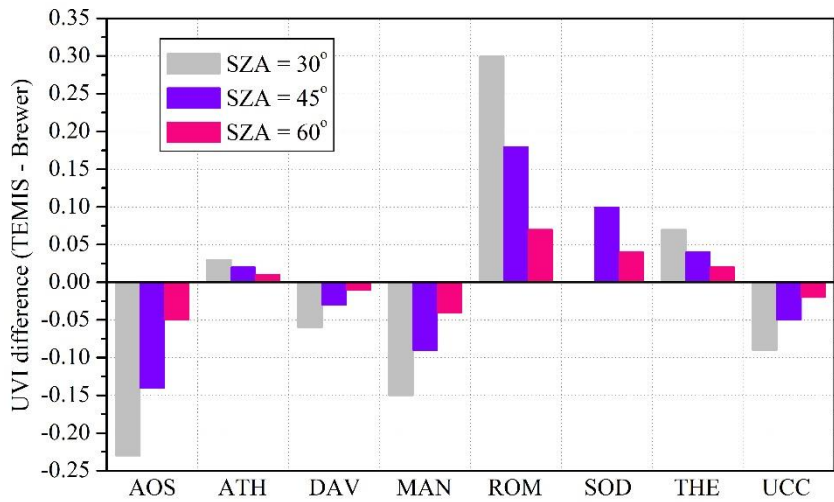
1114
1115
1116
1117
1118
1119
1120
1121
1122
1123
1124
1125
1126
1127
1128
1129

Table 4: Mean bias error of the TEMIS TOC as compared to the WOUDC ground-based measurements.

Station	AOS	ATH	DAV	MAN	ROM	SOD	THE	UCC
MBE TOC (DU)	7.6	-0.9	1.9	5.0	-9.9	-5.4	-2.2	2.9
RMSE TOC (DU)	15.8	10.0	9.1	11.3	12.5	13.1	6.2	7.8
r	0.92	0.95	0.97	0.97	0.94	0.97	0.99	0.98

1130
1131
1132
1133
1134
1135
1136
1137
1138
1139
1140
1141
1142
1143

1144
1145
1146
1147
1148
1149
1150
1151
1152
1153
1154
1155



1156

1157 **Figure 7:** Differences of UVI derived by the UVIOS using as input the TEMIS and the Brewer TOC respectively at all stations with available
1158 data. (lower possible SOD SZA is 44 degrees).

1159

1160

1161

1162

1163

1164

1165

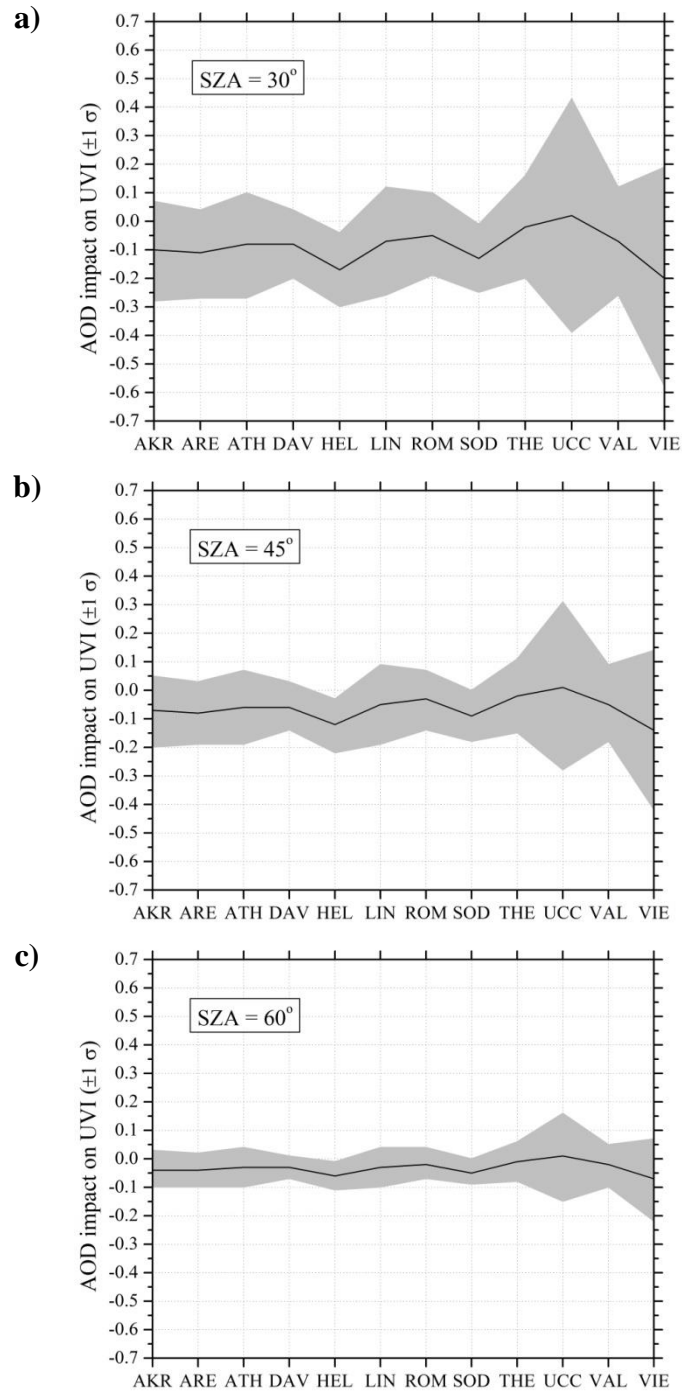
1166

1167
1168
1169
1170
1171
1172
1173
1174
1175
1176
1177
1178
1179
1180
1181
1182
1183

1184
1185
1186
1187
1188
1189
1190
1191
1192
1193
1194
1195
1196

Table 5: Comparison results between CAMS forecasted AOD values used as UVIOS input and AERONET ground-based AOD measurements. The AOD MBE and RMSE statistical scores are shown in absolute units, along with correlation coefficient.

Station	AKR	ARE	ATH	DAV	HEL	LIN	ROM	SOD	THE	UCC	VAL	VIE
MBE	0.037	0.042	0.030	0.029	0.062	0.026	0.017	0.047	0.008	-0.007	0.024	0.071
RMSE	0.074	0.070	0.074	0.053	0.078	0.074	0.056	0.065	0.066	0.150	0.073	0.157
r	0.77	0.91	0.80	0.73	0.70	0.69	0.80	0.63	0.76	0.50	0.78	0.10



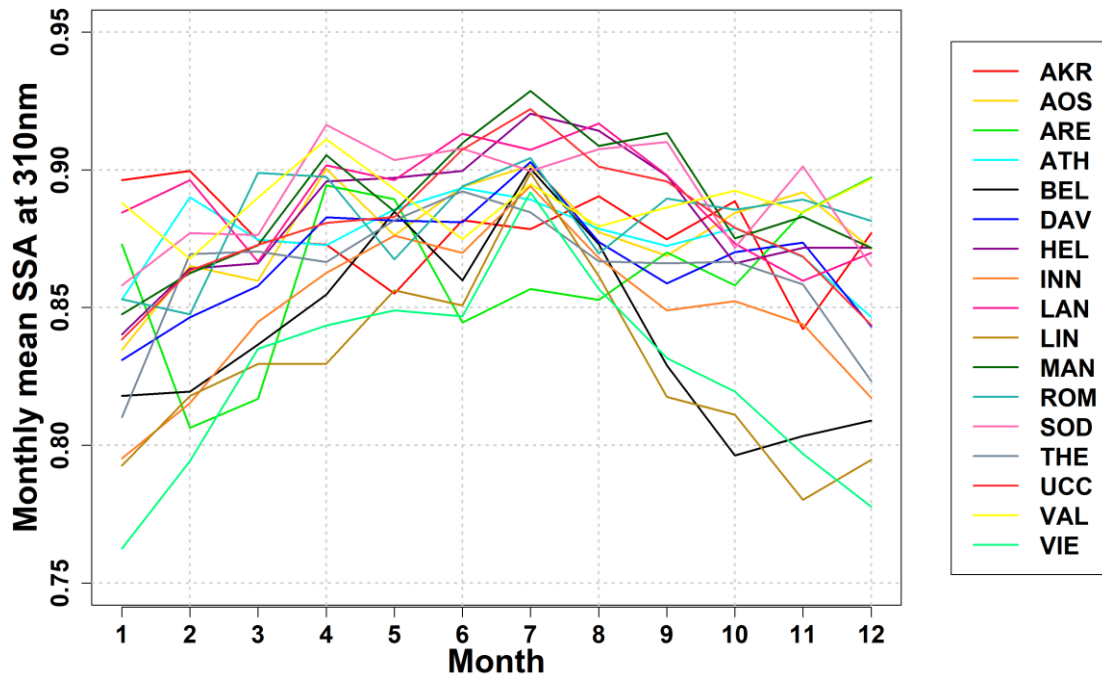
1197

1198

1199

Figure 8: The mean bias error of the CAMS – AERONET AOD impact on UVI for all stations with available data as a function of SZA at 30 (a), 45 (b) and 60 (c) degrees together with the uncertainty range ($\pm 1 \sigma$).

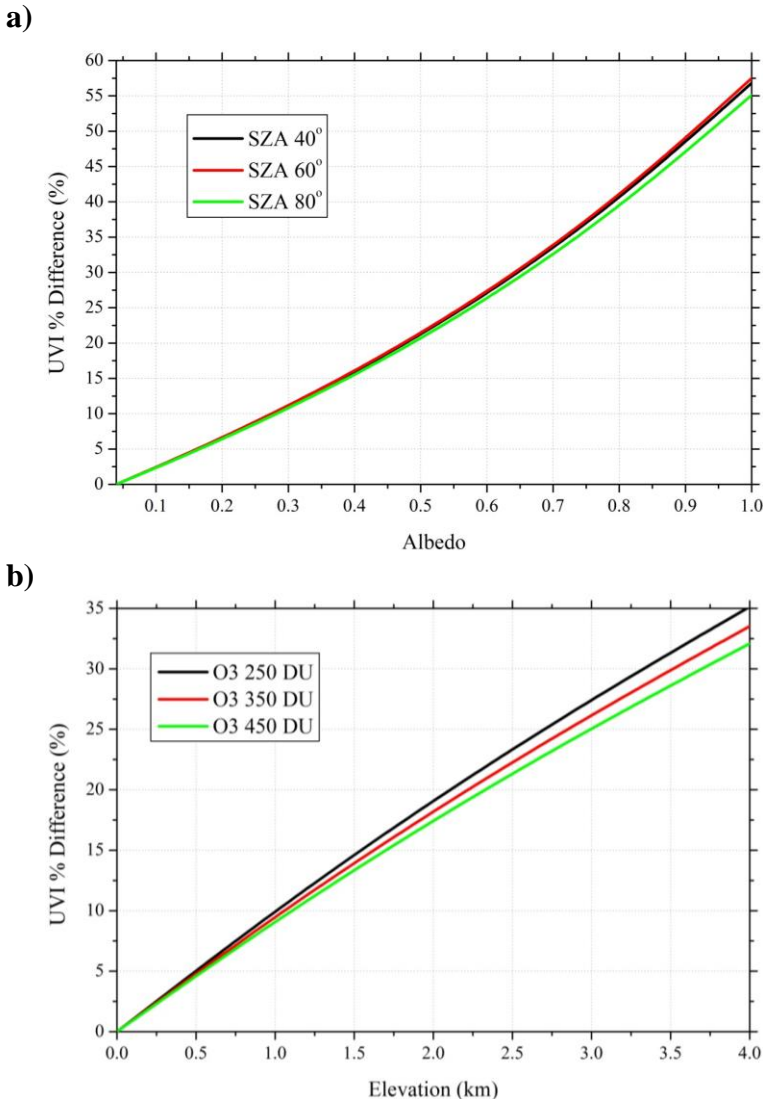
1200
1201
1202
1203
1204
1205
1206
1207



1208
1209
1210
1211
1212
1213
1214
1215
1216

Figure 9: The monthly mean (i.e. 1-12 = Jan-Dec) SSA levels for all ground stations as derived by the MACv2 database.

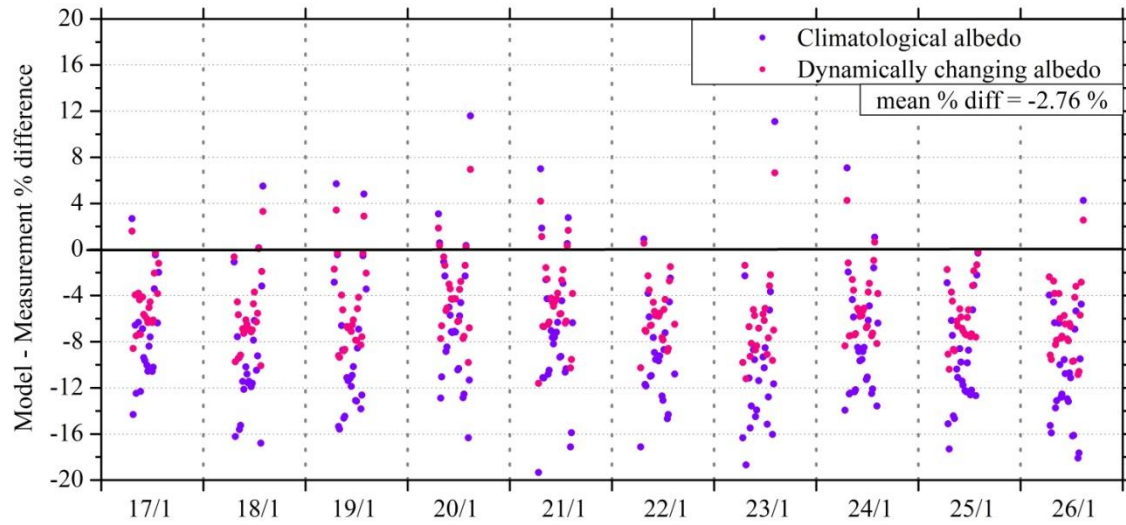
1217
1218
1219
1220
1221



1222
1223
1224
1225
1226

Figure 10: The surface albedo effect on UVI as a function of percentage difference for various SZAs (a). The surface elevation effect on UVI as a function of percentage difference for various total ozone columns (b).

1227
1228
1229
1230
1231
1232
1233
1234
1235
1236
1237
1238

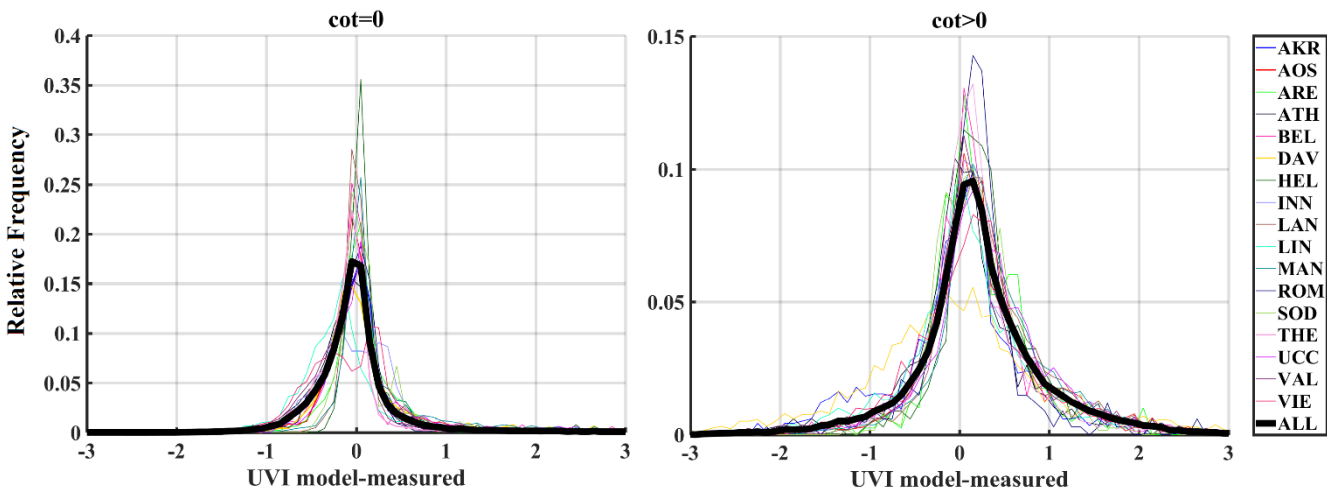


1239
1240
1241
1242

Figure 11: The effect of surface albedo correction on UVI for the Davos station. The climatological and the dynamically changing albedo in terms of percentage differences of modelled and ground measurements during a snow covered period (17/1 - 26/1) under clear sky conditions.

1243
1244
1245
1246
1247
1248
1249
1250

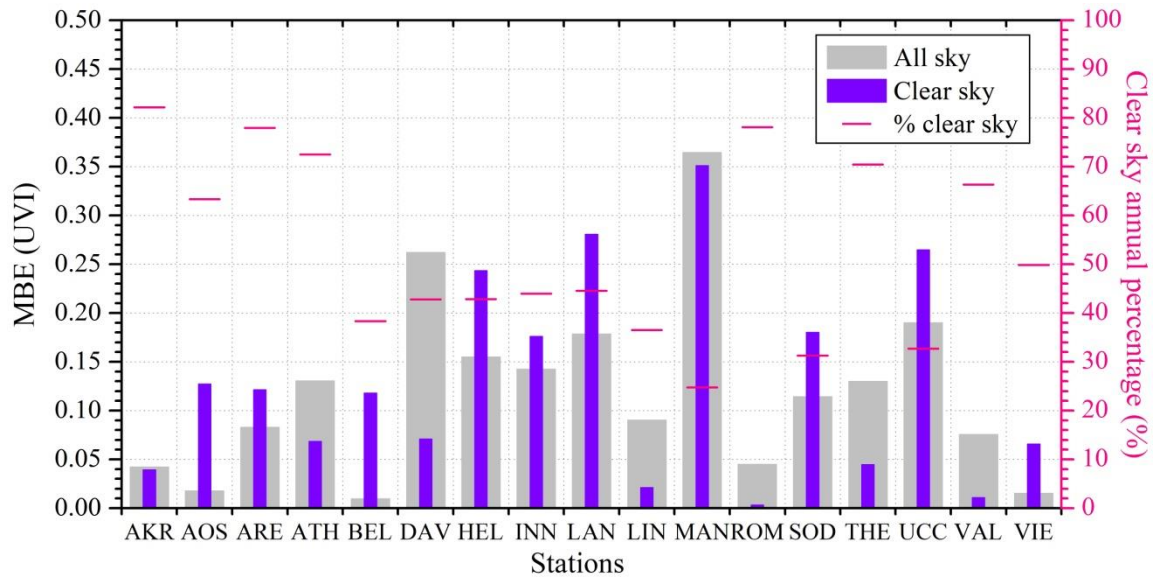
1251
1252
1253
1254
1255
1256
1257
1258
1259
1260
1261
1262



1263
1264
1265
1266
1267
1268
1269
1270
1271
1272
1273

Figure 12: Relative frequency distribution of UVI residuals for all stations (coloured lines) and the mean (bold black line) for cloudless (left plot) and cloudy (right plot) conditions.

1274
1275
1276
1277
1278
1279
1280
1281
1282
1283
1284
1285



1286
1287
1288
1289
1290
1291
1292
1293
1294
1295

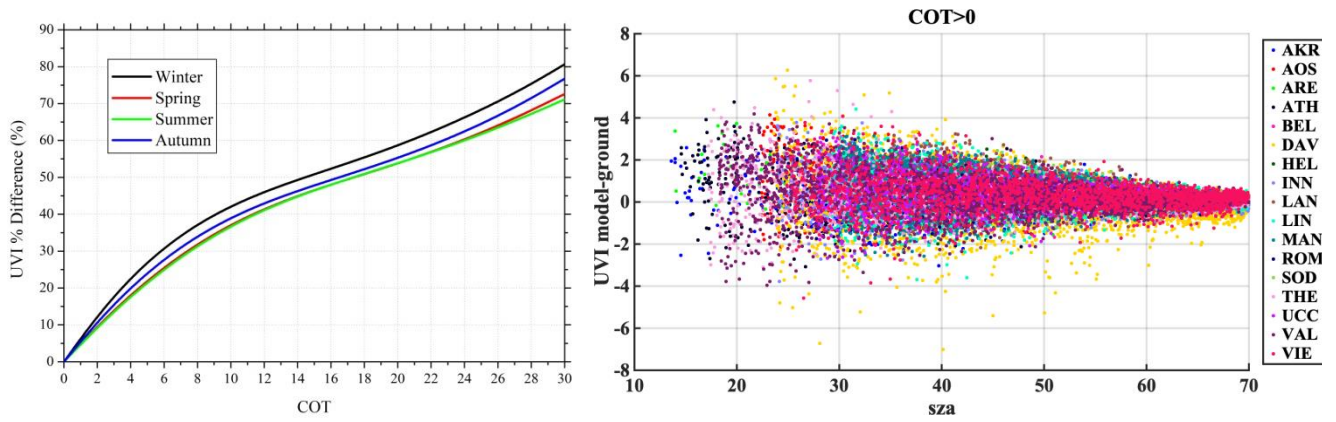
Figure 13: Mean bias error of the modelled UVI as compared to the ground-based measurements for all and clear sky conditions. The percentage of clear sky data time steps was also plotted with red lines.

1296
1297
1298
1299
1300
1301
1302
1303
1304
1305
1306
1307
1308
1309
1310
1311
1312
1313
1314
1315
1316
1317
1318
1319
1320
1321
1322
1323
1324
1325
1326

Table 6: Percentage of data for UVIOS underestimation (A1-A3) and overestimation (B1-B3) under clear and cloudy sky conditions for various UVI difference (modelled-ground) classes.

Difference of UVI	< -1.0 (A1)	< -0.5 (A2)	< 0.0 (A3)	> 0.0 (B3)	> 0.5 (B2)	> 1.0 (B1)
% of data COT > 0	3.6	11.5	37.5	62.5	24.8	11.1
% of data COT = 0	0.9	10.2	45.4	54.6	11.4	4.2

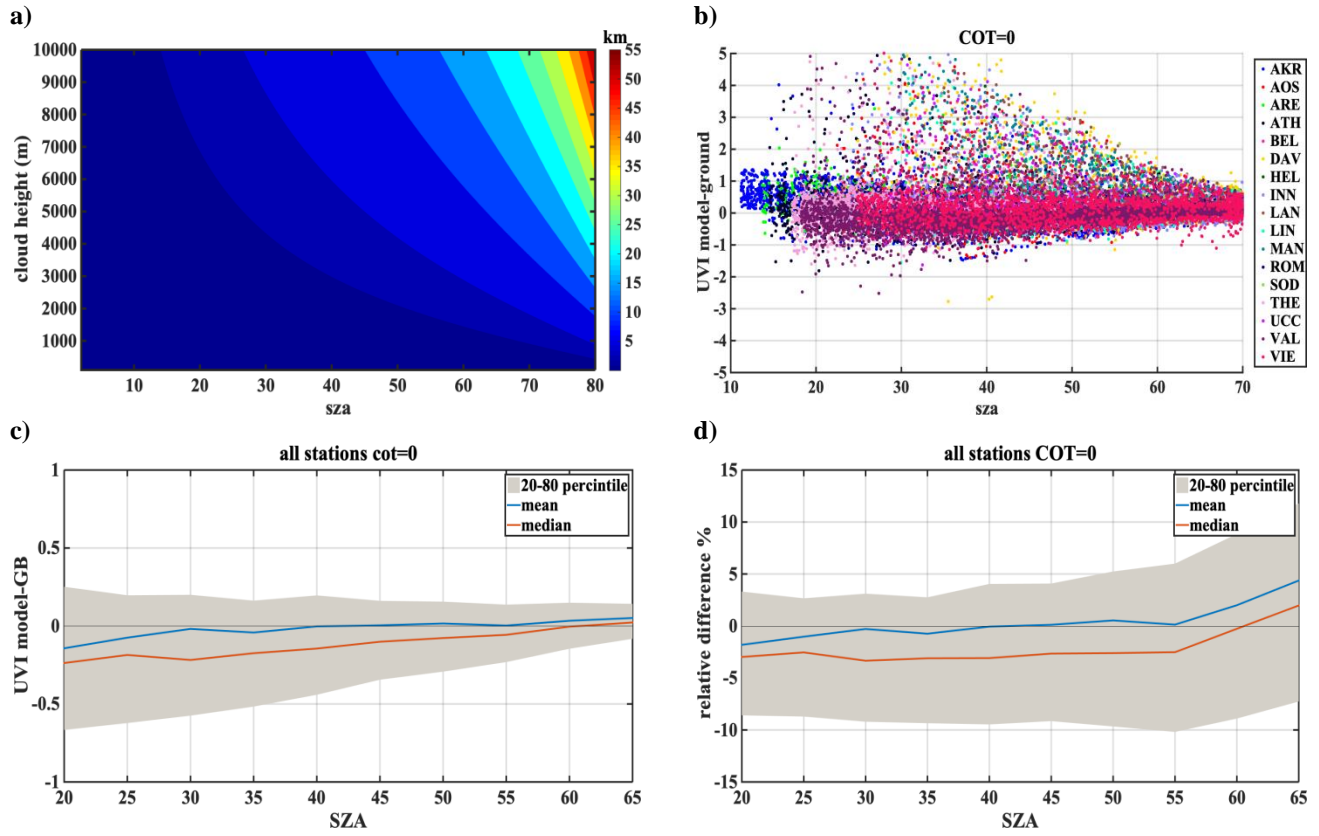
1327
1328
1329
1330
1331
1332
1333
1334
1335
1336
1337
1338
1339



1340 **Figure 14:** The average COT effect on UVI as a function of percentage difference for all seasons (left) and scatterplot of the UVI difference
1341 under cloudy sky conditions for all stations (right).

1342
1343
1344
1345
1346
1347
1348
1349
1350
1351

1352
1353
1354
1355
1356
1357
1358



1359
1360
1361
1362
1363
1364
1365
1366

Figure 15: The shadow volume at the surface level of a cloud relative to the SEVIRI angle view, as a function of cloud height and SZA (a). Scatterplot of the UVI difference under clear sky conditions for all stations (b). UVI mean, median and 20-80 percentile differences (c) and percentage differences (d) derived by the UVIOS as compared to the ground-based measurements for clear sky conditions as a function of SZA.

1367 Appendix A

1368 The following set of Figures (A.1 – A.17) show ~~for all stations~~ for all stations, in the upper row, density scatterplots of
1369 measured and modeled UVI for all sky and clear sky conditions ~~(upper row),~~ followed by the correlation coefficient (R) and
1370 the number of data points (N) used in the analysis. In the middle row, the normalized probability histogram of differences is
1371 depicted (middle row), while the lower row presents ~~and the~~ boxplot of differences ~~(lower row)~~ as a function of SZA,
1372 representing median (red lines), mean (blue dotted lines), 25-75 percentiles (blue boxes) and 5-95 whiskers (dotted lines). ~~Table~~
1373 ~~A.1 shows additionally the amount of data points that represent both all sky and clear sky conditions for the studied stations.~~

1374 We have categorized the stations mostly based on cloud cover as Mediterranean, Central Europe, High altitude and High
1375 latitude. Each of the station has its own characteristics in terms of atmospheric conditions and parameters affecting the UVI
1376 reaching the ground. A summary of the results with possible explanation of the differences observed are shown here. The
1377 Mediterranean region includes the stations THE, ATH, AKR, ROM, VAL and ARE. Analysis of TOC showed that in most of
1378 the cases UVI mean differences are less than 0.1 in general while a negative bias between TOC and the ground measurements
1379 was seen to be highest for ROM (-9.9) that corresponds to the UVI difference of 0.3. Impact of AOD uncertainty showed the
1380 correlation coefficient between the modelled and the measured UVI values above 0.7 for most of the stations while it was as
1381 high as 0.91 for ARE. The mean bias between the modelled and measured UVI for clear sky condition was found to be less
1382 than that for the all sky condition for the stations AKR, ATH and THE that had most days of the year as cloud-free (the clear
1383 sky percentage is above 70%). The mean bias between the modelled and measured UVI for clear sky condition was more than
1384 the all sky condition for ARE even though it had mostly clear skies throughout the year. The analysis of the combined effect
1385 of the aerosol and ozone at Thessaloniki revealed that the model showed a slight underestimation with real inputs (AERONET
1386 and Brewer) while overestimations for forecasted inputs (CAM5 and TEMIS). However, the coefficient of correlation was
1387 found to be as 0.989 and 0.992 for the model with forecasted and real inputs, respectively. Stations of this classification have
1388 the single scattering albedo ranging from 0.76 to 0.93, with most of them having SSA values between 0.83 to 0.93 except
1389 stations ARE and THE that had relatively smaller SSA values (0.76-0.9) and greater variability, and large MBE. AKR station
1390 comparison showed some UVIOS calculated UVI at higher levels than the ground-based measurements especially in low
1391 SZA's. However, ground-based UVI measurements seem more unrealistic than the UVIOS calculated UVI for summer local
1392 noon conditions as modeled UVIs with real AOD and TOC measurements at the area tend to agree with UVIOS outputs.

1393 The second classification is the Central European regions including AOS, UCC, BEL, MAN, LIN, VIE and INN. The median
1394 of the absolute UVI differences between the model and the measurement for all sky condition were higher for MAN and UCC
1395 while for others it was close to zero. Larger UVI difference of -0.22 due to TOC uncertainty impact was observed for AOS
1396 which might be due to large values of UVI at higher altitude as the positive bias is highest for AOS station (7.6). The UVIOS
1397 MBE and RMSE statistical scores for analyzing AOD uncertainty impact showed a mean positive bias up to 0.071 for all the
1398 stations except UCC which is showed a mean negative bias of 0.007. The mean bias between the modelled and measured UVI
1399 for clear sky condition was more than the all sky condition for AOS even though it had mostly clear skies throughout the year.

1400 BEL, UCC and VIE showed more MBE for clear sky condition than the all sky condition as they have mostly cloudy skies
 1401 throughout the year (clear sky annual percentage less than 50%). However, stations LIN and MAN also have more MBE for
 1402 clear sky condition even though they have most days of the year as cloudy (clear sky annual percentage less than 45%).
 1403 Analysis of AOD uncertainty showed that UVI difference was highest for VIE than the other stations. The monthly values of
 1404 the single scattering albedo used in UVIOS ranged from 0.76 to 0.93 for stations AOS, UCC and MAN, with most of them
 1405 having SSA values between 0.83 to 0.93, and relatively small variability. While, the stations BEL, INN, LIN and VIE had
 1406 relatively smaller SSA values (0.76-0.9) and greater variability than the other stations and most of these stations have shown
 1407 large MBE.

1408 The high altitude station is DAV and high latitude stations include LAN, HEL and SOD. DAV have less MBE for clear sky
 1409 condition even though they have most days of the year as cloudy (clear sky annual percentage less than 45%). DAV and MAN
 1410 show worse statistical behavior for clear sky, which is probably caused by misclassification of cloudy pixels. For DAV this
 1411 could be explained by the complex mountainous topography of the area. Large UVI differences in SOD and HEL indicate
 1412 higher introduced uncertainties over higher latitudes. Higher aerosol levels in the atmosphere tend to lower the UVI. Highest
 1413 difference in UVI is observed for the stations HEL, SOD and VIE. Since, the aerosol level at the stations HEL and SOD is
 1414 very low this leads to higher UVI which can be the reason for the small UVI differences observed for these stations. The
 1415 stations of this classification have mostly cloudy skies throughout the year (clear sky annual percentage less than 50%) and
 1416 have more MBE for clear sky condition than the all sky condition. This might be due the fact that the clouds are not captured
 1417 well at a point station and a cloudy sky might have been considered as a clear sky. Higher UVI difference was observed for
 1418 HEL and SOD as a result of AOD uncertainty analysis which might be due to the low aerosol content of these stations due to
 1419 higher latitude that leads to higher UVI values.

1420

1421

Table A.1 Number of data points and clear sky data points, used in the analysis for each station.

Station	All data	Data-COT=0
AKR	6547	5379
AOS	5607	3551
ARE	1814	1414
ATH	4892	3548
BEL	1317	505
DAV	5635	2410
HEL	595	255
INN	4365	1919
LAN	7409	3302
LIN	3795	1387
MAN	7854	1946
ROM	1532	1196
SOD	860	269
THE	9750	6867
UCC	3007	983
VAL	9795	6497
VIE	4199	2094

1422

AKR

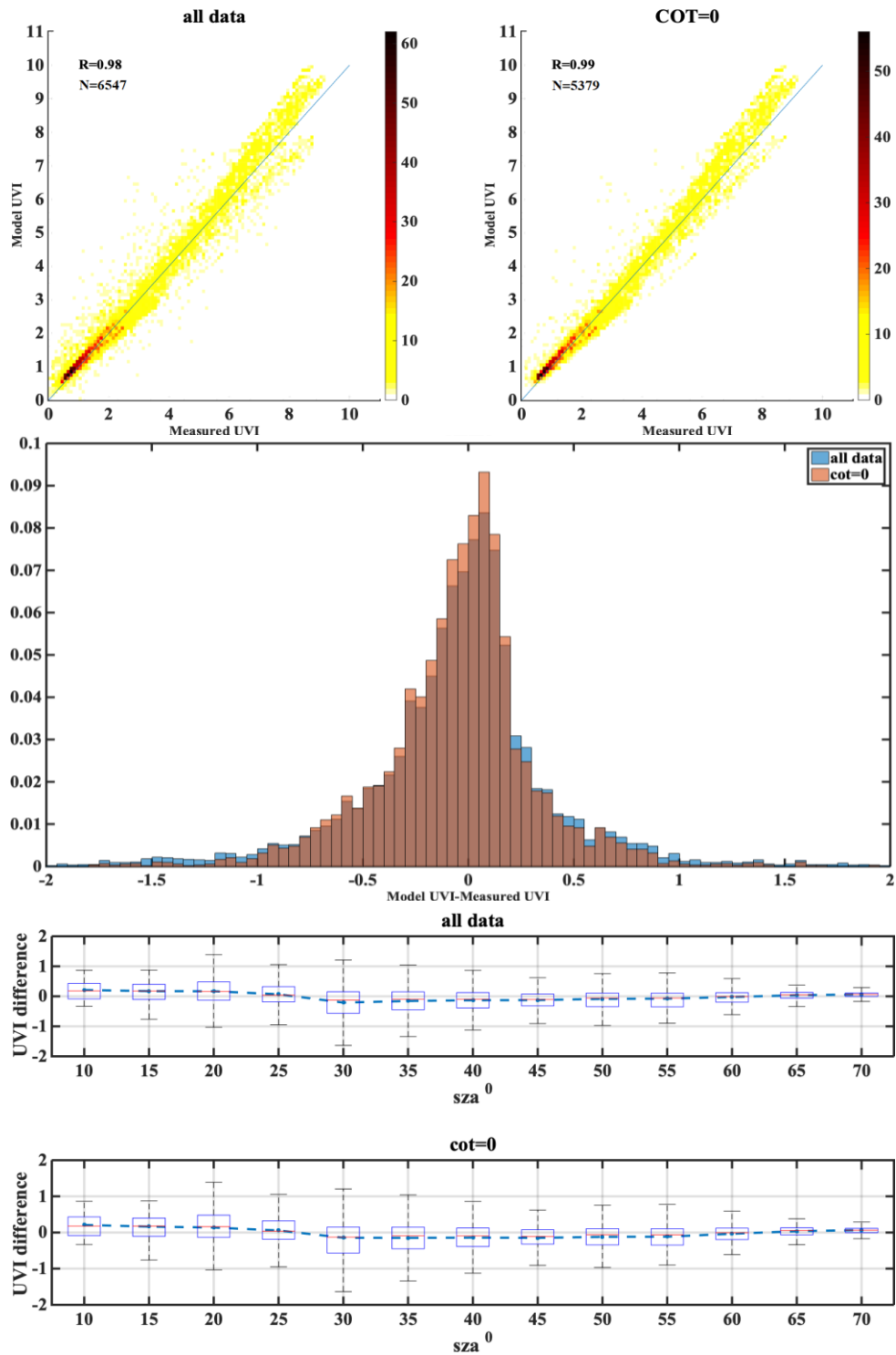


Figure A.1

AOS

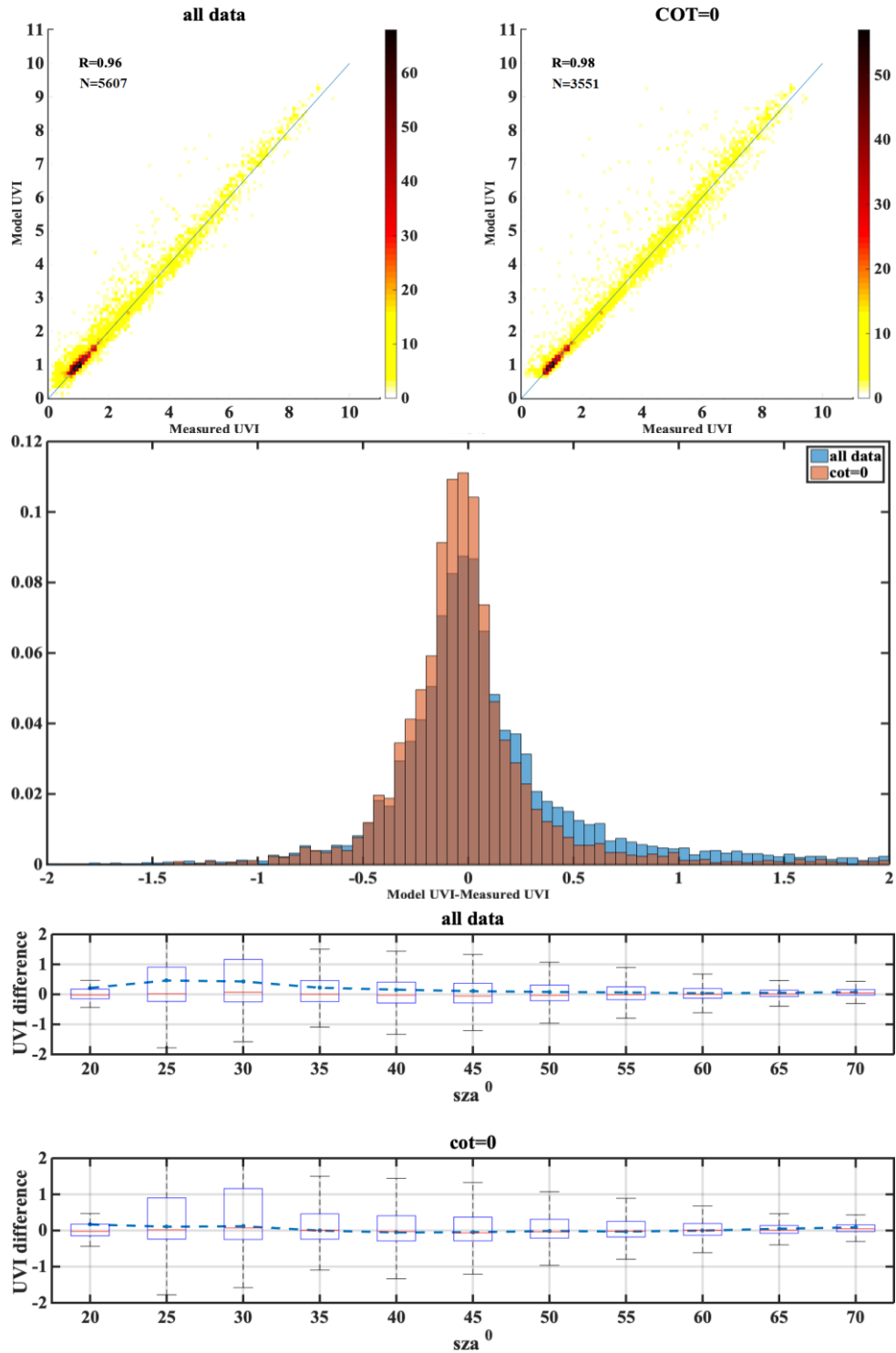


Figure A.2

ARE

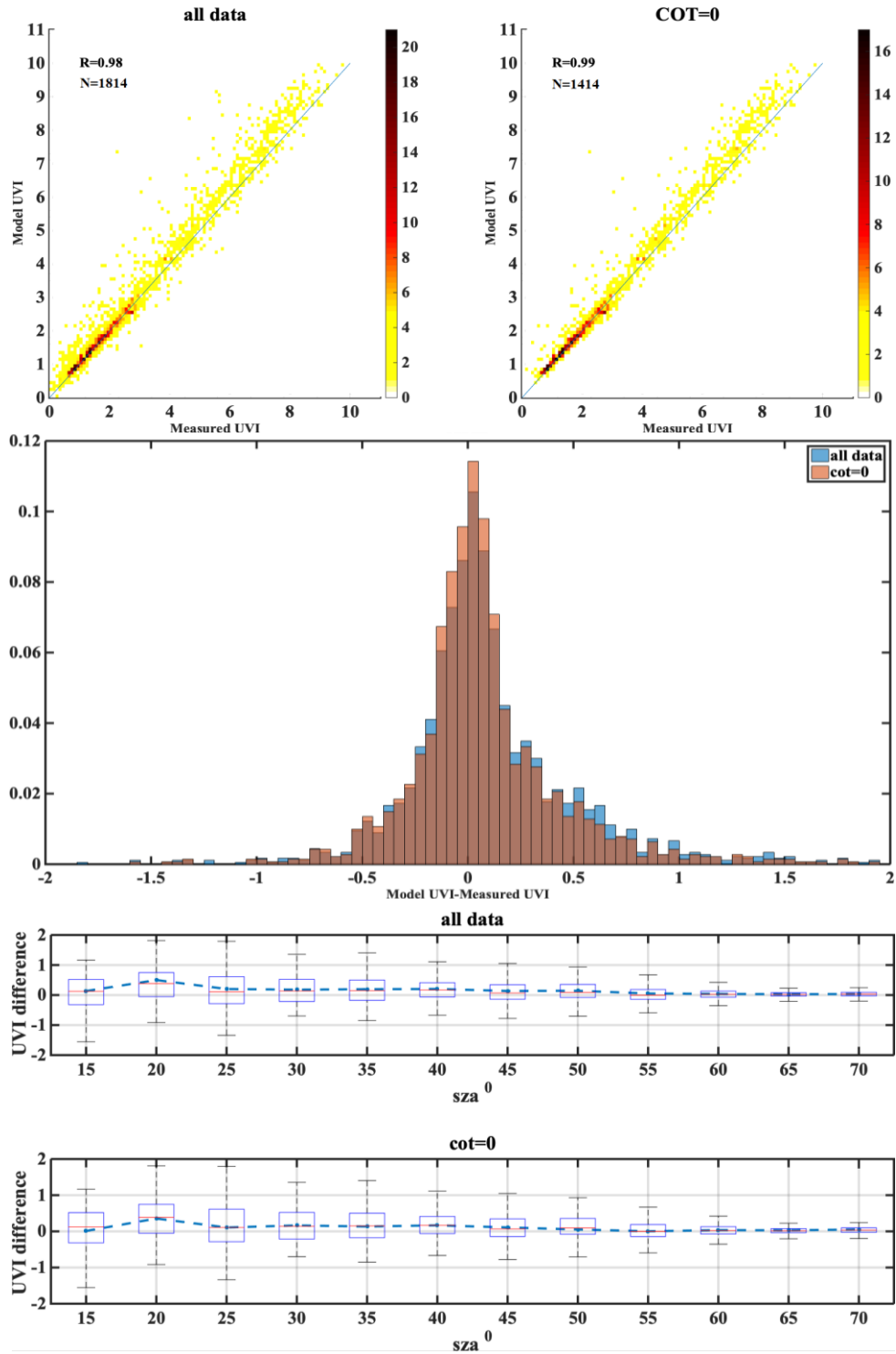


Figure A.3

ATH

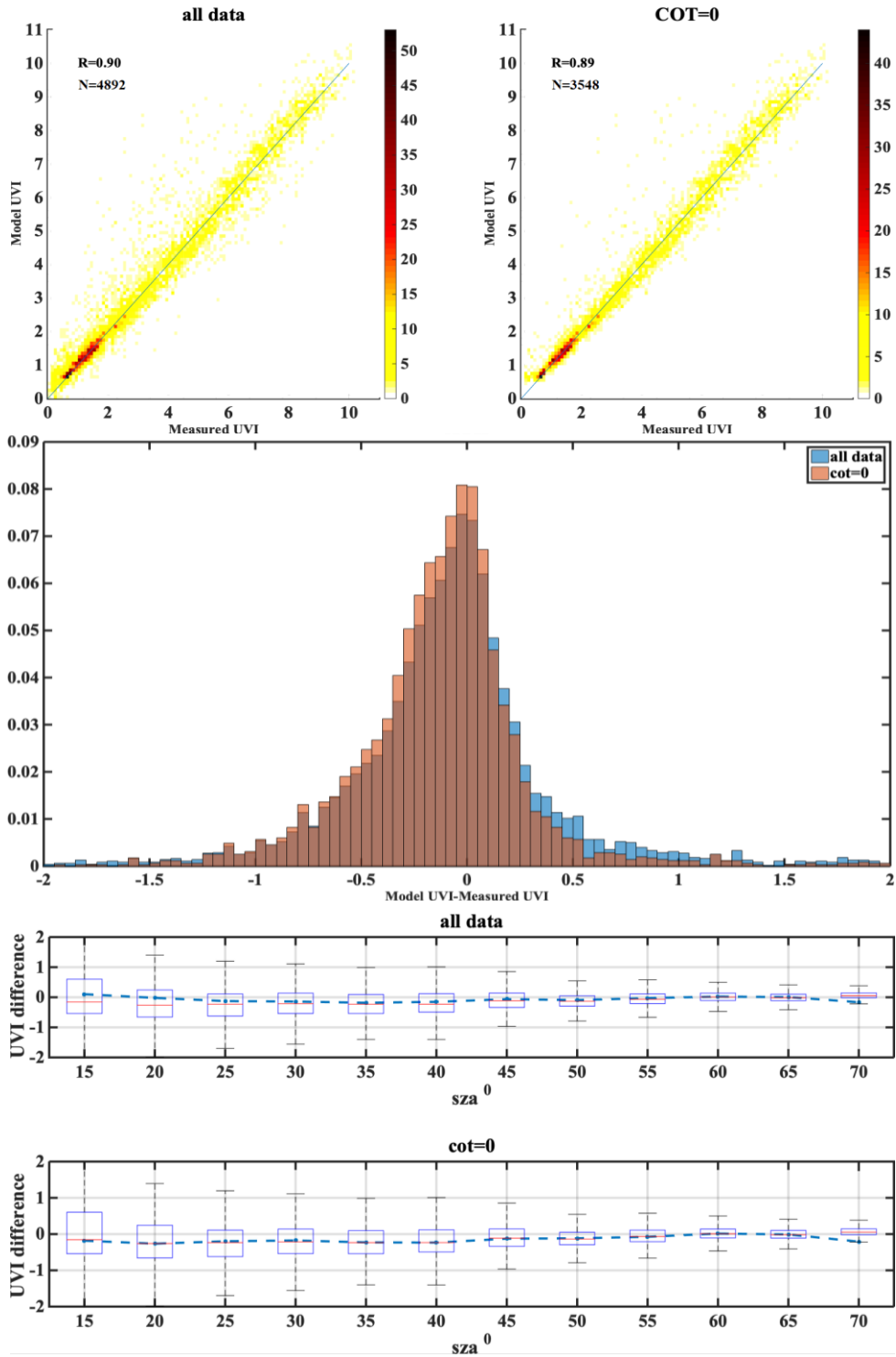


Figure A.4

BEL

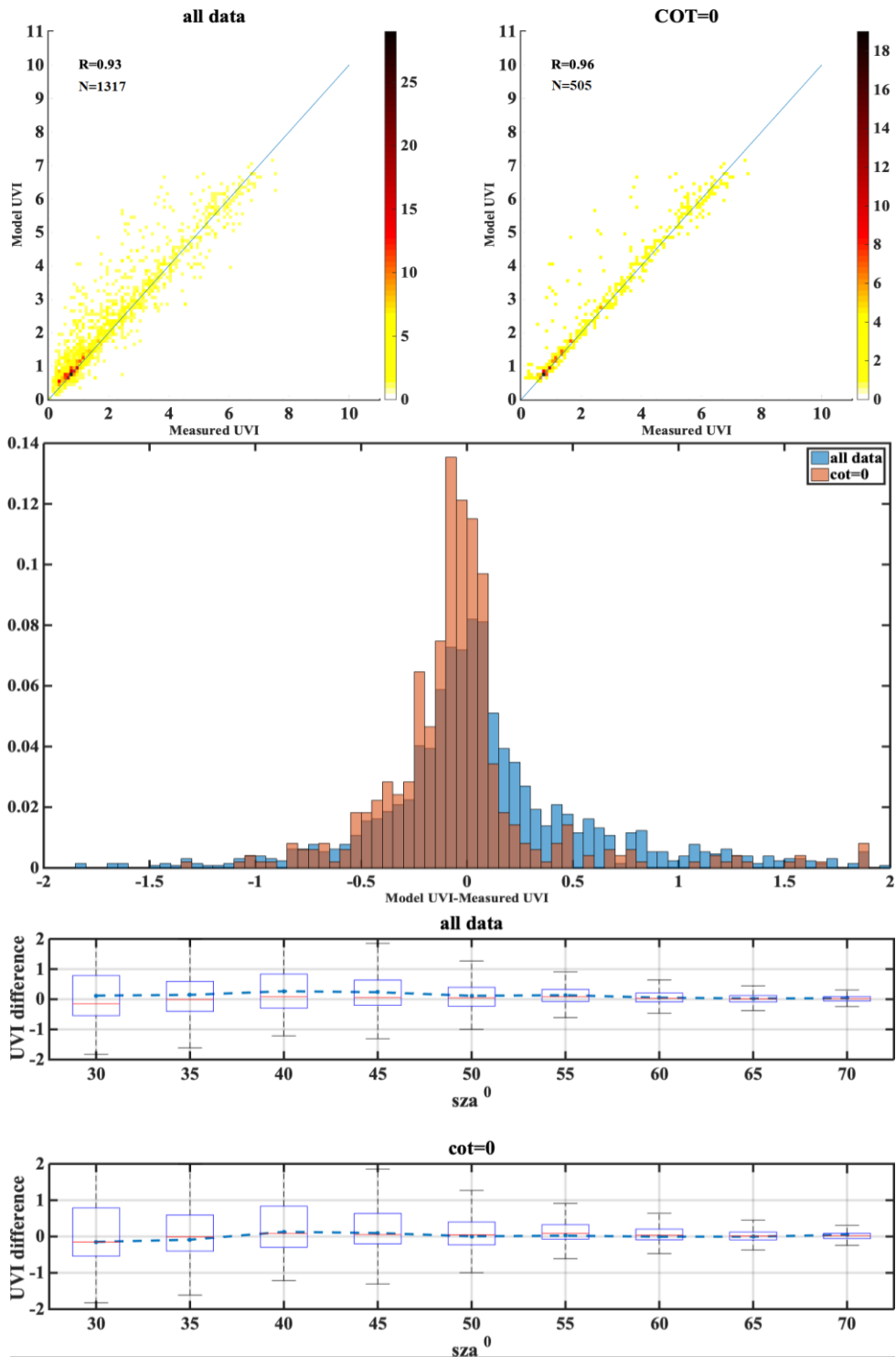


Figure A.5

DAV

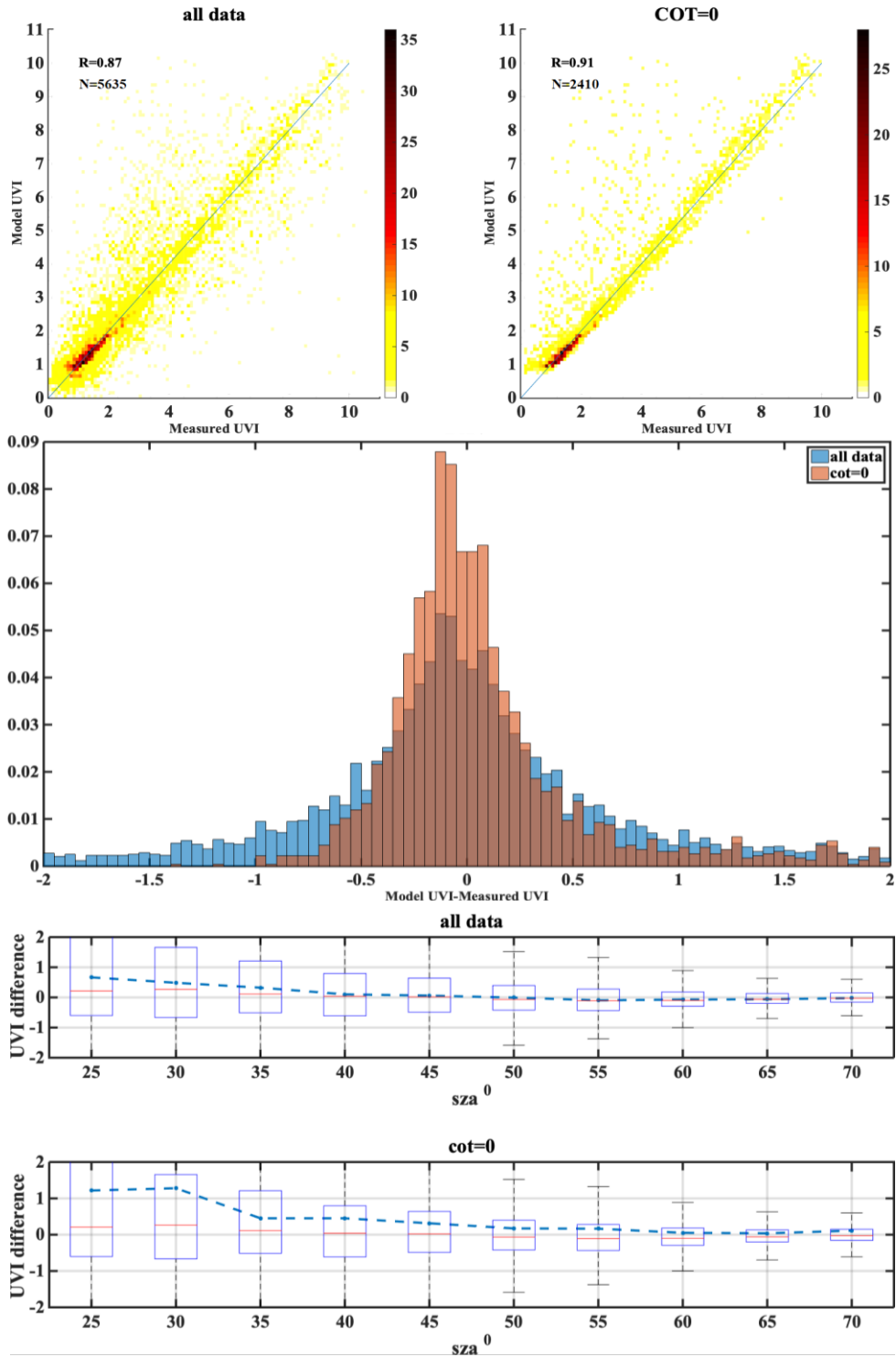


Figure A.6

HEL

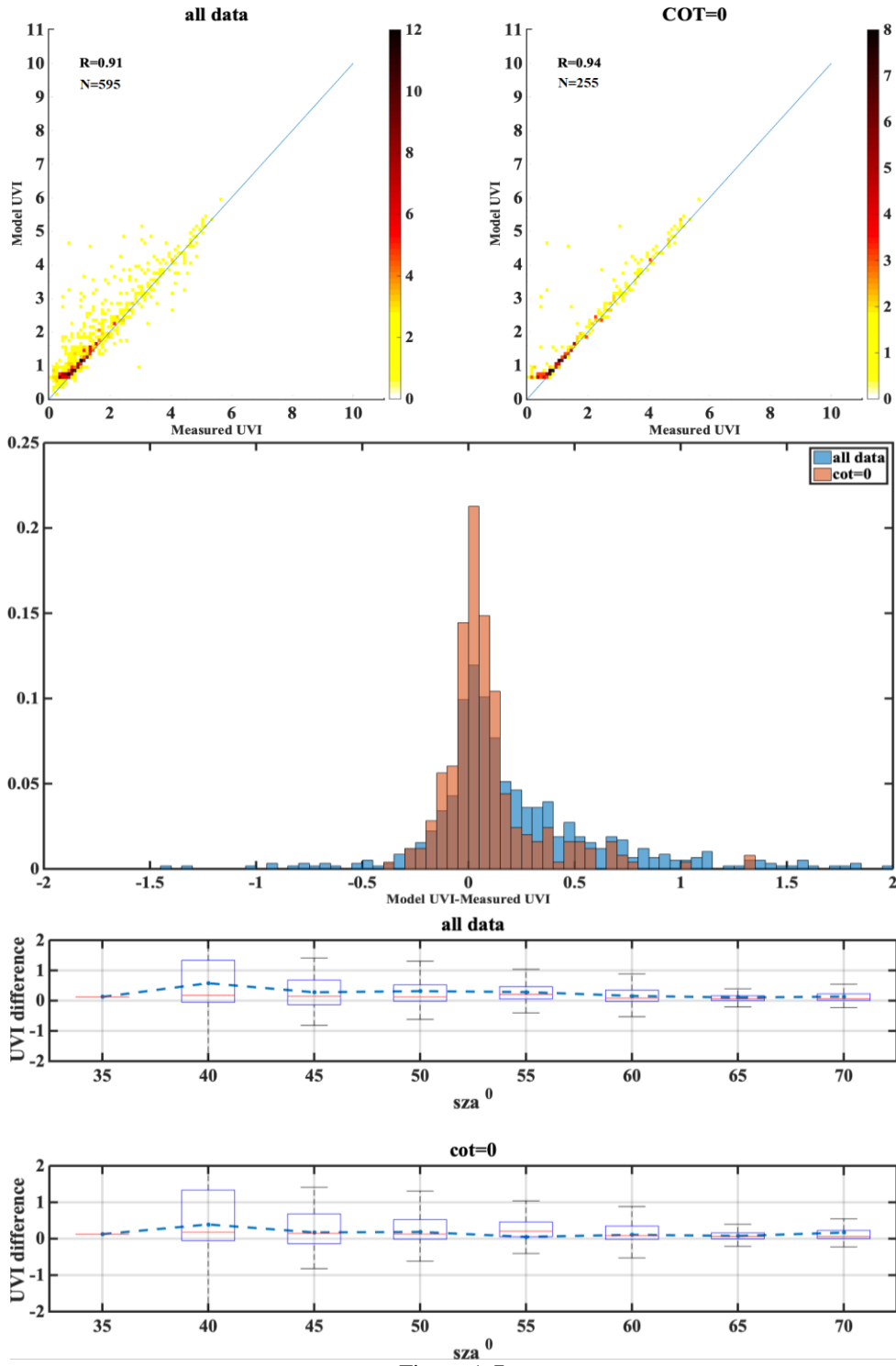


Figure A.7

INN

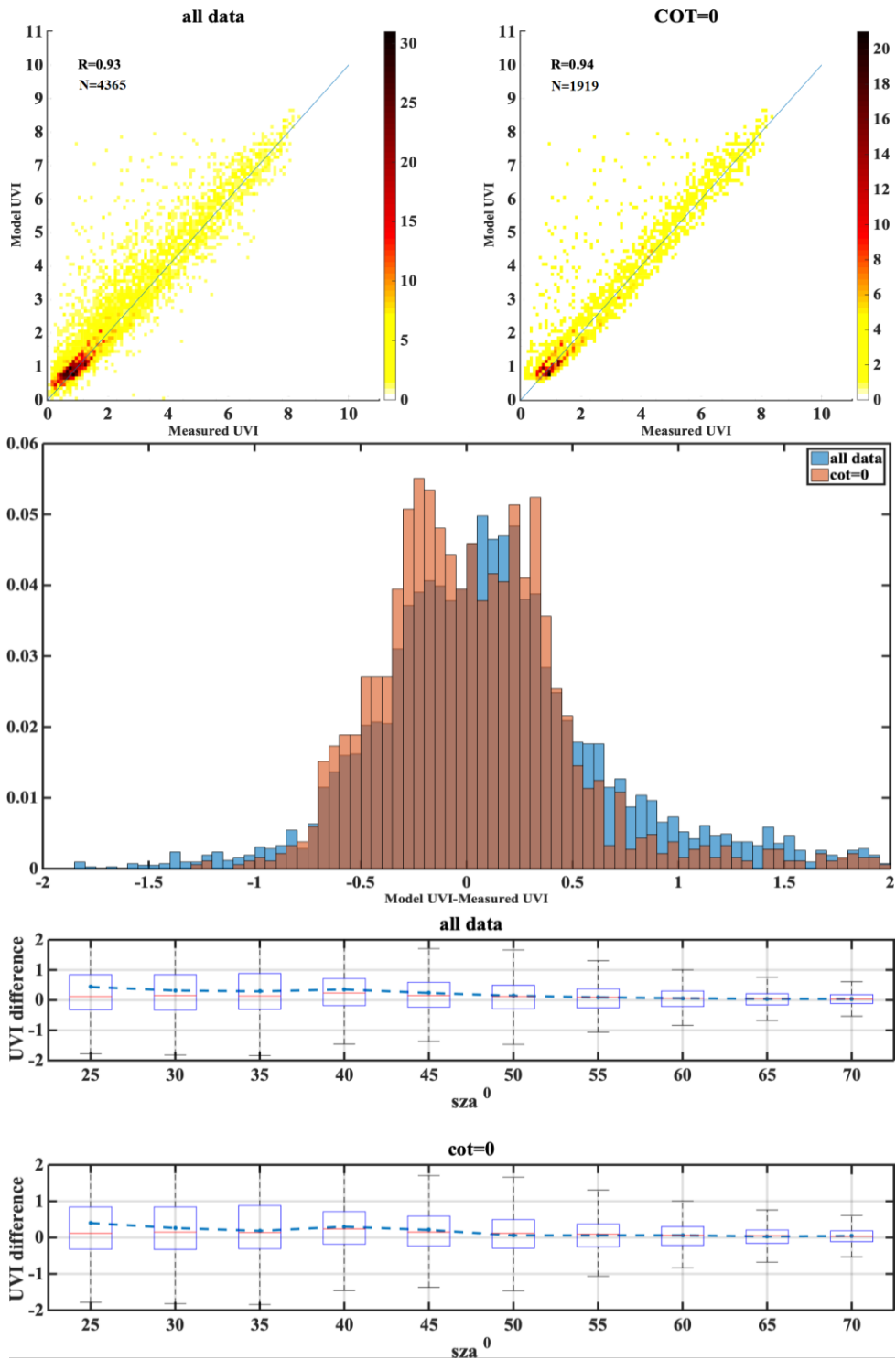


Figure A.8

LAN

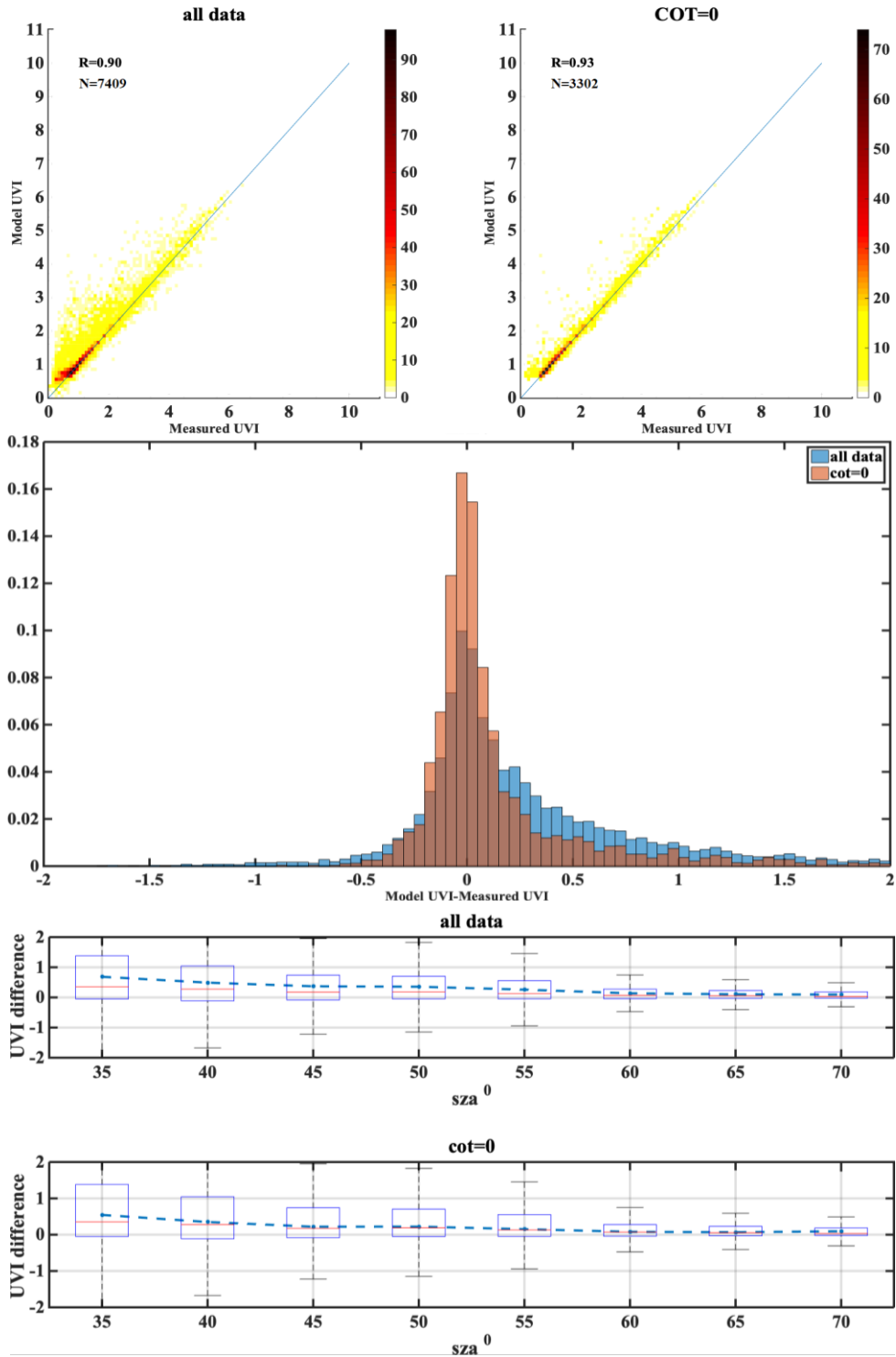


Figure A.9

LIN

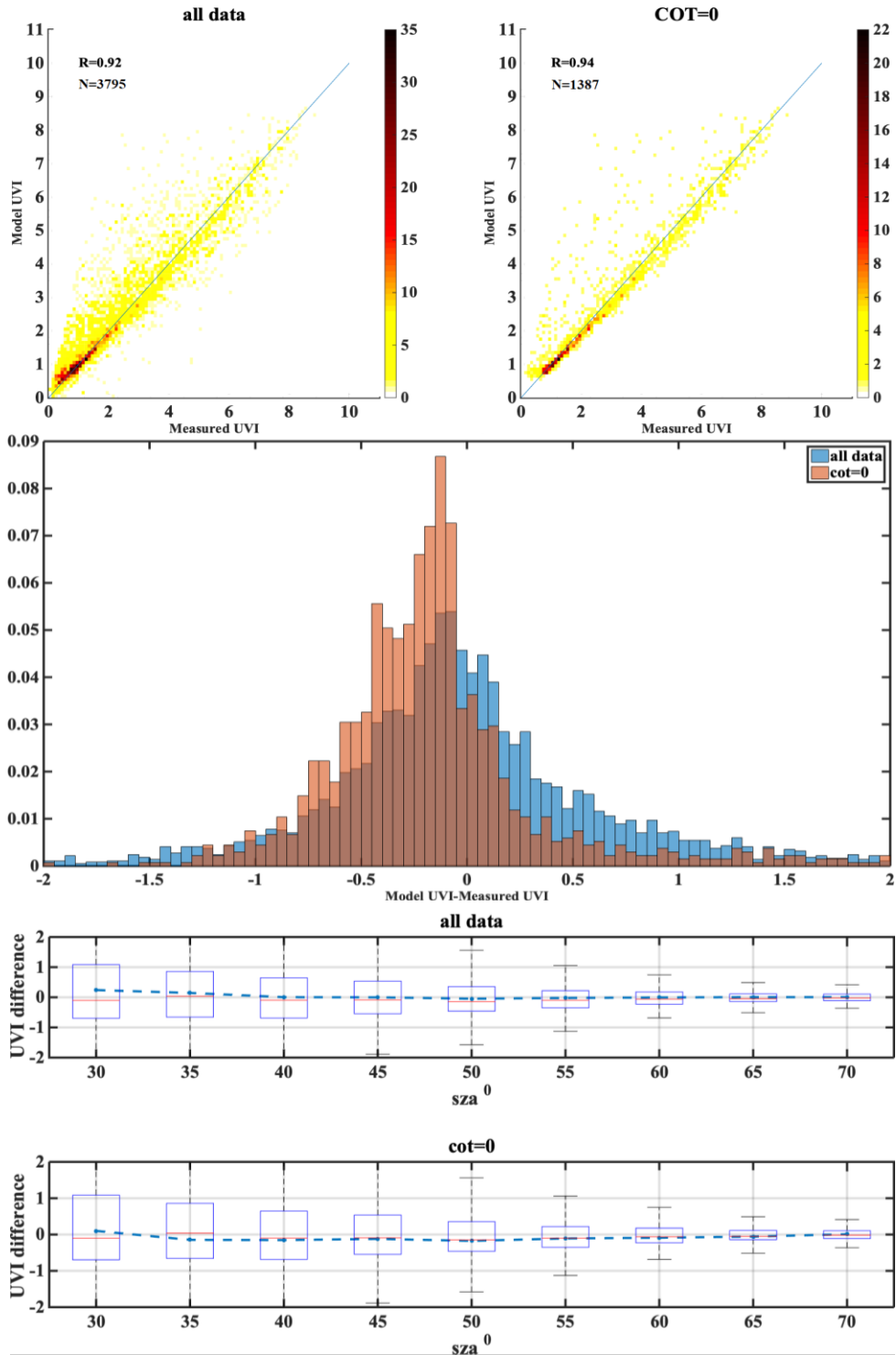


Figure A.10

MAN

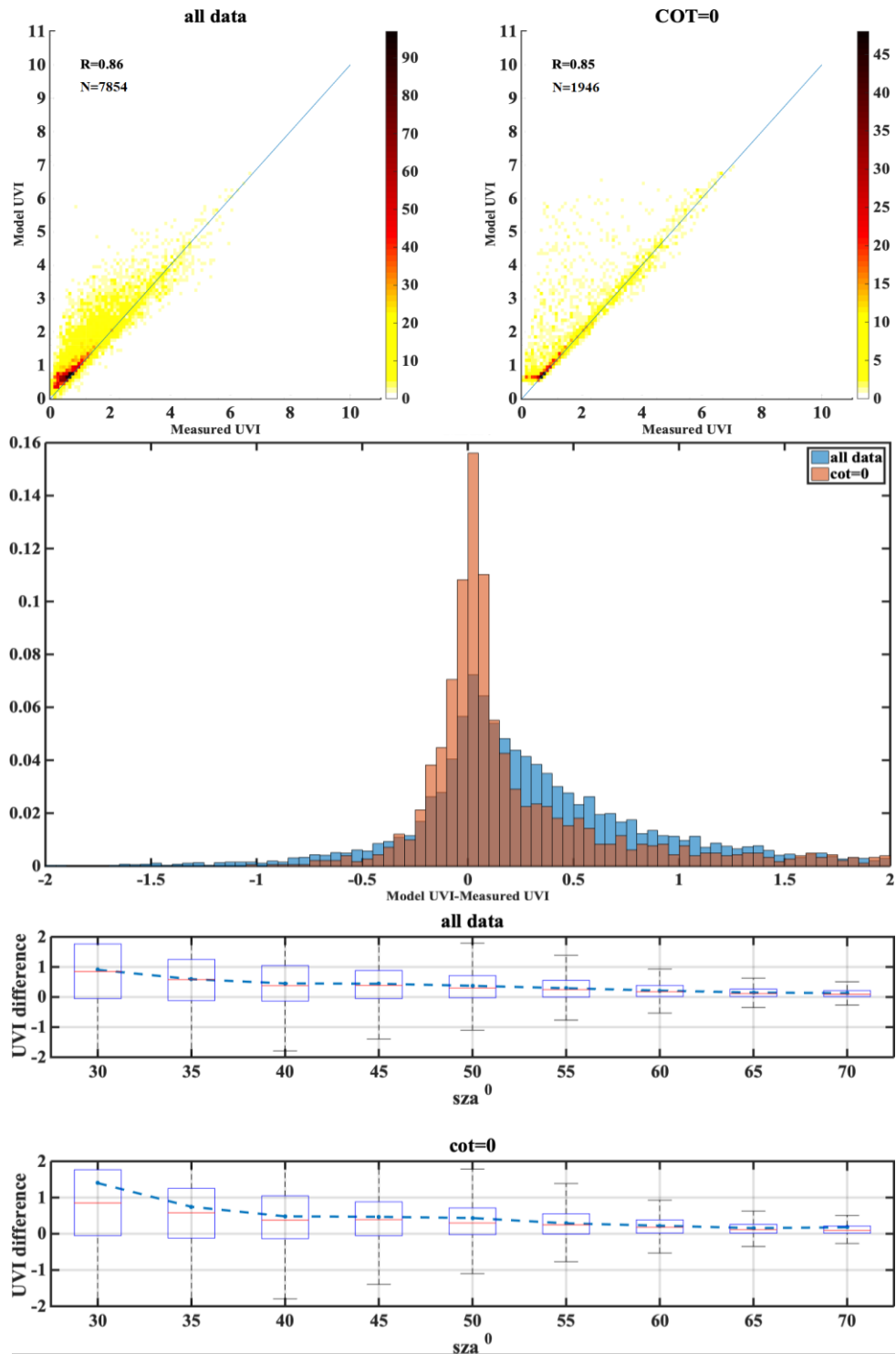


Figure A.11

ROM

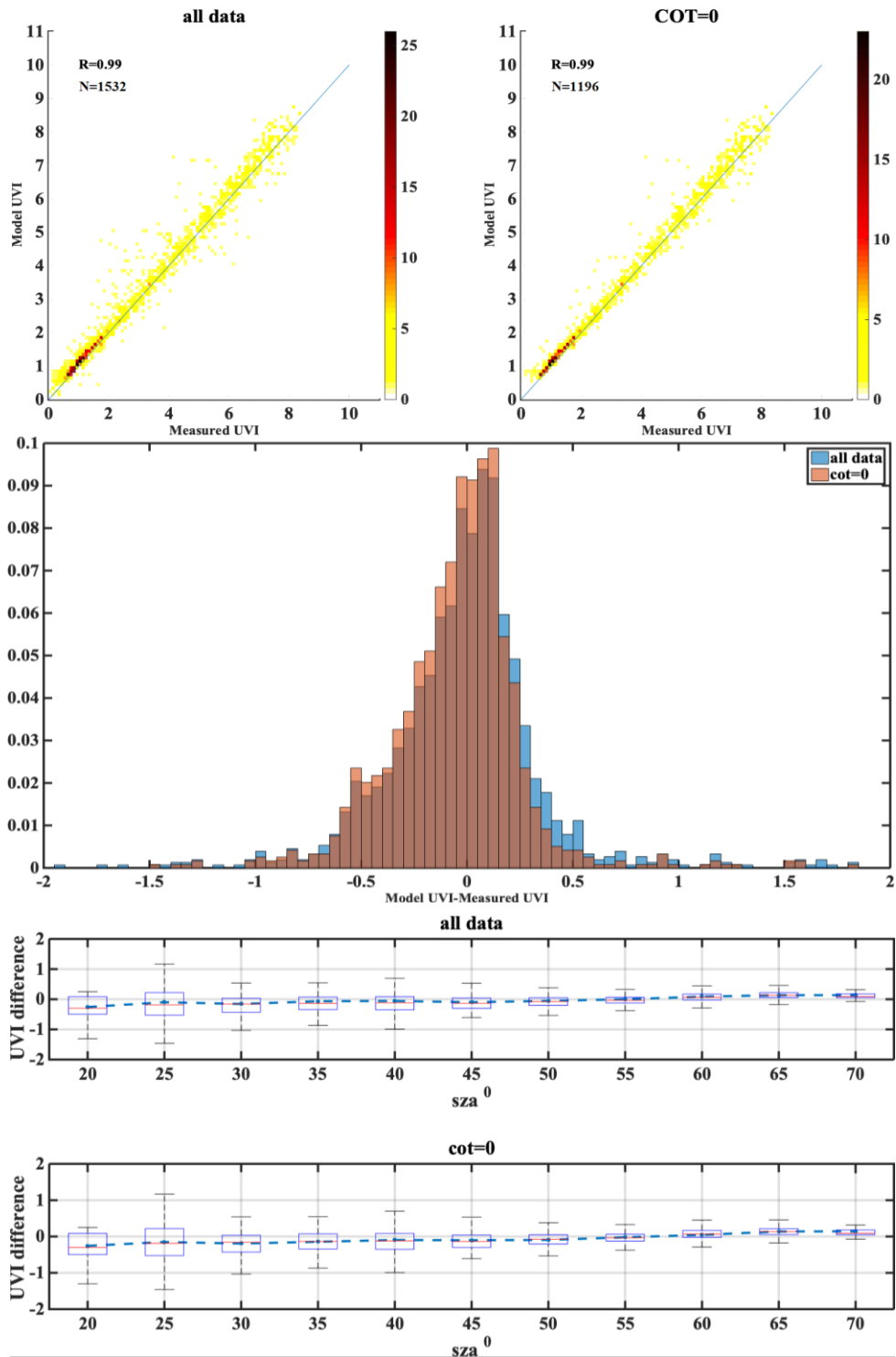


Figure A.12

SOD

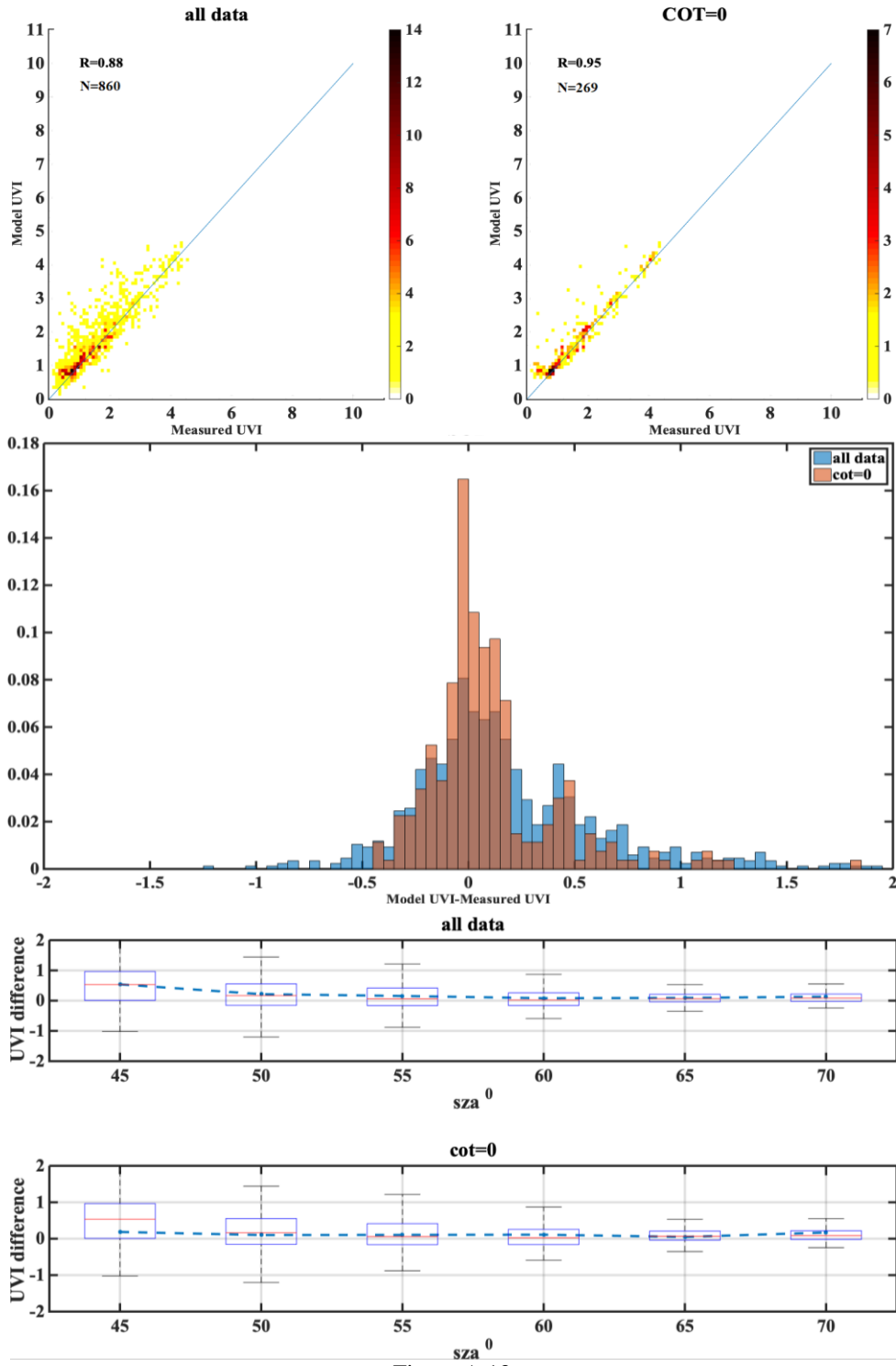


Figure A.13

THE

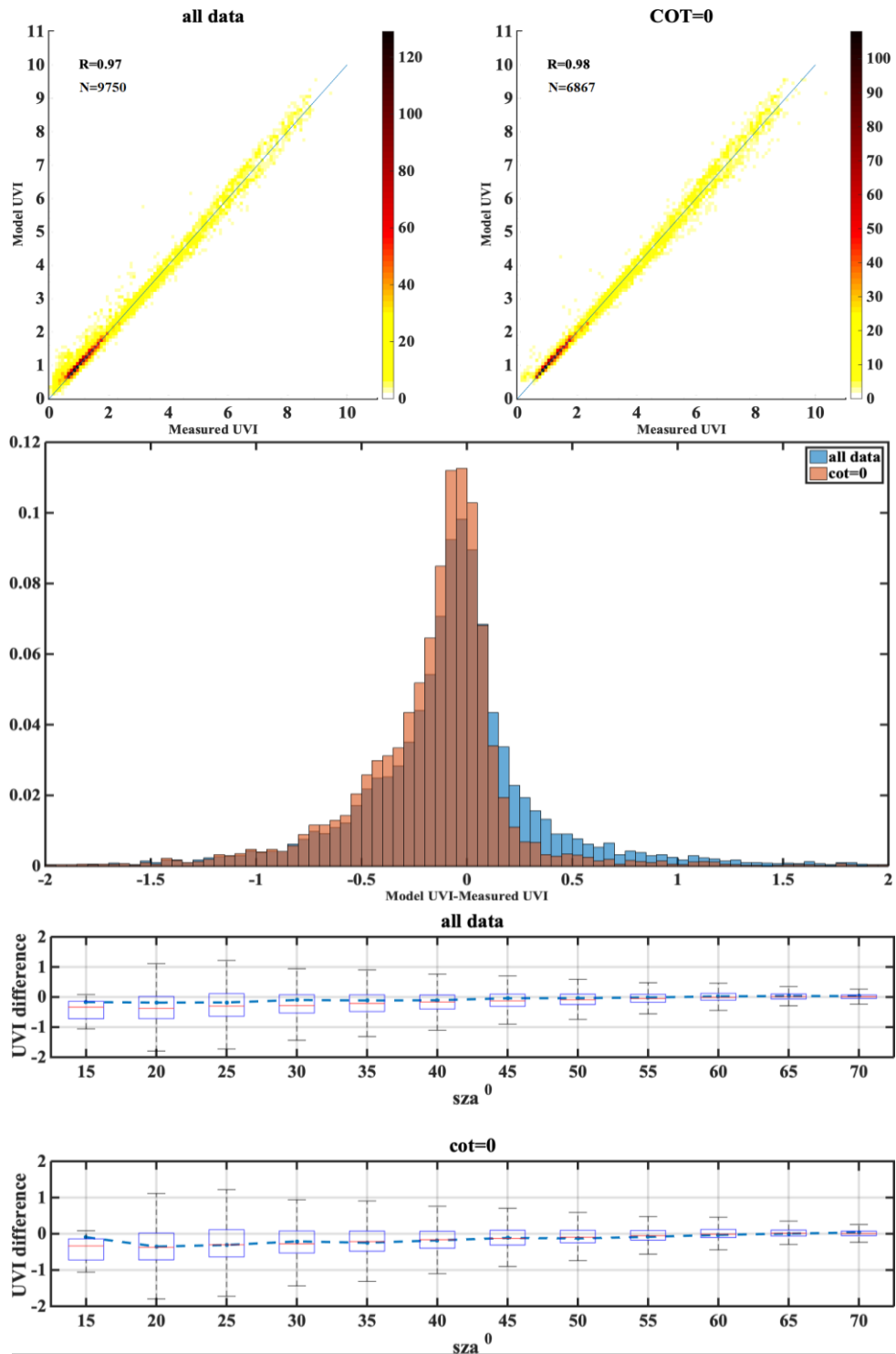


Figure A.14

UCC

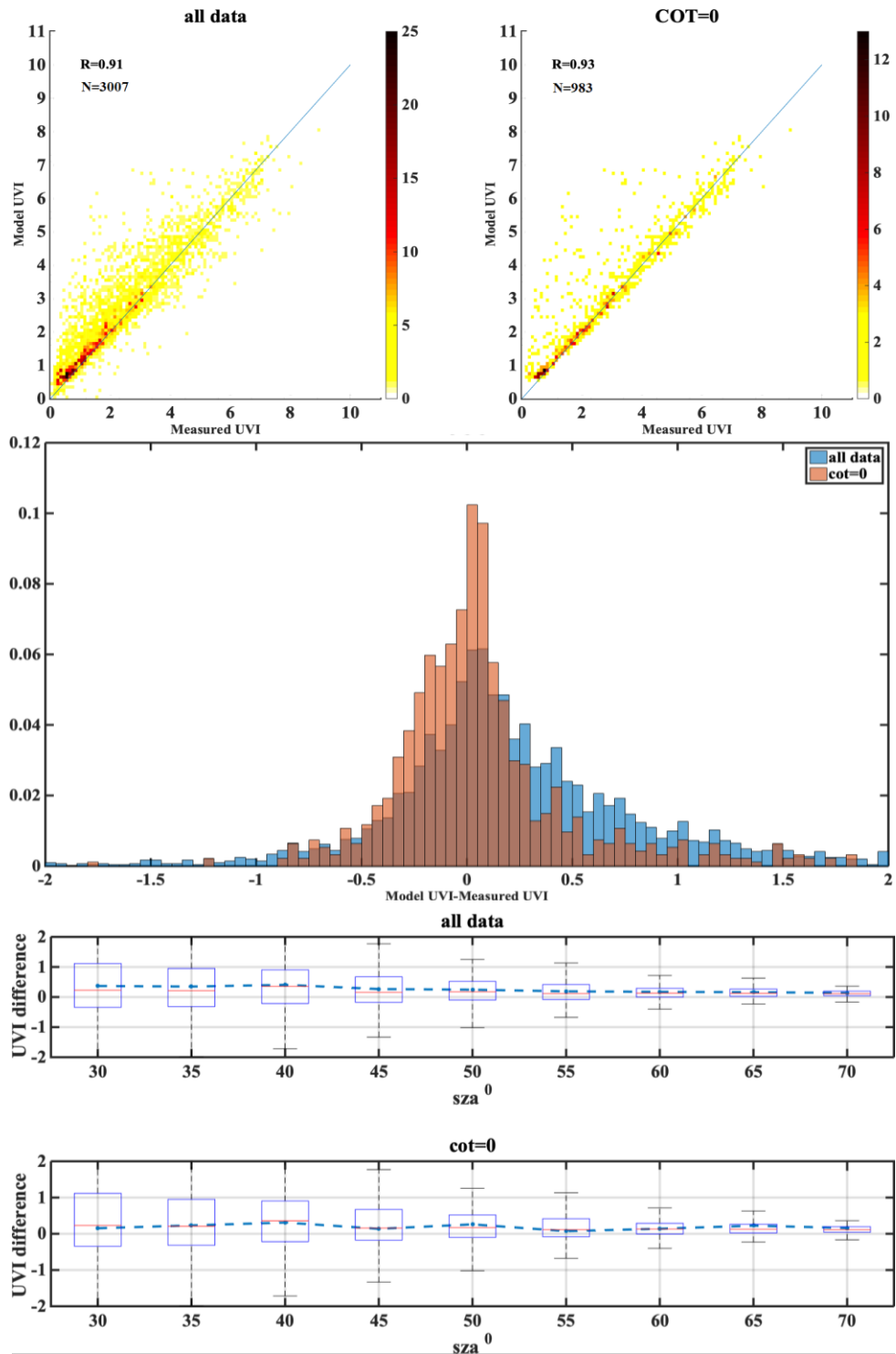


Figure A.15

VAL

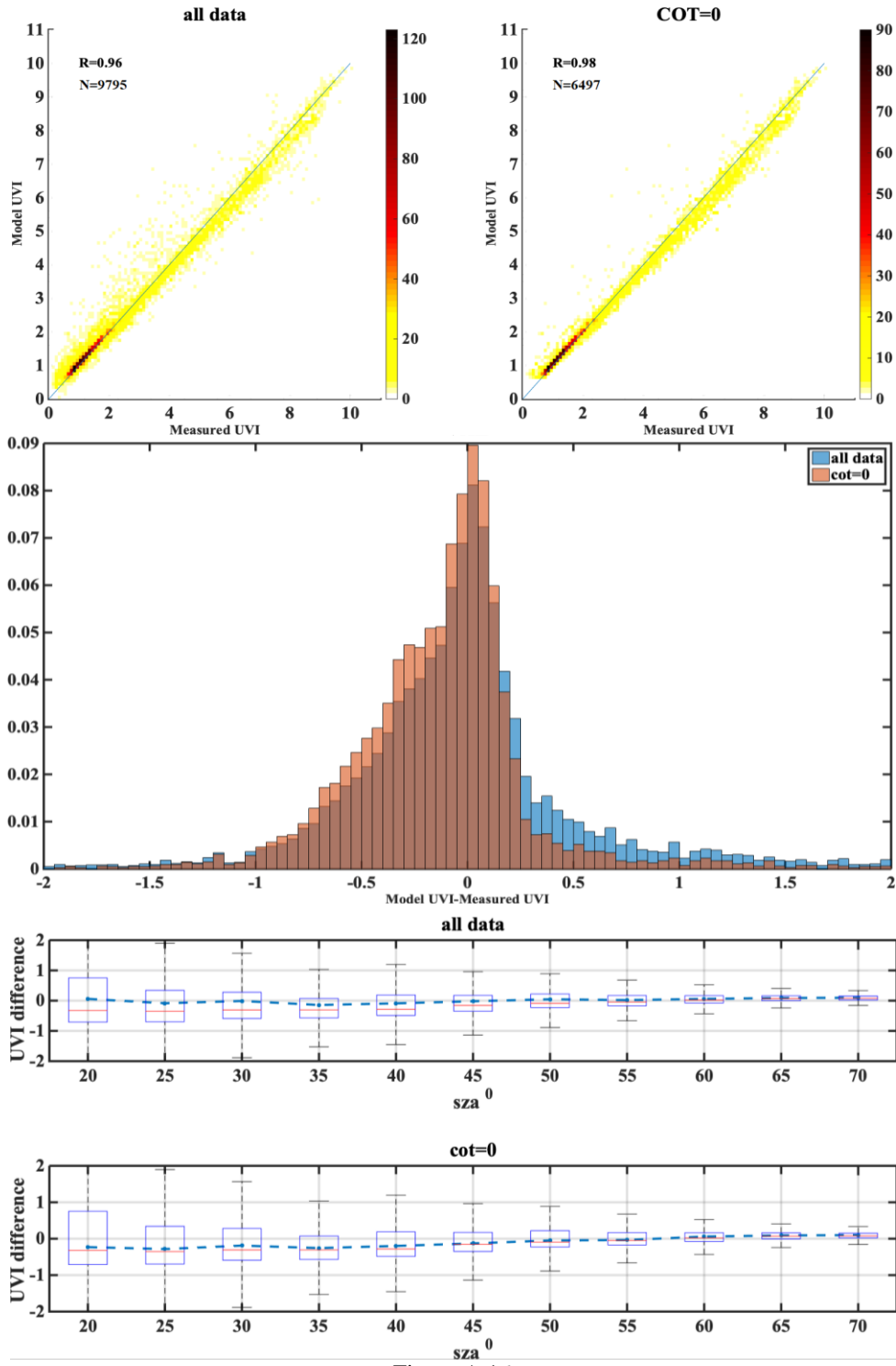


Figure A.16

VIE

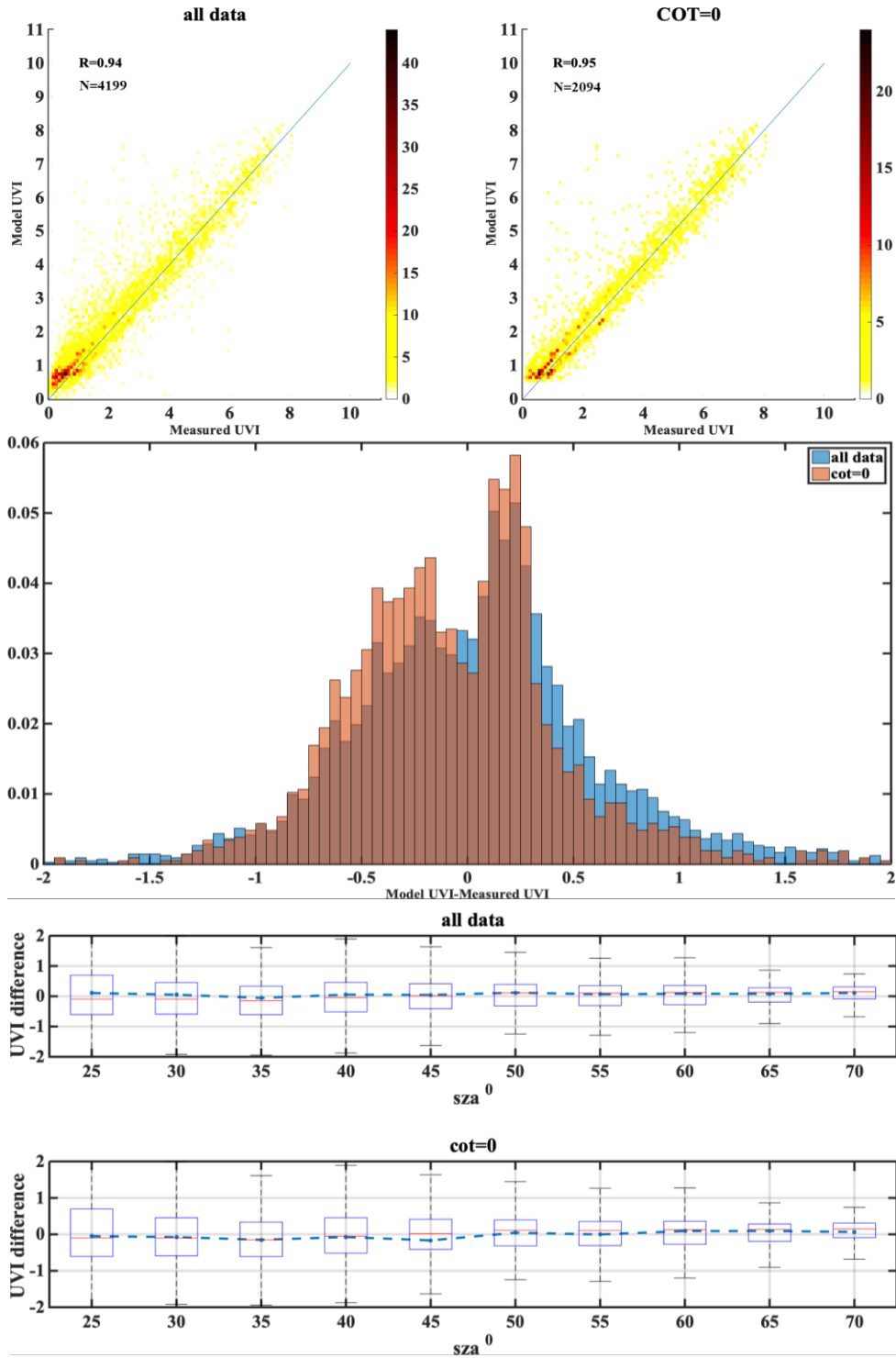


Figure A.17